EVALUATION OF EFFECTIVE STIFFNESS PROCEDURES IN SEISMIC DESIGN OF REINFORCED CONCRETE FRAMES

A Thesis Submitted to
the Graduate School of
İzmir Institute of Technology
in Partial Fulfillment of the Requirements for the Degree of

MASTER OF SCIENCE

in Civil Engineering

by
Duygu ŞENOL

December 2021
İZMİR

ACKNOWLEDGMENTS

I wish to express my gratitude to my supervisor, Assoc. Prof. Cemalettin Dönmez, whose expertise was invaluable in formulating the research questions and methodology. He consistently enabled this study to be my work but guided me in the right direction whenever he thought it was necessary. Also, I would like to thank my family, mother, siblings, and father since they have supported me throughout my life.

I also would like to thank my valuable friend Bora Doğaroğlu due to supporting me and providing motivation during my research process.

I wanted to thank all the Izmir Institute of Technology Civil Engineering Department.

Last but not least, I wish to express my appreciation to my lovely fiancé Emrah Kısa for his understanding and encouragement.

ABSTRACT

EVALUATION OF EFFECTIVE STIFFNESS PROCEDURES IN SEISMIC DESIGN OF REINFORCED CONCRETE FRAMES

This study investigates the success of the effective stiffness procedures defined for the design of reinforced concrete frames in seismic design regulations. The emphasis will be on the effort to model success relations. The origins of the effective stiffness approach could be identified in the effort to use the equal displacement rule for seismic design purposes. The equal displacement rules dictate that if a system's effective stiffness at the sustained drift levels could be identified, the linear and nonlinear system deflection demands are approximately equal. The nonlinear displacement response of a system could be obtained using this "estimated" stiffness value at the sustained displacement levels from the elastic analysis of the system. Hence, there is no consensus about defining the effective stiffness, and different approaches exist for its calculation. In this study, the effective stiffness approaches of the Turkish Earthquake Code (2018), Canadian Standards Association Design of Concrete Structures (CSA A.23.3-14), New Zealand Concrete Structures Standard (NZS3101-2006), Eurocode 8 (EN 1998-3), Building Code Requirement for Structural Concrete of American Concrete Institute (ACI318-19) and Sozen's Method are investigated in terms of effort in their execution to the success of the result. In order to provide a comparison in reference to measured values, the evaluation is based on the shaking table tests of a ten-story-three-bay reinforced concrete frame model. The numerical analysis is performed using the OpenSees platform. The model is formed by defining nonlinear rotational springs at the element ends. The effective stiffness definitions are performed per each regulation, and the results are compared with the test results. Also, a suite of ground motions is selected, and time history analyses are performed using each effective stiffness approach. Results are compared in terms of the maximum and envelope drift levels of the frames obtained by each approach.

ÖZET

BETONARME ÇERÇEVELERİN SİSMİK TASARIMI İÇİN ETKİN RİJİTLİK YÖNTEMLERİNİN DEĞERLENDİRİLMESİ

Bu çalışma, sismik tasarım yönetmeliklerindeki betonarme çerçevelerin tasarımı için tanımlanan etkin rijitlik yöntemlerinin başarısını incelemeyi amaçlamaktadır. Çalışmadaki öncelikli hedef incelenen yönetmeliklerin bu konuda ne denli başarılı olduklarını ortaya koymaktır. Etkin rijitlik yaklaşımı esas olarak eş yer değiştirme kuralını sismik tasarım amaçları için uyarlarken tanımlanmıştır. Eş yer değiştirme kuralı, bir sistemin ulaştığı maksimum öteleme seviyelerindeki etkin rijitliğinin tanımlanabilmesi halinde aynı sistemin doğrusal ve doğrusal olmayan modellerindeki yer değiştirme taleplerinin yaklaşık olarak eşit olacağını belirtmektedir. Böylelikle bir sistemin doğrusal olmayan ötelemesinin hedef öteleme seviyelerindeki "etkin rijitlik" değeri kullanılarak sistemin elastik analizinden elde edilebileceği ortaya çıkmıştır. Ancak, etkin rijitliğin nasıl tanımlanacağına dair bir fikir birliği yoktur ve farklı yaklaşımlar mevcuttur. Bu çalışmada, Türk Deprem Yönetmeliği (2018), Kanada Beton Yapı Tasarım Standardı (CSA A23.3-14), Yeni Zelanda Beton Yapı Tasarım Standardı (NZS3101-2006), Avrupa-8 Yönetmeliği (Eurocode 8- EN1998-3), Amerikan Yapısal Beton Yönetmeliği (ACI318-19) ve Sozen Metodu tarafından tanımlanan etkin rijitlik yaklaşımları incelenmiştir. Sonuçları bir referans değer ile karşılaştırmak amacıyla, on katlı üç açıklıklı bir sarsma tablası deneyler serisinin çerçeveleri tanımlanan yöntemler ile incelenmiştir. Analizler, OpenSees açık platformundaki analiz modülleri kullanılarak yapılmıştır. Doğrusal olmayan sayısal model, eleman uçlarında yığılı plastisite yaklaşımıyla oluşturulmuştur. Her yönetmelik için etkin rijitlik tanımlarına göre analizler yapılmış ve deney sonuçlarıyla karşılaştırılmıştır. Ayrıca, Türk Deprem Yönetmeliğinde yüksek sismik bir bölgeyi temsil eden bir deprem seti seçilmiş ve zaman tanım alanında analizler yapılmıştır. Sonuçlar, maksimum ve zarf ötelenme seviyeleri açısından incelenmiştir.

TABLE OF CONTENTS

LIST OF FIGURES

Figure **Page**

Figure **Page**

LIST OF TABLES

Table **Page**

Table **Page**

CHAPTER 1

INTRODUCTION

1.1. Problem Statement

The seismic design of reinforced concrete (RC) structures mostly relies on linear analysis techniques. Nonetheless, based on either a linear or nonlinear approach, the current design methodology targets a strength less than the required value for an elastic response. The gap in reality and the design approach are compensated using the equal displacement rule, which simply states that the linear and nonlinear maximum displacements are approximately equal. Hence, structures designed for lower strength values could survive the earthquake by sustaining their design strength levels at the expected displacement demands during the ground motions. Some researchers report (Moehle 2015) that the equal displacement rule is an observation made on the averaged results of the structures for a group of ground motions and should not be expected to be observed for every individual ground motion. On the other side, there are experiments (Takeda, Sozen, and Nielsen 1970), (Gulkan and Sozen 1971) and (Otani 1973) showing that it is valid at least for the individual ground motions applied in these studies.

Nevertheless, the equal displacement rule provides a basis for explaining how the structures could survive in earthquakes with a strength much lower than the elastic demands. One important aspect needs attention: the period value which the linear and nonlinear displacements are expected to coincide is not the initial period of the structure. It is rather a value that should consider the softening in the system (Sozen 2003). There is a debate about how to define this softening. There are two major approaches. The first one relies on the fact that cracking in the system is the main source of the softening and calculating the “cracked stiffness” should be the course of action. The other approach embraces the complexity and the difficulty of calculating the representative stiffness value in the nonlinear response, and rather than attempting to perform complicated tasks, make very simplistic assumptions about the calculation of the stiffness.

Different approaches in calculating the effective stiffness are embodied in the seismic regulations. Some of these are Building Code Requirement for Structural

Concrete of American Concrete Institute ACI318 (2019), New Zealand Standard (2006), Canadian Standards Association Design of Concrete structure, Eurocode 8, and Turkish Earthquake Code (2018). A close look at these documents presents methods for calculating effective stiffness of the RC structures as simple as defining a constant reduction in stiffness of all members to the calculation of individual member effective stiffness' based on the individual properties of the members. The effort necessary to apply these procedures varies considerably. The main purpose of the presented study is to investigate whether the complexity in calculating the effective stiffness of the structure with various approaches is worthed for the effort in the obtained results.

1.2. Scope of the Thesis

In this study, the evaluation of the success of the effective stiffness procedures was performed in reference to the measured response of a 10-story scaled moment frame structure. The experiments by (Cecen 1979) were selected for this purpose. The test frame was modeled in the OpenSees platform, and nonlinearity was introduced by concentrated nonlinear springs at the ends of the members. Since the test frame was designed to develop a beam mechanism, the selected nonlinear modeling options were sufficient to simulate the nonlinear action in the experiment.

Six different approaches defined in seismic and structural design codes were utilized for comparison purposes. These are Building Code Requirement for Structural Concrete of American Concrete Institute (ACI318), New Zealand Standard (2006), Canadian Standards Association Design of Concrete Structures (2014), Eurocode8 (1998) Turkish Earthquake Code (2018), and a simple approach recommended by Prof. Mete (Sozen 2003).

The reference frame is also subjected to a suite of ground motions selected and scaled to represent the soil type ZD in the Turkish Earthquake Code (2018). This exercise aims to observe the differences in the results of different effective stiffness approaches under different earthquake demands.

1.3. Outline of the Thesis

The comparisons are performed by forming linear and non-linear models of the test frames. Hence, corresponding frame models were built by using OpenSees software. The first set of these models is linear frames, which are used for linear time history analyses. The second set of frames, which have concentrated nonlinear springs at member ends, was used for nonlinear time history analyses. The effective stiffnesses of the members of these frames were changed according to the six procedures listed above. Chapter 1 involves the problem statement and the scope of the study. Chapter 2 contains the literature review on the effective stiffness of RC structures and the detailed information of the corresponding seismic regulations. Chapter 3 presents the details and geometric properties of the numerical models and the explanations about the analyses. Chapter 4 contains the discussion of the results obtained from all performed analyses. And, Chapter 5, includes the summary and conclusions of the thesis, and the motivation for future studies.

CHAPTER 2

EFFECTIVE STIFFNESS DEFINITIONS

2.1. Introduction

The key relation of correlating the linear and nonlinear displacement under seismic demands necessitates the calculation of effective stiffness values for nonlinear analysis. There are various approaches in this matter. A brief history of the development of effective stiffness and the existing approaches in the literature to estimate effective stiffness will be presented in this section.

2.2. Effective Stiffness Definitions

The effective stiffness approach is not only employed for seismic purposes. Hence, it is necessary to discuss different purposes of effective stiffness usage. Broadly, it could be said that if a structure is being assessed for the responses beyond the service level loads, it is necessary to consider the effective stiffness of the members. As stated in ACI318, the selection of appropriate effective stiffness values depends on the intended performance of the structure (ACI318, 2019). If the wind loads are considered, an effective stiffness beyond cracking but at pre-yield level is appropriate. If the secondary analysis of a frame is performed, a different set of effective stiffness representing the members' stiffness immediately prior to failure should be defined. The effective stiffness definition for earthquake loading is reported to have relied on the intended structural performance and the demand of the earthquake considered. As summarized in ACI318-19, it is necessary to have a target nonlinearity for defining the effective stiffness. (Sozen 2003) states that for the seismic response, the effective stiffness should be related to maximum displacement attained during the ground motion. Sozen proposed that simple arbitrary amplification of the drift (de-amplifying the stiffness) could be sufficient to obtain the intended result. On the other side, (Elwood and Moehle 2006) stated that the precise estimation of a section stiffness is necessary to predict the yield displacement for nonlinear analysis reasonably. It is also mentioned that accurate stiffness estimation

largely influences the displacement ductility demands. Since the precise prediction of effective stiffness is not a simple task for the practical design of RC buildings under seismic excitation, (Elwood and Moehle 2006) proposed certain coefficients for elements mainly dependent on the axial load levels and the probable reinforcement detailing.

Nevertheless, this simplification sometimes causes overestimation of the effective stiffness of RC structures (Paulay and Priestly 1992). (Sözen 2013) proposed that the decline in the stiffness could be reflected by using one-half of the gross section properties of members. Other approaches demand detailed procedures to the same effect. However, it is not clear whether the detailed analysis results in more accurate stiffness values. The contradiction of the detailed approaches is the approximate nature of the definitions or simplifications for the local type of elements. Sozen's proposal of using an arbitrary scaling of the stiffness to reach the intended results could be as effective as using a relatively complicated procedure. ACI318 and Eurocode 8 propose Sozen's proposal as an alternative to the detailed procedures. The presented study will attempt to provide further evidence about the effectiveness of the proposed procedures. The experimental study performed by (Cecen 1979) will be used as a reference for this purpose. The success of the listed procedures will be evaluated in reference to Cecen's data.

2.3. Effective Stiffness Definitions in the Selected Seismic Design Codes

Effective stiffness approaches of the selected seismic and structural design specifications were evaluated. These were Turkish Earthquake Code (2018), Eurocode 8 (EN 1998), American Concrete Institute Building Code Requirements for Structural Concrete (ACI318-19), New Zealand Concrete Structures Standard (NZS 3101-2006), Canadian Design of Concrete Structures (CSA A23.3-14) and a simple method by proposed by Prof. Mete Sozen. The effective stiffness definitions of these documents are presented in the coming sections.

2.3.1. Turkish Earthquake Code (2018)

Turkish Earthquake Code (2018) contains three different procedures for determining the effective stiffness based on the analysis type. If a linear analysis is

performed, a procedure that relies on pre-defined coefficients for the elements is defined. If the analysis is nonlinear with concentrated plastic hinges, the effective stiffness of the members is defined through a formulation that relies on a set of parameters based on individual member properties. Finally, if the analysis is nonlinear with distributed plasticity, there is no definition for effective stiffness. It is accepted that distributed plasticity modeling is sufficient for the purpose.

Interestingly, the effective stiffness of flexural members for evaluation of existing structures are defined to be (Sec. 15.4.11) the values assigned for linear analysis in Section 4.5.8., regardless the analysis is linear or nonlinear.

2.3.1.1. Rules for Linear Analysis

Beams and columns should be modeled as frame finite elements. The effective stiffness coefficients of the individual elements are defined as presented in Table 1.

Table 1. Effective stiffness coefficients of reinforced concrete bar elements for linear analysis method

Coefficients for Linear Analysis		
Element	**Effective Stiffness Coefficient**	
	Bending Flexure	**Shear**
Bond Beams	0.15	1.00
Beams	0.35	1.00
Columns	0.70	1.00
Shear Wall (Equivalent Frame Element)	0.50	0.50

2.3.1.2. Rules for Nonlinear Analysis with Concentrated Plasticity

Beams and columns should be modeled as frame elements similar to linear analysis. Nonlinear behavior is simulated with concentrated nonlinear hinges at the ends

of the elements. The plastic hinges could be located at the ends of the clear spans of beams and columns. Beams and columns should be modeled linearly along their lengths. The effective stiffnesses of the members are defined in Section 5.4.5.2 of TEC (2018), and these definitions are presented below. The effective stiffness of the slabs modeled linearly is defined as in Table 2.

$$(EI)_e = \frac{M_y}{\theta_y}\frac{L_s}{3} \tag{1.1}$$

M_y: Effective yielding moment

L_s: Shear span (Ratio of the moment to shear force)

(L_s shall be taken as half of the length for beams and columns.)

θ_y: Yielding rotation

θ_y could be calculated as below,

$$\theta_y = \frac{\phi_y L_s}{3} + 0.0015\eta\left(1 + 1.5\frac{h}{Ls}\right) + \frac{\phi_y d_b f_{ye}}{8\sqrt{f_{ce}}} \tag{1.2}$$

η = 1.0 for beams and columns

η = 0.5 for shear walls

h: Height of cross-section (m)

d_b: Average diameter of longitudinal reinforcements (m)

f_{ce}: Expected compression strength of concrete (MPa)

f_{ye}: Expected tension strength of reinforcements (MPa)

ϕ_y: Yield curvature

2.3.2. Eurocode 8 (EN 1998)

Eurocode 8 demands that the effect of the cracking should be taken into consideration for seismic analysis and design of RC structures. It is regulated by Section 4.3.1 that for new structures, effective stiffness should be calculated either in reference to

yield point or could be taken as half of the gross stiffness based on the uncracked section. The definition in reference to yield point is based on bilinearization of the moment rotation relation. It is stated that "the elastic stiffness of a bilinear relation should be the secant stiffness to the yield-point."

Annex A.3.2 of Eurocode 8 (EN 1998-3) regulates the effective stiffness definitions of the existing structures. It provides a set of equations based on moment-shear ratio, yield rotation, plastic hinge length, material strengths, and main bar diameter. The formulation is given in Eq. 1.4 and 1.5. It is a similar formulation to TEC2018. Considering the release dates, the Turkish regulation approach for nonlinear modeling of new structures for concentrated hinges adopted the Eurocode8 approach.

$$(EI)_{effective} = \frac{M_y}{\theta_y}\frac{L_v}{3} \tag{1.4}$$

$$\theta_y = \varphi_y \frac{L_v + a_v}{3} z + 0.0014\left(1 + 1.5\frac{h}{L_v}\right) + \varphi_y \frac{d_{bl} f_y}{8\sqrt{f_c}} \tag{1.5}$$

θ_y: Chord rotation at yield (rad)

φ_y: Yield curvature at the end section (m^{-1})

L_v = M/V Ratio of moment/shear at the end section (m)

h: Depth of cross-section (m)

a_v = 1.0 If shear cracking is expected to precede flexural yielding at the end section

a_v = 0.0 If yield moment is smaller than shear resistance of the member

z: Length of internal lever arm, taken equal to *d-d'* in beams, columns (m)

f_y: Steel yield stress (MPa)

f_c: Concrete strength (MPa)

d_{bl}: Mean diameter of tension reinforcement (m)

2.3.3. American Concrete Institute Building Code Requirements for Structural Concrete (ACI318-19)

ACI318-19 discusses and defines effective stiffness in two different sections. It appears first in Section 6.6.3 in a linear first-order analysis discussion. The definitions in this section are for linear analysis at factored load levels. It is stated that either the predefined values presented in Table 2 or half of the gross section stiffness could be used. It is also permitted to perform more rigorous analysis. The second appearance of the effective stiffness definition is in Appendix A, where requirements and recommendations about nonlinear time history analysis are presented. It is discussed in the commentary of RA.8 that the intent of the effective stiffness is to specifically introduce the effects of bar slip at the member ends. It is stated that software's are capable of modelling all the other components such as deformations due to flexure, shear, and axial elongation or shortening. However, it is not explicitly told what type of modeling is intended. Discussion about the fiber section modeled shear walls in RA.8.4 clarifies that intention is the frame members with concentrated nonlinear springs hinges in the ends. It is stated that the defined values are in reference to yield level deformations, Table 3. Values are defined based on the member type and the axial load levels.

Table 2. Effective section properties of concrete elements in linear elastic analyses in ACI318-19

Reinforced Concrete Elements	**Stiffness Reduction Factors**
Beams	$0.35I_g$
Columns	$0.70I_g$

Table 3. Effective section properties of concrete elements in inelastic dynamic analyses in ACI318-19

Reinforced Concrete Elements		**Stiffness Reduction Factors**	
		Axial	**Flexural**
Beams	Nonprestressed	$1.0I_g$	$0.3E_cI_g$
Columns with compression caused by design gravity loads[1]	$\geq 0.5A_g f_c'$	$1.0E_cA_g$	$0.7E_cI_g$
	$\leq 0.1A_g f_c'$ or with tension	$1.0E_cA_g$*(compression)* $1.0E_sA_{st}$ *(tension)*	$0.3E_cI_g$

(I_g and E_c refer to the gross section second moment of area and modulus of elasticity of concrete, respectively. A_{st} means the areas of longitudinal reinforcements)

[1]for columns with axial compression falling between the limits provided, flexural stiffness shall be determined by linear interpolation.

2.3.4. New Zealand Concrete Structures Standard (NZS 3101-2006)

NZS 3101 states in Section C2.6.1.4 that the stiffness of reinforced concrete members depends on many factors, such as the quantity of reinforcement and grade, level of axial load, and the extent of cracking in the member. Where elastic analysis methods (equivalent static, modal response spectrum, and elastic time history) form the basis for defining seismic design actions, the stiffness of members which are designed to sustain inelastic deformation should be based on a member stiffness which is equal to the stiffness at the first yield of the longitudinal reinforcement.

Clause C6.3.5 of NZS 3101 does not give specific values for stiffness to be used in the elastic analysis for strength design. It only requires that sensible assumptions to represent the limit state. Also, these assumptions should be applied consistently to the structure. Under these conditions, the designer is free to select suitable stiffness values. A common assumption is adopted for member stiffnesses to calculate design moment actions for the ultimate and serviceability limit states. These values are 0.8 (EcIg) for columns and 0.4 (EcIg) for flexural members' elastic analysis. Ig refers to the gross section second moment of area, and Ec, however, represents modulus of elasticity of the concrete. It is stated that the changes in the stiffness of the RC sections have an

insignificant effect on the magnitudes of critical design moments. Nonetheless, where plastic hinge rotations or deflections take place, it is stated that realistic stiffness calculations are important. For this purpose, the stiffness values at potential plastic zones are directed to be calculated as in Section 6.8 of NZS 3101-2006. Besides, the EI value should be based on cross-section properties, coherent with the principles set out in Sections 6.8.1 and either 6.8.2 or 6.8.3 of the code.

NZS 1170.5 Supplement 1:2004 states that if cracking and yielding are modeled, the elastic member stiffness's for reinforced concrete and composite steel/concrete members should be based on gross section properties. On the other hand, if only yielding is modeled, then the elastic stiffness should be the effective stiffness values specified by the material Standards. The material Standard NZS 3101 defines that the effective stiffness values should be based on Table 4. The choices of the reduction factors vary for both the type of element, reinforcement strength, axial load level, and the limit states. It could be summarized that the set effective stiffness values are proposed if concentrated nonlinear springs at the member end are used. It is accepted that the distributed plasticity is inherently taking care of the drop in stiffness. The designer is permitted to perform more rigorous modeling.

Table 4. Effective section properties as a ratio of gross section properties in NZS 3101-2006

Member	**Ultimate Limit State**		**Serviceability Limit State**		
	f_y = 300 MPa	**f_y = 500 MPa**	**μ=1.25**	**μ=3**	**μ= 6**
Beams					
Rectangular ж	0.43I_g (0.5%≤ρ≤1.75%)	0.32 I_g (0.3%≤ρ≤1.4%)	I_g	0.7 I_g	0.5 I_g
T and L Beams ж	0.40 I_g (0.75%≤ρ≤1.75)	0.30 I_g (0.45%≤ρ≤1.75)	I_g	0.7 I_g	0.5 I_g
Columns					
$N^*/A_g f_c' >$ 0.5	0.8 I_g (1.0 I_g) ŧ	0.8 I_g (1.0 I_g) ŧ	I_g	1.0 I_g	As for the ultimate limit state values in brackets
$N^*/A_g f_c' = 0.2$	0.55 I_g (0.66 I_g) ŧ	0.50 I_g (0.66 I_g) ŧ	I_g	0.8 I_g	
$N^*/A_g f_c' = 0.0$	0.40 I_g (0.45 I_g) ŧ	0.30 I_g (0.35 I_g) ŧ	I_g	0.7 I_g	
NOTE					
ж for additional flexibility, within joint zones and conventionally reinforced coupling beams refer to the text.					
ŧ the values in brackets apply to columns that have a high level of protection against plastic hinge formation in the ultimate limit state.					

Note: For columns with axial compression falling between the limits provided, flexural stiffness shall be determined by linear interpolation.

2.3.5. Canadian Design of Concrete Structures (CSA A23.3-14)

According to CSA A23.3-14, the member stiffnesses used in analyses for lateral deflection or second-order frame analyses shall represent the degree of member cracking and inelastic action at the limit state for which the analysis is being carried out.

National Building Code of Canada 2015 (NBC, 2015) states that linear analysis could be performed using the reduced section properties defined in Section 21.2.5 of CSA A23.3-1 and shown in Table 5. On the other hand, it is left to peer review for nonlinear dynamic analysis.

Table 5. Effective properties of sections in CSA A23.3-14

Element Type	**Effective Property**
Beam	$I_e = 0.4\ I_g$
Column	$I_e = \alpha_c\ I_g$
Coupling Beam	$A_{ve} = 0.15A_g$; $I_e = 0.4I_g$
Coupling Beam	$A_{ve} = 0.45A_g$; $I_e = 0.25I_g$
Slab frame element	$I_e = 0.2\ I_g$
NOTE: $\alpha_c = 0.5+0.6\ \frac{Ps}{fc'Ag} \leq 1.0$	
A_g: Gross area of section (mm^2)	
P_s: Axial force at section resulting from factored dead load plus factored live load using earthquake load factors (N)	
f_c': Specified compressive strength of concrete (MPa)	

2.3.6. Sozen's Method

The effective stiffness idea originated from (Shibata and Sozen 1976) study. The idea was to define a substitute linear structure with a similar displacement with the nonlinear structure. (Sözen 2013) stated later that the loading cycle interested in determining the drift under seismic loading is the cycle with the largest displacement amplitude, and that is the drift levels in which effective stiffness is organized for seismic analysis purposes (Sözen 2013). It is mentioned that the cracked stiffness value is defined in reference to yield point, and it is "quite different from the effective stiffness at the time of attainment of the maximum drift." Hence, as a conclusion, even though cracked-section idea is plausible, it should be used as a tool to increase the calculated drift. It

should not be presented as being “realistic.” It is proposed that “it may be more effective to amplify the drift arbitrarily by a plausible factor rather than asking the designer to go on a chase to determine how much the columns would crack vs. how much the girders or the walls would crack.” (Sözen 2013)

(Sözen 2013) proposed to use half of the gross uncracked stiffness of the members as the effective stiffness for the frame members in an RC structure.

CHAPTER 3

CECEN'S EXPERIMENTS, NUMERICAL MODEL AND THE ANALYSES

3.1. Introduction

The goal of the study necessitates the evaluation of the success of the different equivalent stiffness approaches. Shake table experiments performed by Cecen (1979) are selected for this purpose. Scaled reinforced concrete moment-frames were tested in the experiments. Frames were three-bay, ten-story structures with a strong-column weak-beam design. It was ensured to develop beam mechanism as the failure mode. Hence, these are ideal moment frames as specified by the contemporary seismic design codes. The frames were subjected to a series of ground motions with increasing intensity. Therefore, it will be possible to check the success of the equivalent stiffness procedures at different demand levels. There are two equivalent frames. The first frame was subjected to three different ground motions, and the second frame was subjected to seven different ground motions. The maximum intensity of ground motions in both frames is similar.

The analyses of the frames are performed in OpenSees platform. It is an open-access platform with strong nonlinear modeling capabilities, widely used in the literature. The test frames and the developed numerical model of the frames are presented in the following sections. The results of the analysis will follow. In addition, the test frames are subjected to a suite of ground motions in numerical analysis. This set is representative of the soil type ZD in the Turkish Earthquake Code (2018.) The motions were scaled with the rules defined in TEC 2018. The results of these excitations are presented in the rest of the chapter.

3.2. The Reference Frame

One of the main difficulties of performing an investigation to compare the available procedures is the availability of the reference data upon which the comparison could be made. The difficulty arises due to the availability of the physical observations

that cover the full domain of the procedures. On the other side, performing a study that relies on simulated data always carries the risk of being carried away with the unavoidable assumptions to obtain the reference data. As a well-known general rule, comparing a calculation with another calculation does not have to give information about the real behavior. Nevertheless, the current study is organized to have an experimental study as its comparison base. Cecen's Study (Cecen 1979) is selected for this purpose.

3.2.1. Properties of the Test Frame

The frames test by Cecen (1979) were three-bay, ten-story double planar frames subjected to uniaxial earthquake ground motions through a shaking table. The setup contains two "identical" frames, Fig. 3.1 and 3.2, connected by steel plates. The plates form the platform to attach the necessary masses to the system to reach the intended period. The reason for having the double frame was to provide room for the mass attachment. The probability of having different responses from the "identical" double frames was closely observed during the test, and it had verified that the system had planar behavior. Each story had a 227-kg mass, and the effect was distributed equally to the columns of the frame.

Due to the physical limitation of the testing facility, test frames were scaled with a ratio of 1/12. The calculated elastic period of the resulting structure was 0.2 sec. The frame's story height and bay lengths were 229 and 305 mm (Fig. 3.2), respectively. The cross-sectional dimension of columns was 38x51 mm, and that of beams was 38x38 mm (Fig.3.3). The material strengths were 30 MPa for concrete and 480 MPa for reinforcing steel. The reinforcement details of the test frames are presented in Table 6.

The tests were intended to carry out at periods beyond the constant acceleration zone of the code spectra. Hence, the applied ground motion was also scaled to reach this result. El Centro (1940) ground motion was scaled to different amplitudes during the tests and compressed by a scale of 2.5 in time to achieve the intended period location in the design spectrum. After this scaling, the test frame period in the full-scale ground motion corresponds to 0.34 seconds for H1 and H2 runs.

Experiments contained two sets of test frames. Frame H1 was subjected to three scaled motions of the El Centro motion with an increasing intensity from Run1 to Run3. The peak accelerations are 0.36g, 0.68g, and 1.6g consecutively for Runs 1 to 3. Here g

refers to the acceleration of gravity. Frame reported to be reached to 29, 53, 101 mm roof drift displacements for the listed motions. A second test frame, H2, was subjected to a similar range of earthquake amplitudes but with smaller increments for the applied motions. There were seven excitations for this specimen. The peak accelerations were 0.19g, 0.34g, 0.51g, 0.48g, 0.72g, 1.01g, 2.25g. Run-3 (0.51g) and run-4 (0.48g) were organized to have identical peak accelerations to demonstrate the repetition of the ground for the same frame. Frame reached 9, 18, 24, 26, 39, 60, 100 mm roof drift displacements for the excitations of the frame H2. The range of roof drifts reached in the tests allows comparisons at different damage levels. Therefore, comparisons are provided at each level.

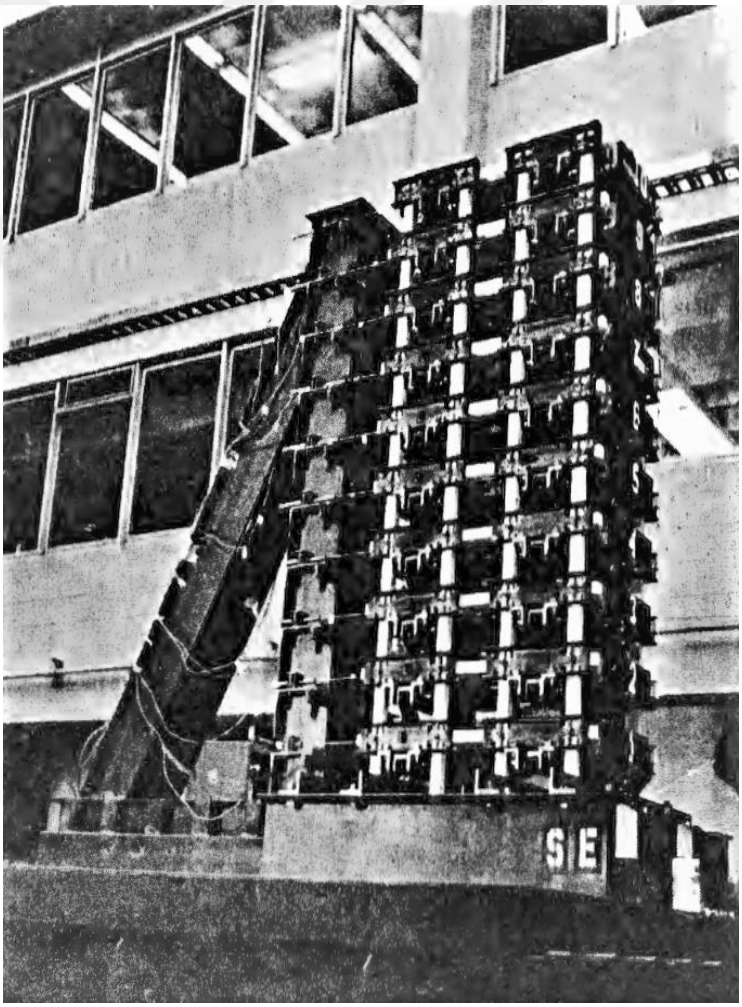

Figure 1. Cecen's test setup

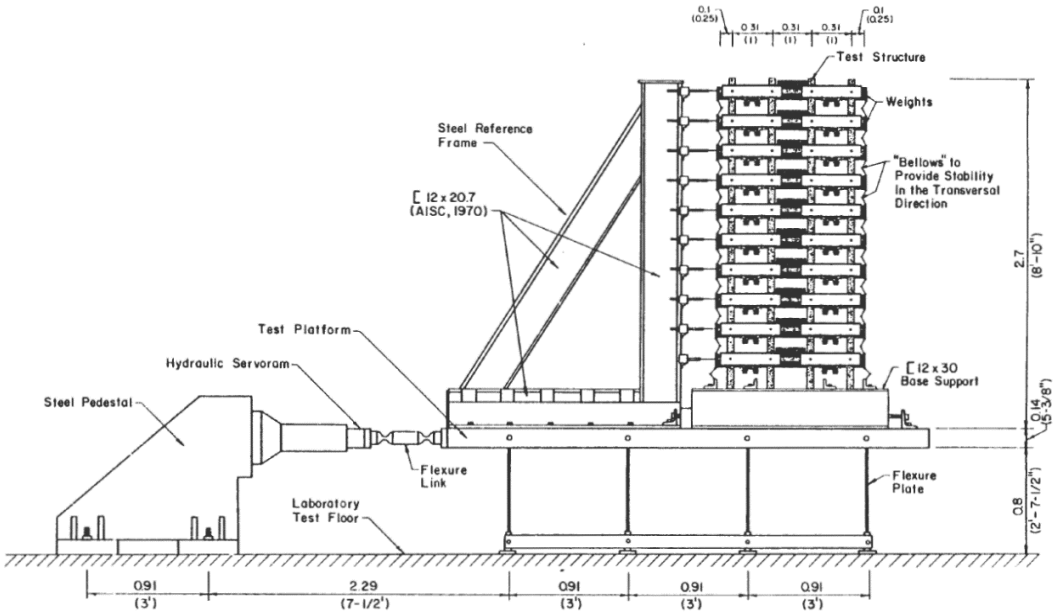

Figure 2. General view of the Cecen's test setup and the shaking table

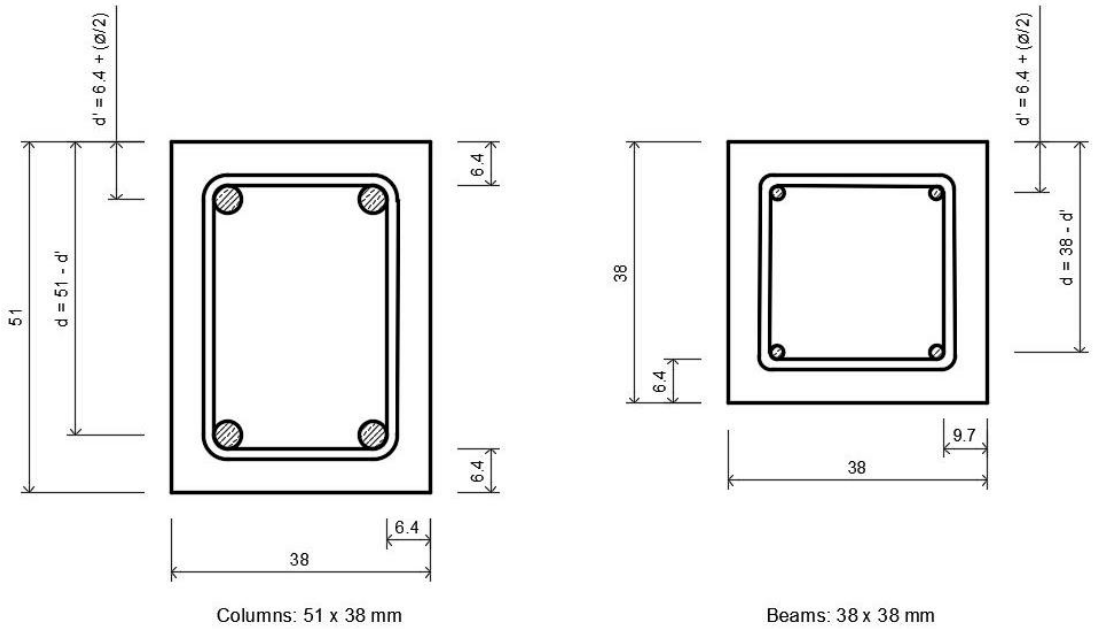

Figure 3. Columns and beams cross-sections, respectively.

(All dimensions in millimeters.)

Table 6. Reinforcements of Cecen's test setup

Member	Story #	Longitudinal Reinforcement	Transverse Reinforcement
External Columns	1-4	4 x 4.5 mm	dt=1.6 mm Pitch= 8.89 mm
	5-10	4 x 3.4 mm	
Internal Columns	1-4	4 x 4.1 mm	dt=1.6 mm Pitch= 8.89 mm
	5-10	4 x 2.3 mm	
Beams	1-4	4 x 2.3 mm	dt=1.6 mm Pitch= 7.62 mm
	5-10	6 x 1.6 mm	

3.2.2. The Numerical Model

It was necessary to prepare numerical models of the system to compare the success of the different effective stiffness approaches. It has to be mentioned that, as it is presented in Chapter 2, the specifications define the effective stiffness for different modeling options. Typically, it is defined for linear and nonlinear models. The definitions for nonlinear models are for modeling with concentrated plasticity. Hence two types of models are prepared to cover both definitions. The OpenSees platform is used for this purpose (Open System for Earthquake Engineering Simulation). As it is mentioned, it is an open-source software framework. It could simulate both structural and geotechnical systems through the use of finite element methods. OpenSees is released and maintained by the Pacific Earthquake Engineering Research Center at the University of California, Berkeley. It has many capabilities to model and analysis, especially the nonlinear response range of the systems. Furthermore, it has a rich material, element library, and solution algorithms. Based on the experience obtained in this study, it could be said that OpenSees is fast, stable, and efficient in solving considered nonlinear models with multiple runs. The input of the OpeenSees platform necessitates a code in Tcl language. Tcl is a dynamic programming tool with a string-based command language.

3.2.3. Basic Features of OpenSees Platform

OpenSees is an object-oriented framework for finite element analysis. A key feature of OpenSees is the interchangeability of components and the ability to integrate existing libraries and new components into the framework (not just new element classes) without changing the existing code. Core components, the abstract base classes, define the minimal interface (minimal to make the addition of new component classes easier but large enough to ensure all required can be accommodated). The OpenSees interface is built on a command-driven scripting language to build variable input files. OpenSees enables users to create linear and nonlinear, structural and geotechnical models. It supports many simulations such as static pushover analyses, static reversed-cyclic analyses, dynamic time-series analyses, uniform-support excitation, and multi-support excitation. The working principle of OpenSees could be followed in Figures 4 and 5.

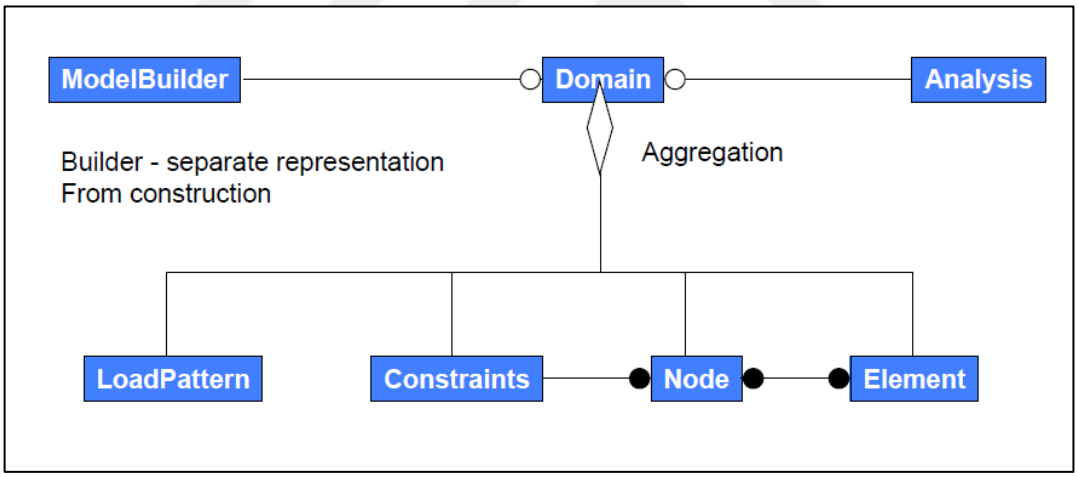

Figure 4. The working principle of OpenSees
(Source:Https://Opensees.Berkeley.Edu/Wiki/Index.Php/OpenSees_User)

ModelBuilder, separate from the computational and problem-solving classes, is used to build models. In addition, OpenSees includes a general model-builder for creating three-dimensional frame and continuum models using TCL. Users could generate structural or geotechnical models using TCL procedures and are encouraged to share these generation procedures with other users.

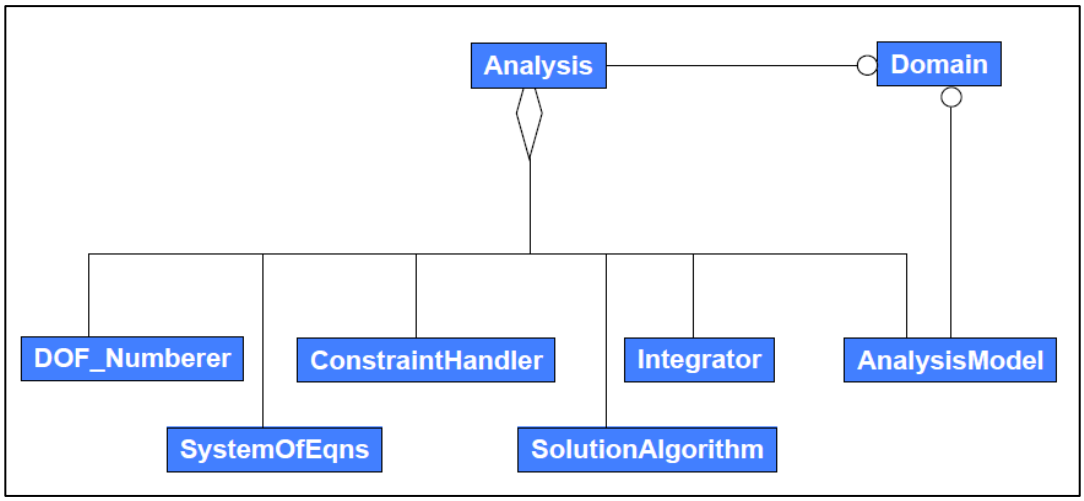

Figure 5. Analysis class for simulation
(Source:Https://Opensees.Berkeley.Edu/Wiki/Index.Php/OpenSees_User)

Linear equation solvers, time integration schemes, and solution algorithms are the basis of the OpenSees framework. The components of a solution strategy are interchangeable, enabling users to find and use sets suited to their particular problem. Also, addition to the available solution methods, new parts of the solution strategy may be seamlessly plugged in to the existing framework.

3.2.4. Numerical Model of the Test Frame

Two distinct models of the test frame are prepared. First, a wireframe linear model is formed using the elastic properties of the elements. The system is accepted to be fixed at the supports, Fig.6. Also, second second-order effects (P-Delta) are considered in the model. This model is used to observe the effect of the effective stiffness procedures on the system dynamic properties and the maximum linear displacement demands.

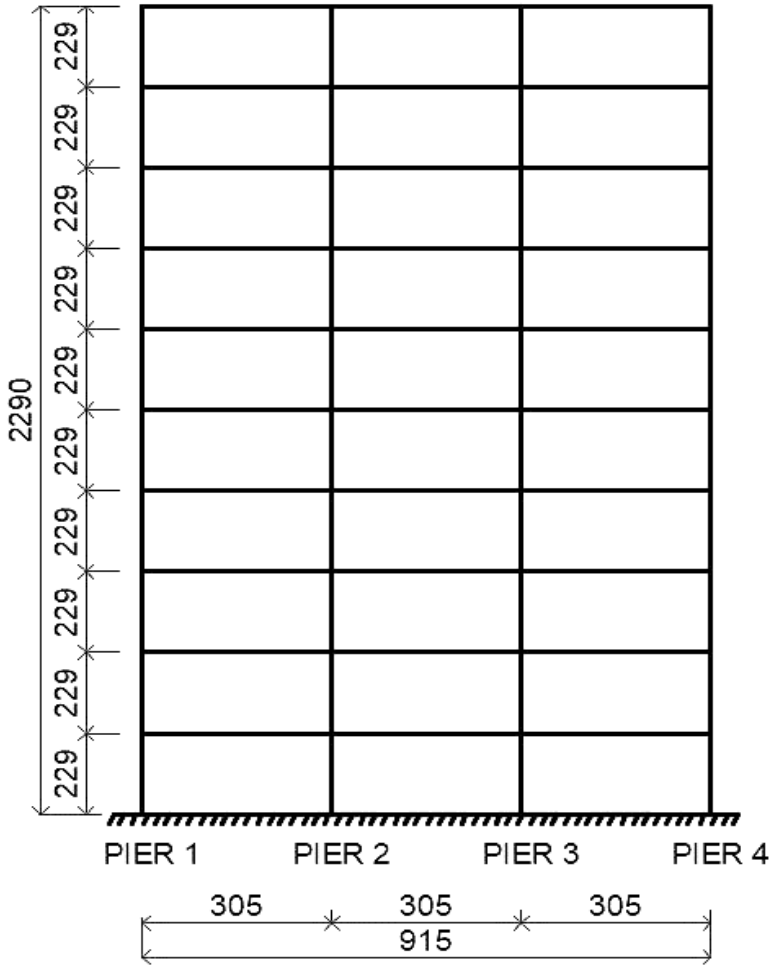

Figure 6. The linear frame
(All dimensions in millimeters.)

The elastic beam-column element model of OpenSees library was used for the elastic regions. The definition of this element model necessitates the modulus of elasticity and the moment of inertia of the sections. The material properties used in the model are presented in Table 7. These values are based on the data provided by Cecen (1979).

Table 7. Input properties of the elements of the frames

Input Properties of the Elastic Beam-Column Element Model			
Element	**Modulus of Elasticity (MPa)**	**Area of Cross Sections (mm^2)**	**Moment of Inertia ($mm^{4)}$**
Beams	20000	1444	173761
Columns	20000	1938	420062

The nonlinear model is a wireframe model as well. Elements are modeled as elastic elements, and the system's nonlinearity is represented by concentrated zero-length nonlinear hinges at the ends of each member, Fig.7. Second-order effects (P-Delta) are also taken into consideration in the model. Stiffness values of the elastic elements are defined per the effective stiffness procedures. The nonlinear springs are defined as moment-rotation springs based on the moment-curvature relation of the corresponding element and the defined plastic hinge length, which is universally accepted to be half of the member dimension in the bending direction.

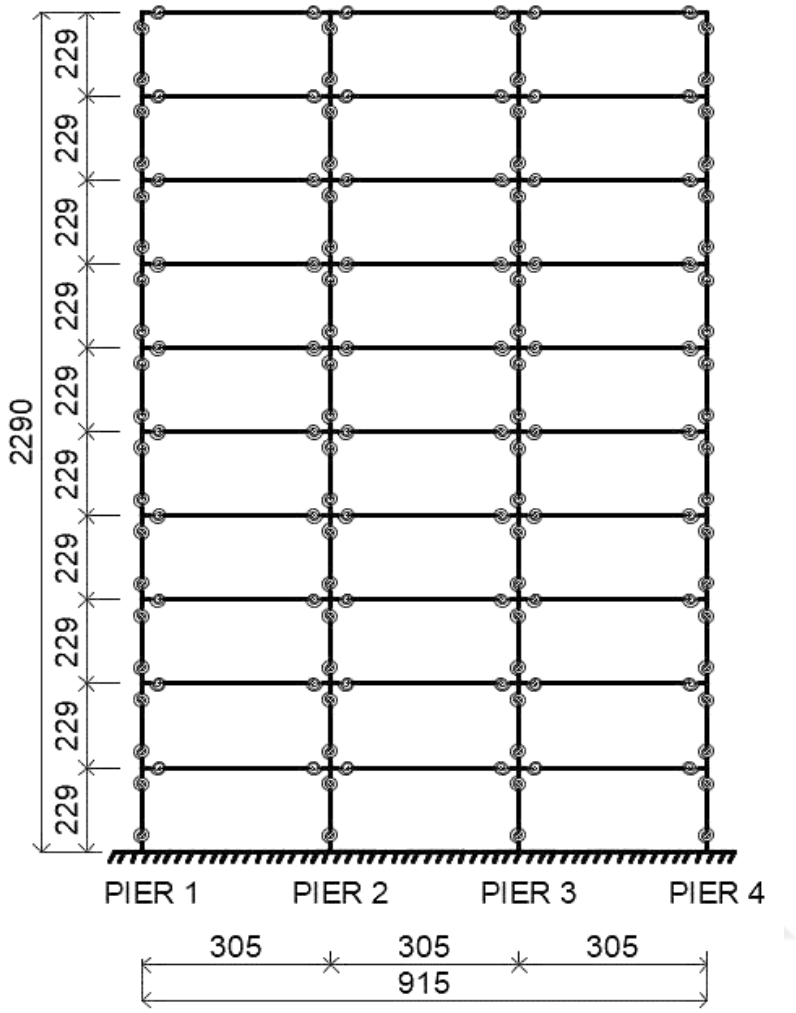

Figure 7. The nonlinear frame with rotational springs
(All dimensions in millimeters.)

The rotational springs at the element ends are modeled with the uniaxial material model with a bilinear hysteretic response. This model is called ‘Steel01’ in the OpenSees library.

It is required to define the yield moment and the initial and post-yield slopes to define the model. The original definitions of the axes are presented in Fig.8. The program permits adaptation of the model to represent moment-rotation response with the same pattern. Horizontal and vertical axes become rotation and moment in this usage. The post-yield slope (b) is selected to be equal to 0.02.

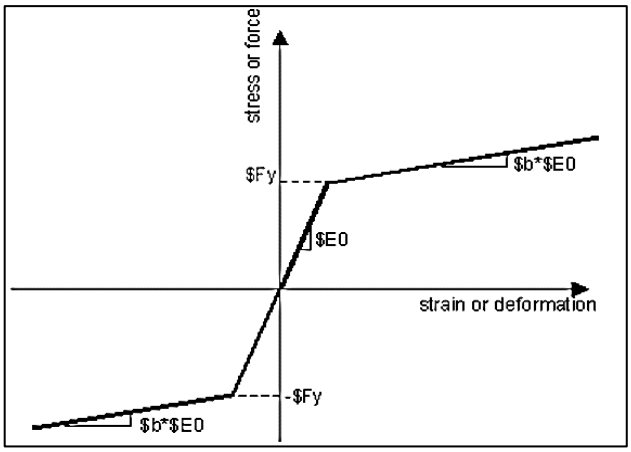

Figure 8. Steel01 material-hysteretic behavior

(Source: Https://Opensees.Berkeley.Edu/Wiki/Index.Php/OpenSees_User)

The moment-curvature relations of the springs are obtained for every two stories of the frame by analyzing the cross-sections on Response2000 software (Https://Www.Ecf.Utoronto.ca/~bentz/R2k.Htm) Bilinear moment rotations curves are obtained from the calculated moment-curvature curves as needed by the selected nonlinear spring in Opensees. The initial slope is defined in reference to yield point and the second slope is obtained as defined above. The lengths of rotational springs are accepted to be half of the cross-section heights as indicated in the seismic codes. Then, properties of the rotational springs are obtained per equations 3.1. and 3.2. Obtained values are presented in Table 8.

$$\theta_y = \phi_y * L_{spring} \quad (3.1)$$

$$k_\Theta = M_y / \theta_y \quad (3.2)$$

θ_y : yield rotation of section (rad)

L_{spring} : length of rotational spring (half of cross-section height) (m)

ϕ_y : yield curvature of section (rad/m)

M_y : yield moment of section (N.m)

k_Θ : tangent of moment- rotation curve (N.m/rad)

Table 8. Properties of the rotational springs of the frame

Properties of the Rotational Springs					
	Story	**Moment (N.m)**	**Curvature (m^{-1})**	**Rot (rad)**	**Tangent of Moment-Rotation Curve (N.m/rad)**
Beams	1-4	111	0.1	0.0019	58421
	5-10	82	0.099	0.00188	43617
External Columns	1-2	620	0.099	0.00252	246032
	3-4	605	0.099	0.00252	240079
	5-6	495	0.099	0.00252	196429
	7-8	370	0.08	0.00204	181373
	9-10	350	0.08	0.00204	171569
Internal Columns	1-2	543	0.099	0.00252	215476
	3-4	515	0.099	0.00252	204365
	5-6	380	0.09	0.0023	165217
	7-8	205	0.08	0.00204	100490
	9-10	185	0.082	0.00204	90686

Before running the dynamic analyses, the first mode shape of the nonlinear system is obtained to compare with that reported in the Cecen's report. This comparison is presented in Table 9 and Fig.9.

Table 9. Comparing the first mode shape of the numerical test setup with that of Cecen's test setup

Comparing First Mode Shapes of Numerical and Experimental Models		
Story #	**OpenSeeS**	**CECEN's Test Setup**
1	0.09	0.11
2	0.25	0.28
3	0.43	0.46
4	0.60	0.63
5	0.78	0.79
6	0.94	0.94
7	1.08	1.07
8	1.18	1.17
9	1.26	1.26
10	1.31	1.31
Note: Mode shapes were obtained by multiplying the eigenvectors with participation factors in Cecen's report		

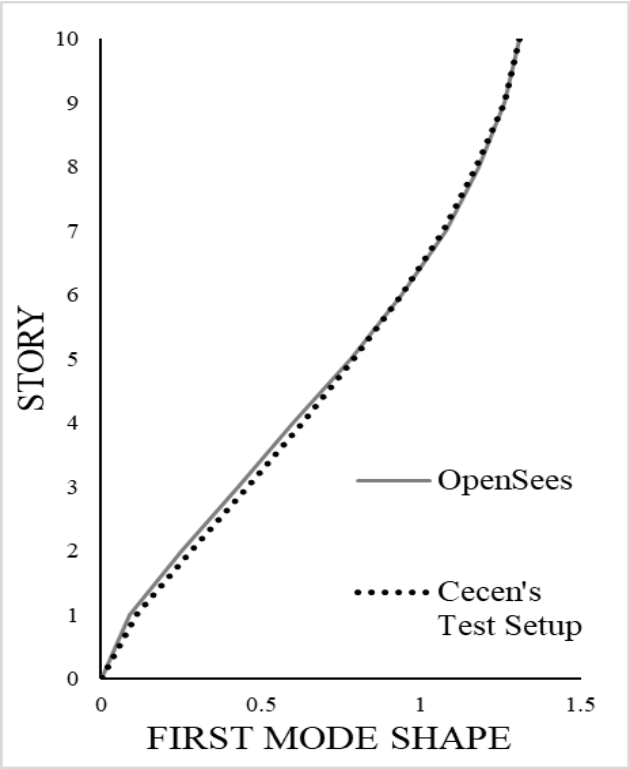

Figure 9. Comparing the first mode shapes

3.2.5. Input Effective Stiffness Definitions

As explained in Chapter 2, different approaches exist in the seismic codes for both linear and nonlinear analyses. The effective stiffness definitions of the test frames are defined following the listed regulations and Sozen's approach. Calculated effective stiffness factors for the test frame are presented in Tables 10 to 15.

Table 10. Stiffness reduction factors per the Sozen's Approach

Stiffness Reduction Factors				
Sozen's Approach	**Linear Analysis**		**Nonlinear Analysis**	
	Beams	**Columns**	**Beams**	**Columns**
	0.5	0.5	0.5	0.5

Table 11. Stiffness reduction factors per the TEC 2018

Stiffness Reduction Factors				
	Element	**Story**	**Linear Analysis**	**Nonlinear Analysis**
TEC 2018	**Beams**	1-4	0.35	0.17
		5-10	0.35	0.15
	External Columns	1-2	0.7	0.24
		3-4	0.7	0.239
		5-6	0.7	0.225
		7-8	0.7	0.17
		9-10	0.7	0.16
	Internal Columns	1-2	0.7	0.224
		3-4	0.7	0.213
		5-6	0.7	0.19
		7-8	0.7	0.1
		9-10	0.7	0.09

Table 12. Stiffness reduction factors per the Eurocode 8

Stiffness Reduction Factors				
	Element	**Story**	**Linear Analysis**	**Nonlinear Analysis**
Eurocode 8 (EN 1998)	**Beams**	1-4	0.5	0.17
		5-10	0.5	0.15
	External Columns	1-2	0.5	0.24
		3-4	0.5	0.24
		5-6	0.5	0.23
		7-8	0.5	0.17
		9-10	0.5	0.16
	Internal Columns	1-2	0.5	0.22
		3-4	0.5	0.21
		5-6	0.5	0.19
		7-8	0.5	0.10
		9-10	0.5	0.09

Table 13. Stiffness reduction factors per the CSA A23.3-14

Stiffness Reduction Factors			
	Element	**Story**	**Linear Analysis**
CSA A23.3-14	**Beams**	1-4	0.4
		5-10	0.4
	External Columns	1-2	0.56
		3-4	0.54
		5-6	0.53
		7-8	0.52
		9-10	0.51
	Internal Columns	1-2	0.56
		3-4	0.54
		5-6	0.53
		7-8	0.52
		9-10	0.51

Table 14. Stiffness reduction factors per the ACI318-19

	Stiffness Reduction Factors			
	Element	**Story**	**Linear Analysis**	**Nonlinear Analysis**
ACI318-19	**Beams**	1-4	0.35	0.3
		5-10	0.35	0.3
	External Columns	1-2	0.7	0.3
		3-4	0.7	0.3
		5-6	0.7	0.3
		7-8	0.7	0.3
		9-10	0.7	0.3
	Internal Columns	1-2	0.7	0.3
		3-4	0.7	0.3
		5-6	0.7	0.3
		7-8	0.7	0.3
		9-10	0.7	0.3

Table 15. Stiffness reduction factors per the NZS3101-2006

	Stiffness Reduction Factors		
	Element	**Story**	**Linear & Nonlinear Analysis**
NZS3101-2006	**Beams**	1-4	0.32
		5-10	0.32
	External Columns	1-2	0.50
		3-4	0.45
		5-6	0.44
		7-8	0.41
		9-10	0.38
	Internal Columns	1-2	0.50
		3-4	0.45
		5-6	0.44
		7-8	0.41
		9-10	0.38

3.3. Dynamic Time History Analyses

The linear and nonlinear RC frame models of the Cecen test frames are subjected to the ground excitations recorded during the experiment at the base block of the corresponding test frames. Related digital data is served to general use by ("Datacenterhub - DEEDS" n.d.). Cecen tested two identical frame twins. Therefore, the same numerical models are used for the simulations. The first twin-frame was named H1, and as explained, there were three base excitations. These are named H1-R1, H1-R2, and H1- R3. The second twin-frame was named H2 and subjected to seven base excitations, H2-R1, H2-R2, H2-R3, H2-R4, H2-R5, H2-R6, and H2-R7. Original base excitations were the 1940 El Centro Earthquake. In order to position the test frames after the constant acceleration region, the motion was compressed in time. Also, it was scaled in amplitude to develop the needed intensity levels. The ultimate intensity level of both ground motion sets was similar. It means that H1-R3 and H2-R7 had similar intensity levels. The intermediate runs were designed to obtain responses at the selected intensity levels. The intensity of H2-R3 and H2-R4 excitations were selected to observe the effect of two consecutive same magnitude motions on the same structure.

The model frame is also subjected to a selected set of ground motions to observe the responses of different effective stiffness schemes. Eleven ground motions to represent a high-seismic location in Turkey, which represents the DD2 level motion with soil type ZD, are selected. The original selection of the ground motion set was performed by (Sönmez 2020). Further details about the selection process could be followed in Sonmez's study. The selected ground motion set is used in the dynamic time-history analyses for the linear, and nonlinear models of the test frame developed. The properties input ground motions and the results of the analyses are explained in the following sections.

The numerical model of the test frame did not have the twin frames. In order to save run time and considering that it will not provide any further information single frame is modeled to represent the test frame. The mass and load levels were organized accordingly. Two different viscous damping ratios for linear and nonlinear models were taken. It was taken as 5% and 2% for the linear and nonlinear analyses, respectively.

3.3.1. Characteristics of Base Accelerations in Cecen's Test

In Cecen's experiments, three runs were exerted for the first test setup. Runs were named H1-R1 to R3. H1-R1 had the lowest spectrum intensity, and H1-R3 had the largest spectrum intensity. The second frame excitations were organized similarly. There were seven runs, H2-R1 to R7. H2-R1 had the lowest, and H2-R7 had the largest spectrum intensity. Properties of input accelerations are presented in Tables 16 to 17. Also, input accelerations of the experiment are presented in Figures 10 to 19. No modifications are applied to reported excitations in the simulations.

Table 16. Properties of the input ground motions of the experimental work H1

Run	**Peak Ground Acceleration (g)**	**Spectrum Intensity (ζ=0.02, mm)**
H1-R1	0.36	160
H1-R2	0.68	350
H1-R3	1.56	500

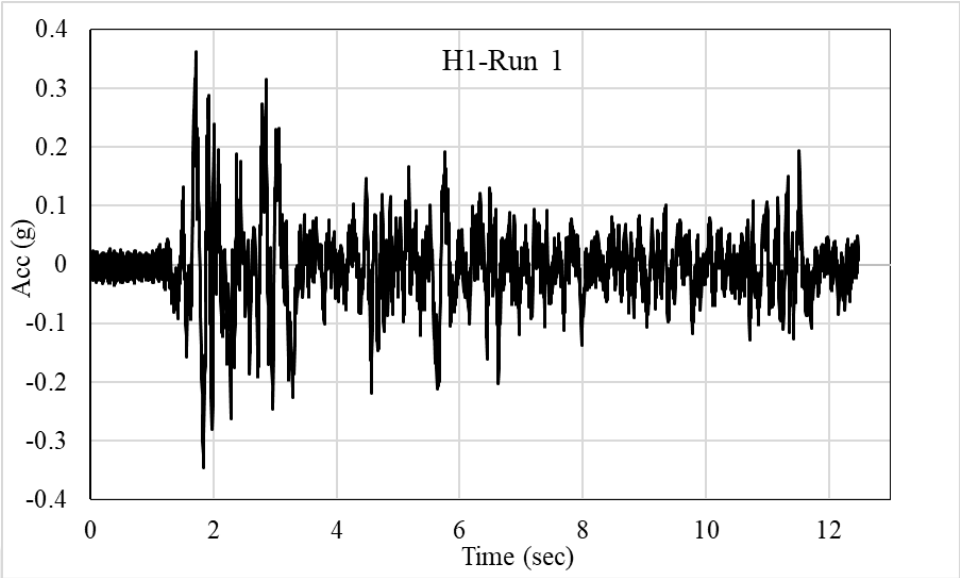

Figure 10. Input acceleration of H1-R1 in Cecen's report

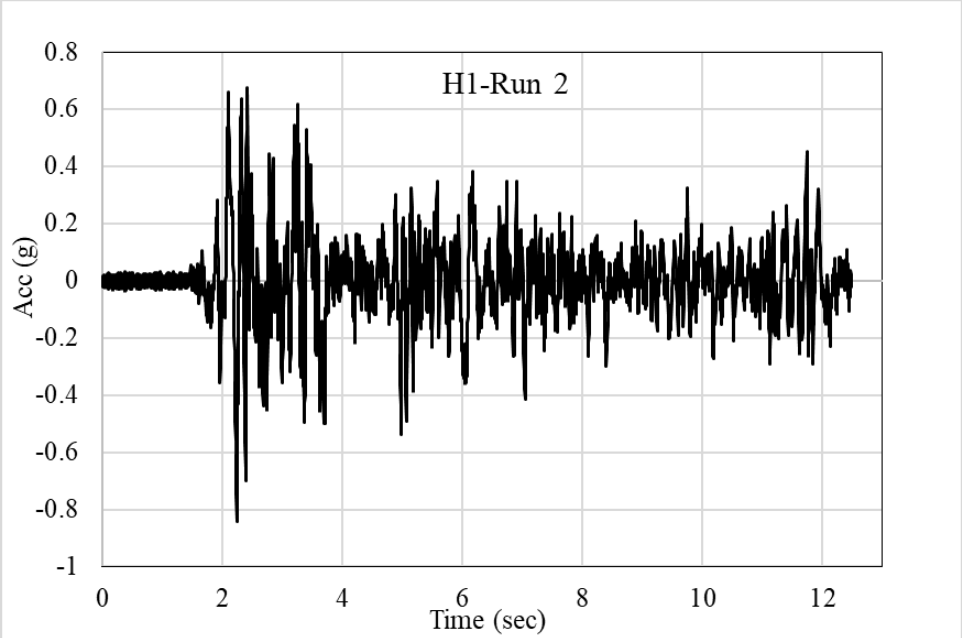

Figure 11. Input acceleration of H1-R2 in Cecen's report

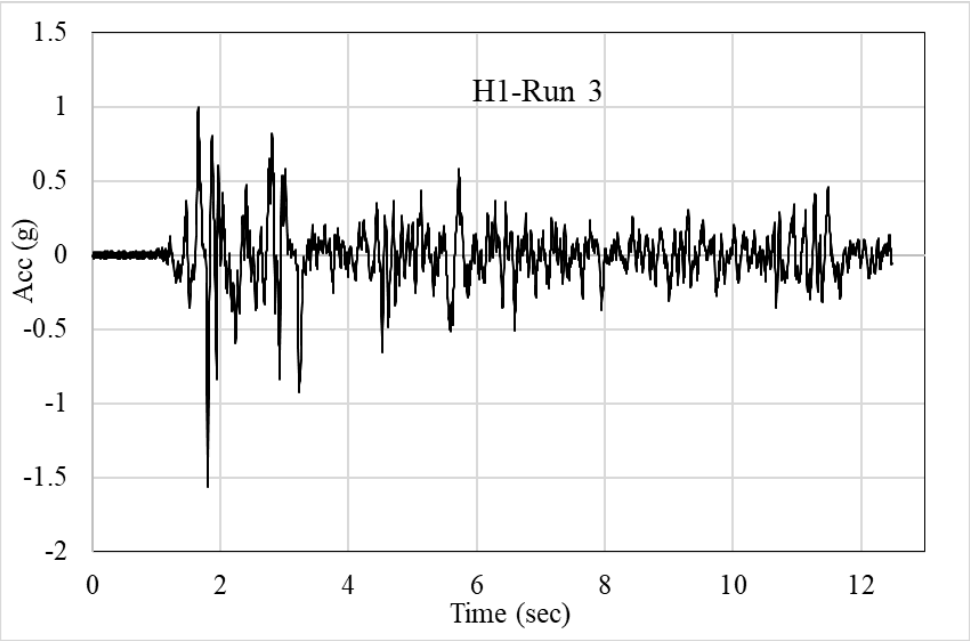

Figure 12. Input accelerations of H1-R3 in Cecen's report

Table 17. Properties of the input ground motions of the experimental work H2

Run	**Peak Ground Acceleration (g)**	**Spectrum Intensity (ζ=0.02, mm)**
H2-R1	0.19	64
H2-R2	0.34	130
H2-R3	0.51	200
H2-R4	0.48	200
H2-R5	0.72	300
H2-R6	1.01	400
H2-R7	2.25	500

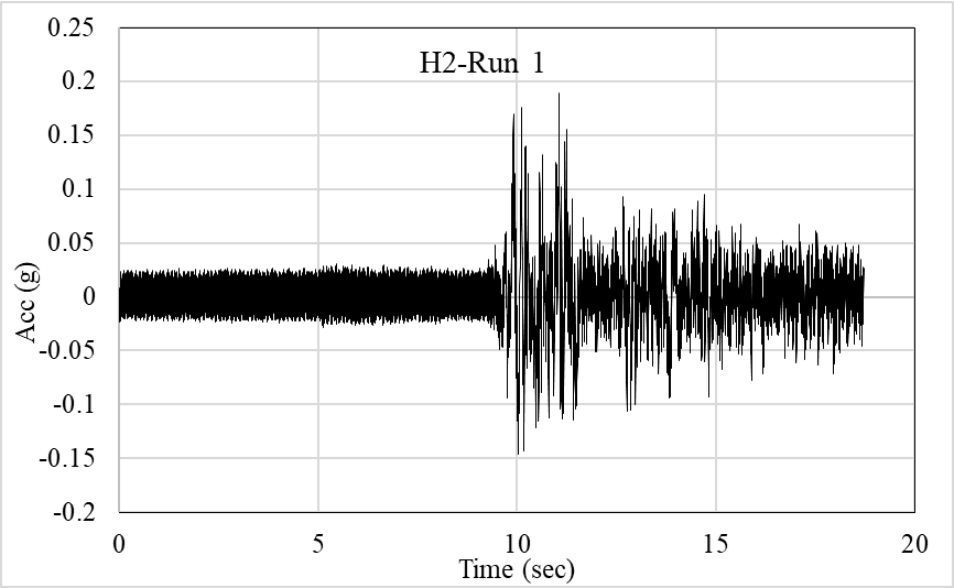

Figure 13. Input acceleration of H2-R1 in Cecen's report

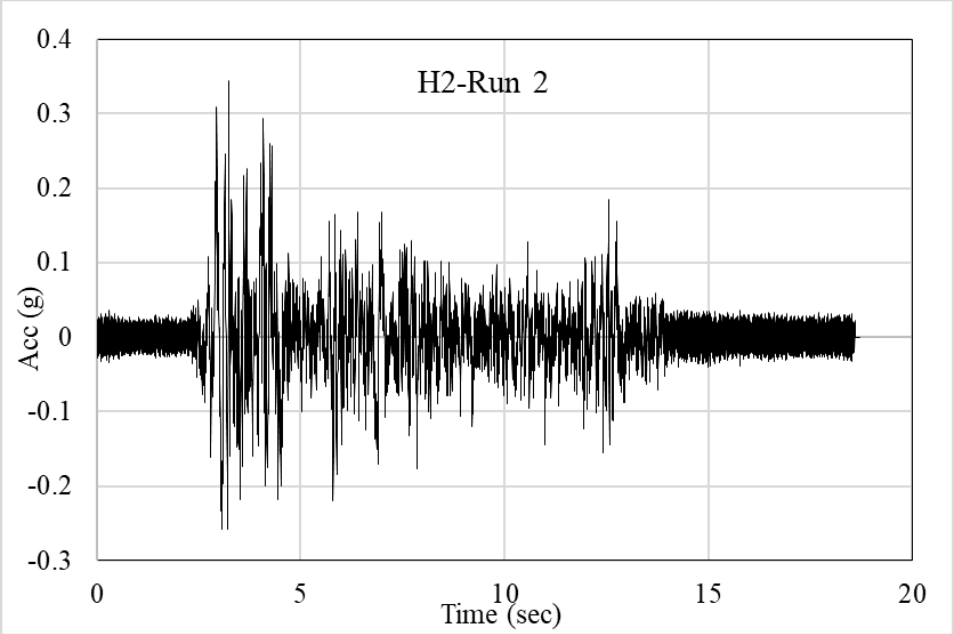

Figure 14. Input acceleration of H2-R2 in Cecen's report

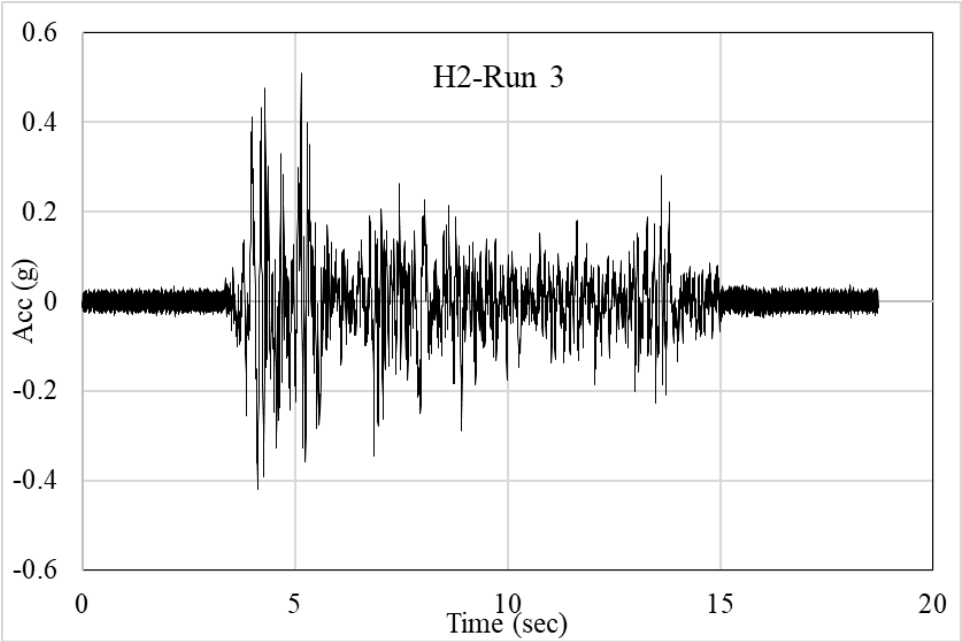

Figure 15. Input acceleration of H2-R3 in Cecen's report

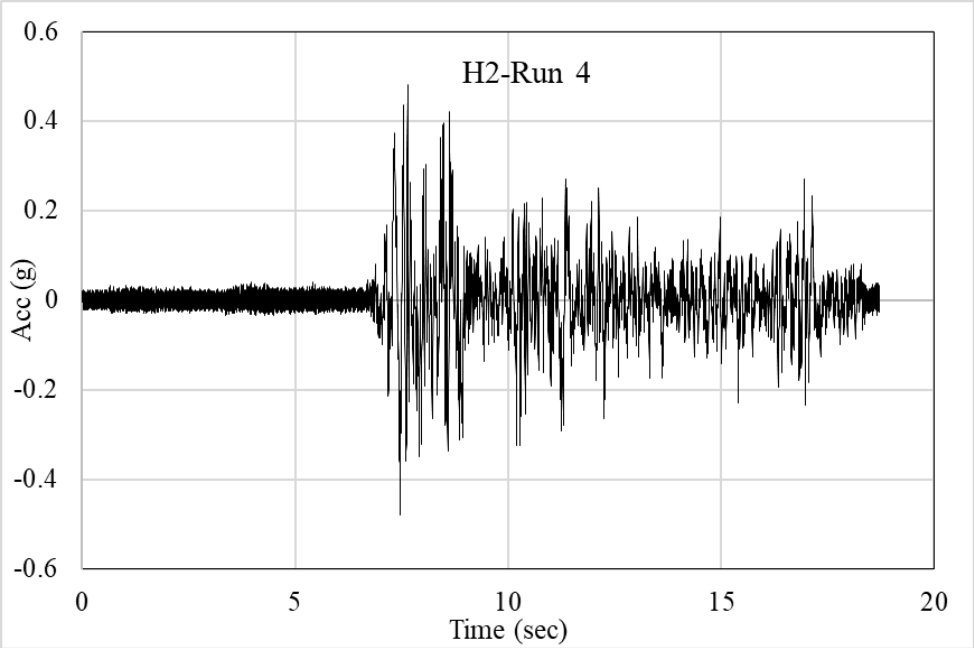

Figure 16. Input acceleration of H2-R4 in Cecen's report

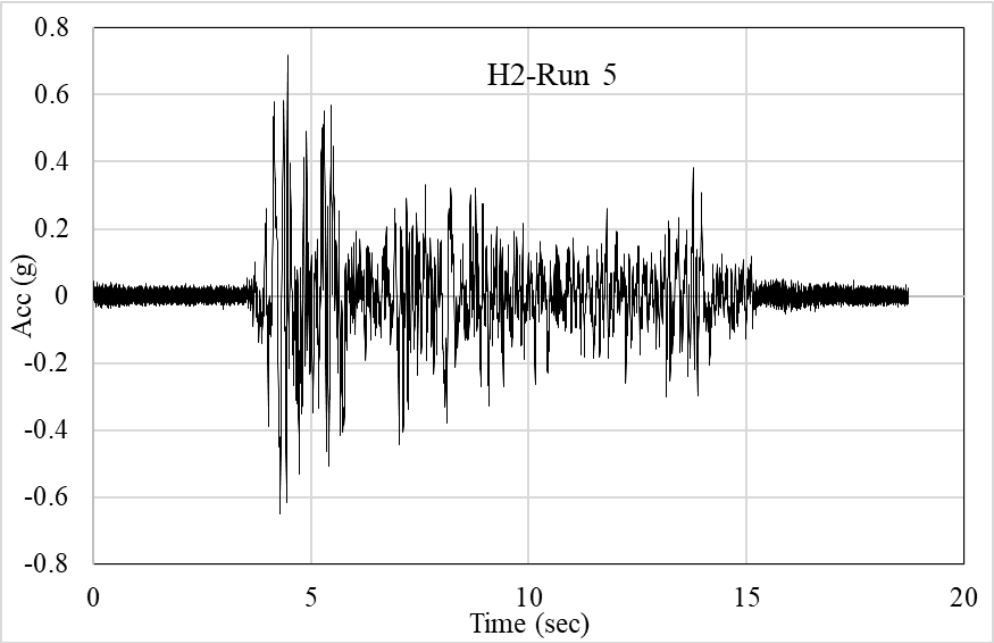

Figure 17. Input acceleration of H2-R5 in Cecen's report

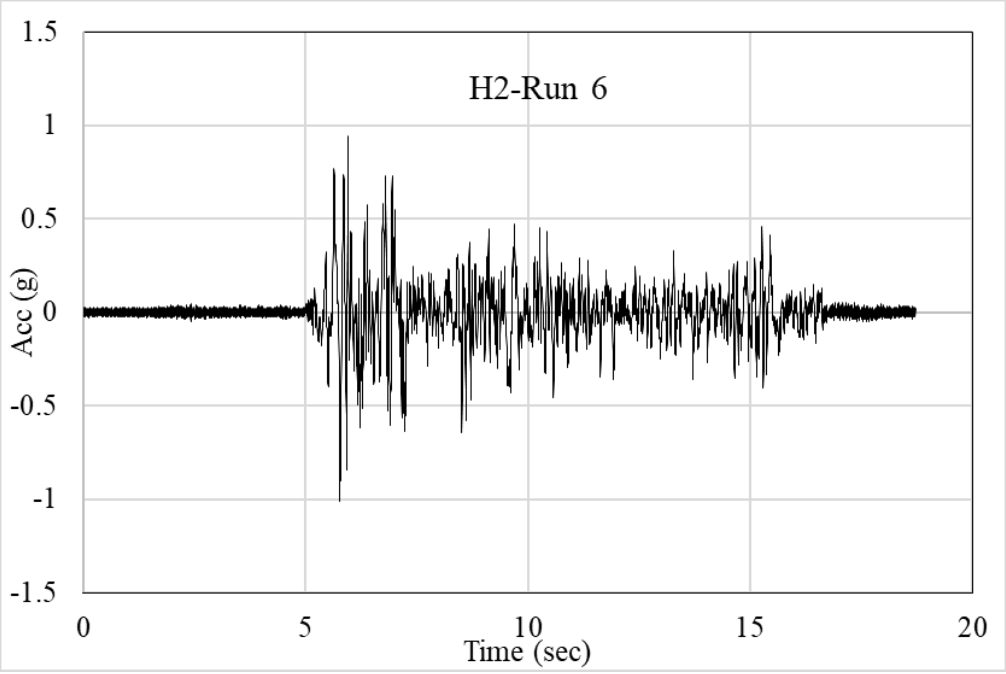

Figure 18. Input acceleration of H2-R6 in Cecen's report

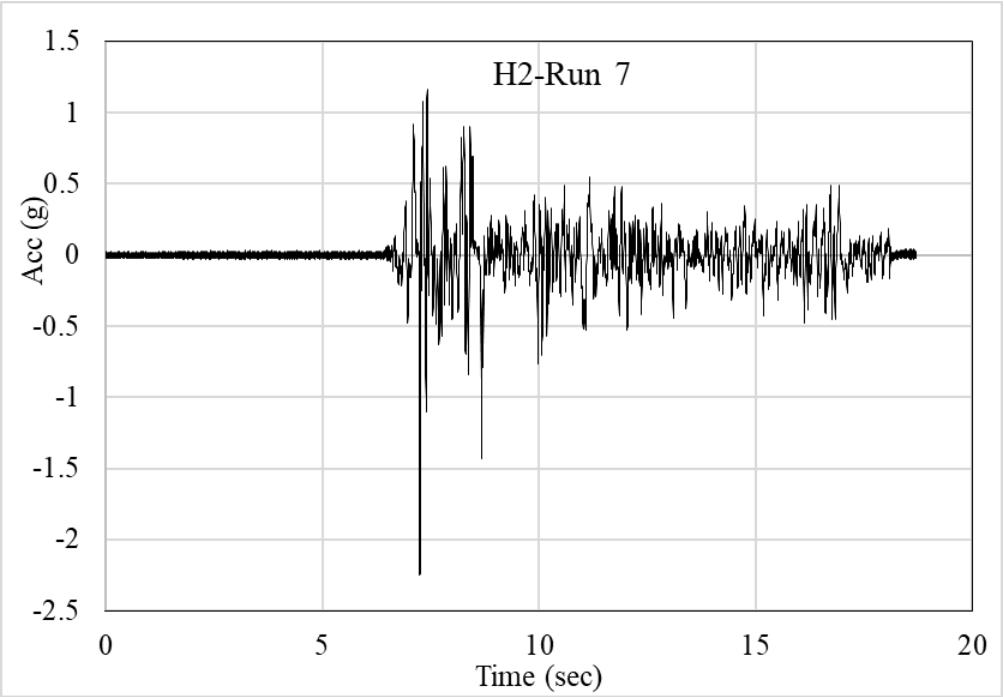

Figure 19. Input acceleration of H2-R7 in Cecen's report

3.3.2. Dynamic Time-History Analysis for Frame H1

As it was mentioned, two sets of simulations are performed. These are linear and nonlinear simulations. In each set, an extra simulation with the gross stiffness is also performed. Runs include frames with the effective stiffness definitions of the Sozen's approach and the Seismic Code approaches listed in Chapter 2.

The results of the analyses are evaluated in terms of maximum roof displacement and the interstory-drift ratio at the instant of maximum roof displacement. Considering that H1-R2 has reached about 2% drift ratios, plastic rotations and envelope drift ratios evaluations are performed for H1-R2 as well. The 2% drift ratio is about the target limit conditions in the TEC 2018.

Deviations from the measured values in Cecen's report were calculated arithmetically by evaluating the maximum roof displacement results of H1 runs.

3.3.2.1. H1-Run 1

Maximum roof displacements (mm), maximum roof drift ratios, periods, and the deviations from the measured values in Cecen's report are presented in Tables 18 and 19. In addition, the interstory drift ratio diagram at the maximum roof displacement instant is also illustrated in Figure 20.

Table 18. Maximum roof displacements for H1-R1

CECEN H1-RUN1				
Linear System				
	Maximum Roof Displacement (mm)	**Maximum Roof Drift Ratio**	**Period (Sec)**	**Deviation from Measured (%)**
Gross Stiffness	16	0.007	0.24	45
ACI 318-19 & TEC2018	28	0.012	0.37	4
Eurocode 8 & SOZEN'S	26	0.011	0.34	11
NZS 3101-2006	29	0.013	0.41	1
CSA A23.3-14	25	0.011	0.36	14
Nonlinear System				
	Maximum Roof Displacement (mm)	**Maximum Roof Drift Ratio**	**Period (Sec)**	**Deviation from Measured (%)**
Gross Stiffness	19	0.008	0.30	35
ACI 318-19	26	0.011	0.48	11
Eurocode 8 & TEC2018	28	0.012	0.62	4
NZS 3101-2006	20	0.009	0.45	32
SOZEN'S	18	0.008	0.39	38
CECEN H1-RUN1	**29**	0.013	**0.34**	**0**

Table 19. Interstory drift ratio at max. roof displacements of nonlinear H1-R1

H1-R1 Interstory Drift Ratio at Max. Roof Displacement, Nonlinear					
STORY #	**ACI318-19**	**EUROCODE8 & TEC2018**	**NZS3101**	**SOZEN'S**	**CECEN H1-R1**
10	0.002	0.002	0.003	0.002	0.006
9	0.004	0.004	0.006	0.004	0.007
8	0.008	0.008	0.010	0.006	0.012
7	0.014	0.015	0.013	0.009	0.013
6	0.019	0.018	0.014	0.011	0.017
5	0.020	0.018	0.012	0.012	0.016
4	0.018	0.017	0.010	0.012	0.020
3	0.015	0.018	0.008	0.010	0.016
2	0.010	0.015	0.006	0.008	0.013
1	0.004	0.007	0.003	0.004	0.008
Base	0.000	0.000	0.000	0.000	0.000

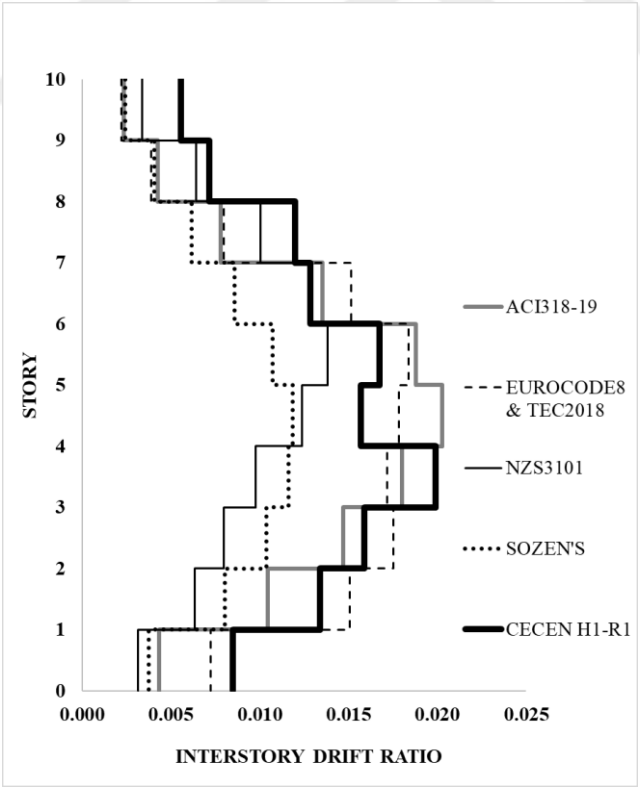

Figure 20. H1-R1 interstory drift ratio diagram at max. roof disp., nonlinear

3.3.2.2. H1-Run 2

Maximum roof displacements (mm), maximum roof drift ratios, periods, and the deviations from the measured values in Cecen's report are presented in Tables 20 and 21. In addition, interstory drift ratio diagram at maximum roof displacement instant and the envelope drift ratio are also illustrated in Fig.21 and 22.

H1-R2 was also inspected for plasticity demand for each effective stiffness procedure. The results of these evaluations are presented in Section 3.2.2.1.

Table 20. Maximum roof displacements for H1-R2

CECEN H1-RUN2				
Linear System				
	Maximum Roof Displacement (mm)	**Maximum Roof Drift Ratio**	**Period (Sec)**	**Deviation from Measured (%)**
Gross Stiffness	32	0.014	0.24	40
ACI 318-19 & TEC2018	56	0.024	0.37	6
Eurocode 8 & SOZEN'S	53	0.023	0.34	0
NZS 3101-2006	59	0.026	0.41	11
CSA A23.3-14	51	0.022	0.36	4
Nonlinear System				
	Maximum Roof Displacement (mm)	**Maximum Roof Drift Ratio**	**Period (Sec)**	**Deviation from Measured (%)**
Gross Stiffness	33	0.014	0.30	38
ACI 318-19	45	0.020	0.48	15
Eurocode 8 & TEC2018	56	0.024	0.62	6
NZS 3101-2006	49	0.021	0.45	8
SOZEN'S	41	0.018	0.39	23
CECEN H1-RUN2	**53**	0.023	**0.34**	**0**

Table 21. Interstory drift ratio at max. roof displacements for H1-R2, nonlinear

H1-R2 Interstory Drift Ratio at Max. Roof Displacement, Nonlinear					
STORY #	**ACI318-19**	**EUROCODE8 & TEC2018**	**NZS3101**	**SOZEN'S**	**CECEN H1-R2**
10	0.006	0.011	0.008	0.005	0.016
9	0.013	0.022	0.017	0.010	0.015
8	0.021	0.033	0.026	0.018	0.024
7	0.026	0.040	0.032	0.024	0.029
6	0.028	0.038	0.033	0.028	0.030
5	0.028	0.033	0.031	0.027	0.027
4	0.026	0.027	0.026	0.025	0.034
3	0.023	0.023	0.020	0.021	0.024
2	0.016	0.014	0.014	0.015	0.020
1	0.007	0.004	0.005	0.006	0.011
Base	0.000	0.000	0.000	0.000	0.000

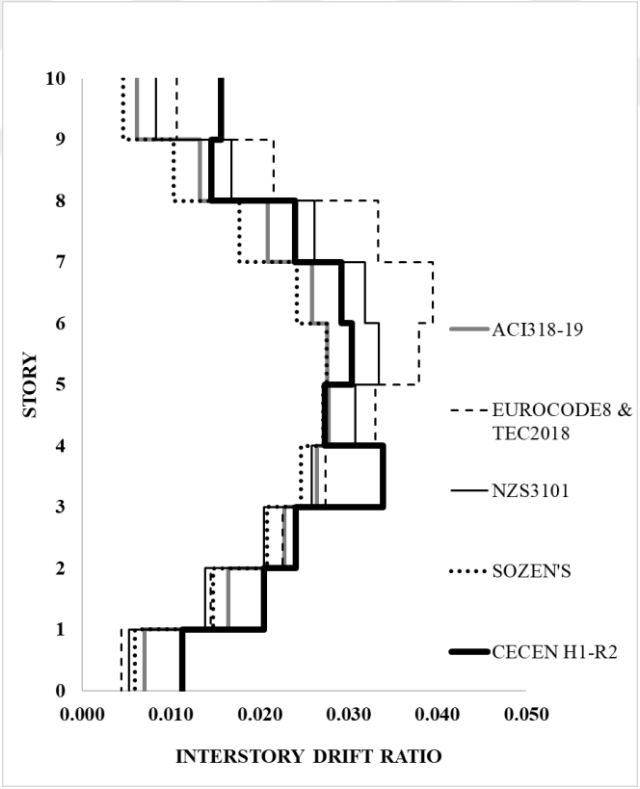

Figure 21. H1-R2 interstory drift ratio diagram at max. roof disp., nonlinear

Table 22. Envelope drift ratio for H1-R2, nonlinear

H1-R2 Envelope Drift Ratio, Nonlinear					
STORY #	**ACI318-19**	**EUROCODE8 & TEC2018**	**NZS3101**	**SOZEN'S**	**CECEN H1-R2**
10	0.009	0.019	0.009	0.006	0.015
9	0.014	0.028	0.017	0.011	0.015
8	0.021	0.036	0.026	0.018	0.024
7	0.027	0.049	0.032	0.025	0.029
6	0.031	0.047	0.034	0.028	0.029
5	0.033	0.038	0.031	0.027	0.025
4	0.028	0.033	0.026	0.025	0.033
3	0.024	0.033	0.022	0.021	0.024
2	0.019	0.029	0.017	0.016	0.023
1	0.011	0.015	0.008	0.007	0.013
Base	0.000	0.000	0.000	0.000	0.000

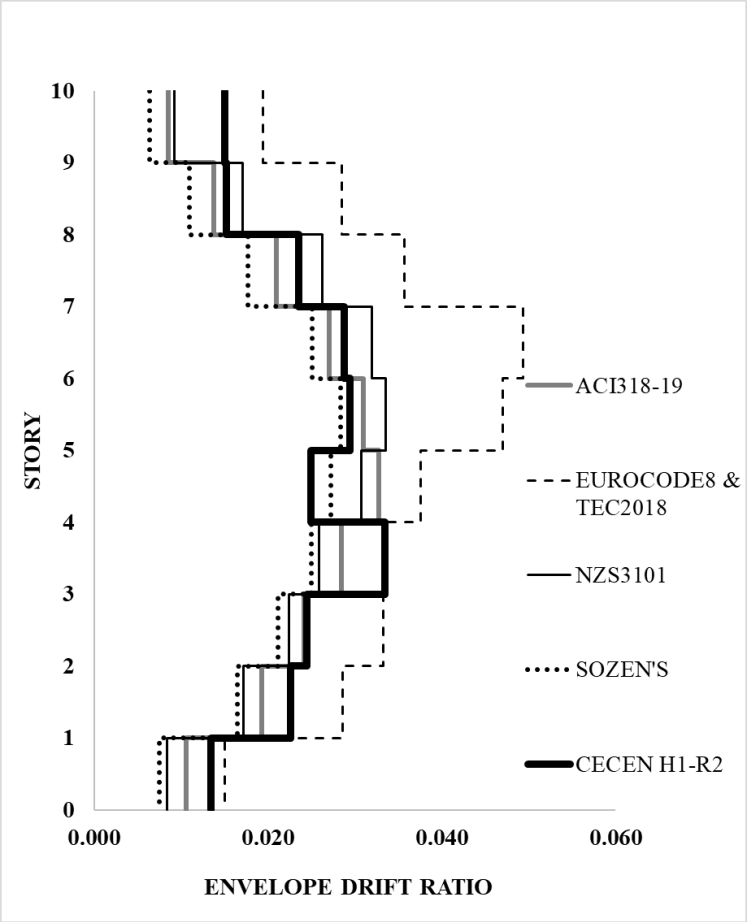

Figure 22. H1-R2 envelope drift ratio diagram, nonlinear

3.3.2.2.1. Plasticity Demands of H1-Run 2

The analysis results of H1-Run 2 were evaluated in terms of its plasticity demands for each effective stiffness procedure. Plasticity demand (PD) is defined as the ratio of plastic rotation ($\Theta_{plastic}$) to yield rotation (Θ_{yield}) at the rotational springs (Equation 3.3.). The plasticity demand of a system could give information about its ductility and the distribution of plasticity. The plastic rotation values and the plasticity demands of the system for each procedure are presented in detail in the following pages.

$$PD = \frac{\Theta_{plastic}}{\Theta_{yield}} \tag{3.3}$$

Table 23. Plastic rotations at max. roof disp. instant of H1-R2 in ACI 318-19

ACI 318-19	**BEAM PLASTIC ROTATIONS (Radian) at Max. Roof Disp.**					
STORY	**COLUMN 1**	**COLUMN 2**		**COLUMN 3**		**COLUMN 4**
10	0.000	-0.001	0.001	-0.001	0.001	0.000
9	0.005	-0.004	0.004	-0.004	0.004	-0.005
8	0.012	-0.011	0.011	-0.011	0.011	-0.012
7	0.018	-0.017	0.017	-0.017	0.017	-0.018
6	0.021	-0.020	0.020	-0.020	0.020	-0.021
5	0.022	-0.021	0.021	-0.021	0.021	-0.022
4	0.020	-0.018	0.018	-0.018	0.018	-0.020
3	0.018	-0.017	0.017	-0.017	0.017	-0.018
2	0.013	-0.012	0.012	-0.012	0.012	-0.013
1	0.009	-0.008	0.008	-0.008	0.008	-0.009
Base Columns Springs	-0.00037	-0.00045		-0.00045		-0.00037

Table 24. Plasticity demand at max. roof disp. instant of H1-R2 in ACI 318-19

ACI 318-19	PLASTICITY DEMAND OF BEAM ROTATIONAL SPRINGS (Θplastic/Θyield)						
STORY	**COLUMN 1**	**COLUMN 2**		**COLUMN 3**		**COLUMN 4**	**Story Average**
10	0.0	0.3	0.3	0.3	0.3	0.0	**0.2**
9	2.6	2.2	2.2	2.2	2.2	2.6	**2**
8	6.3	5.8	5.8	5.8	5.8	6.3	**6**
7	10.2	9.1	9.1	9.1	9.1	9.6	**9**
6	11.8	10.7	10.7	10.7	10.7	11.2	**11**
5	11.8	11.2	11.2	11.2	11.2	11.6	**11**
4	10.3	9.7	9.7	9.7	9.7	10.3	**10**
3	9.5	9.0	9.0	9.0	9.0	9.5	**9**
2	7.0	6.5	6.5	6.5	6.5	7.0	**7**
1	4.8	4.2	4.2	4.2	4.2	4.8	**4**
Base Columns Springs	0.1	0.2		0.2		0.1	**0.2**

Table 25. Plastic rotations at max. roof disp. instant of H1-R2 in Eurocode & TEC

EUROCODE 8 & TEC 2018	BEAM PLASTIC ROTATIONS (Radian) at Max. Roof Disp.					
STORY	**COLUMN 1**	**COLUMN 2**		**COLUMN 3**		**COLUMN 4**
10	-0.004	0.000	0.000	0.000	0.000	0.004
9	-0.006	0.004	-0.003	0.003	-0.004	0.006
8	-0.017	0.014	-0.014	0.014	-0.014	0.017
7	-0.026	0.023	-0.022	0.022	-0.023	0.026
6	-0.028	0.026	-0.026	0.026	-0.026	0.028
5	-0.026	0.025	-0.025	0.025	-0.025	0.026
4	-0.018	0.017	-0.017	0.017	-0.017	0.018
3	-0.020	0.018	-0.018	0.018	-0.018	0.020
2	-0.018	0.017	-0.017	0.017	-0.017	0.018
1	-0.011	0.010	-0.010	0.010	-0.010	0.011
Base Columns Springs	0.00013	0.00013		0.00013		0.00013

Table 26. Plasticity demand at max. roof disp. instant of H1-R2 in Eurocode & TEC

EUROCODE & TEC 2018	**PLASTICITY DEMAND OF BEAM ROTATIONAL SPRINGS (Θplastic/Θyield)**						
STORY	**COLUMN 1**	**COLUMN 2**		**COLUMN 3**		**COLUMN 4**	**Story Average**
10	1.9	0.2	0.2	0.2	0.2	1.9	**0.8**
9	3.3	1.9	1.8	1.8	1.9	3.3	**2**
8	8.9	7.5	7.4	7.4	7.5	8.9	**8**
7	13.5	11.9	11.8	11.8	11.9	13.5	**12**
6	14.6	13.5	13.5	13.5	13.5	14.6	**14**
5	13.6	13.0	13.0	13.0	13.0	13.6	**13**
4	9.7	8.9	8.8	8.8	8.9	9.7	**9**
3	10.3	9.6	9.6	9.6	9.6	10.3	**10**
2	9.5	8.8	8.8	8.8	8.8	9.5	**9**
1	5.9	5.1	5.1	5.1	5.1	5.9	**5**
Base Columns Springs	0.05	0.05		0.05		0.05	**0.05**

Table 27. Plastic rotations at max. roof disp. instant of H1-R2 in NZS3101-2006

NZS 3101	**BEAM PLASTIC ROTATIONS (Radian) at Max. Roof Disp.**					
STORY	**COLUMN 1**	**COLUMN 2**		**COLUMN 3**		**COLUMN 4**
10	0.002	-0.001	0.001	-0.001	0.001	-0.002
9	0.008	-0.007	0.007	-0.007	0.007	-0.008
8	0.017	-0.015	0.015	-0.015	0.015	-0.017
7	0.024	-0.024	0.024	-0.024	0.024	-0.024
6	0.028	-0.027	0.027	-0.027	0.027	-0.028
5	0.027	-0.027	0.027	-0.027	0.027	-0.027
4	0.021	-0.020	0.020	-0.020	0.020	-0.021
3	0.017	-0.017	0.017	-0.017	0.017	-0.017
2	0.013	-0.013	0.013	-0.013	0.013	-0.013
1	0.007	-0.006	0.006	-0.006	0.006	-0.007
Base Columns Springs	-0.0004	-0.0005		-0.0005		-0.0004

Table 28. Plasticity demand at max. roof disp. instant of H1-R2 in NZS3101

NZS 3101	PLASTICITY DEMAND OF BEAM ROTATIONAL SPRINGS (Θplastic/Θyield)						
STORY	**COLUMN 1**	**COLUMN 2**		**COLUMN 3**		**COLUMN 4**	**Story Average**
10	1.1	0.4	0.4	0.4	0.4	1.1	**0.6**
9	4.2	3.8	3.8	3.8	3.8	4.2	**4**
8	8.8	8.1	8.1	8.1	8.1	8.8	**8**
7	12.8	12.5	12.5	12.5	12.5	12.8	**13**
6	14.6	14.2	14.2	14.2	14.2	14.6	**14**
5	14.3	14.0	14.0	14.0	14.0	14.3	**14**
4	11.2	10.8	10.8	10.8	10.8	11.2	**11**
3	9.1	8.8	8.7	8.7	8.8	9.1	**9**
2	7.0	6.6	6.6	6.6	6.6	7.0	**7**
1	3.4	3.1	3.1	3.1	3.1	3.4	**3**
Base Columns Springs	0.17	0.17		0.17		0.17	**0.17**

Table 29. Plastic Rotations at Max. Roof Disp. Moment of H1-R2 in Sozen's

SOZEN'S APPROACH	BEAM PLASTIC ROTATIONS (Radian) at Max. Roof Disp.					
STORY	**COLUMN 1**	**COLUMN 2**		**COLUMN 3**		**COLUMN 4**
10	0.000	-0.001	0.001	-0.001	0.001	0.000
9	0.004	-0.004	0.004	-0.004	0.004	-0.004
8	0.011	-0.010	0.010	-0.010	0.010	-0.011
7	0.018	-0.017	0.017	-0.017	0.017	-0.018
6	0.024	-0.023	0.023	-0.023	0.023	-0.024
5	0.025	-0.024	0.024	-0.024	0.024	-0.025
4	0.021	-0.020	0.020	-0.020	0.020	-0.021
3	0.018	-0.018	0.018	-0.018	0.018	-0.018
2	0.014	-0.014	0.014	-0.014	0.014	-0.014
1	0.008	-0.007	0.007	-0.007	0.007	-0.008
Base Columns Springs	-0.0005	-0.0006		-0.0006		-0.0005

Table 30. Plasticity demand at max. roof disp. instant of H1-R2 in Sozen's

SOZEN'S APPROACH	PLASTICITY DEMAND OF BEAM ROTATIONAL SPRINGS (Θplastic/Θyield)						
STORY	**COLUMN 1**	**COLUMN 2**		**COLUMN 3**		**COLUMN 4**	**Story Average**
10	0.1	0.3	0.3	0.3	0.3	1.3	**0.4**
9	2.2	1.9	1.9	1.9	1.9	3.6	**2**
8	5.6	5.1	5.1	5.1	5.1	7.2	**6**
7	9.5	8.8	8.8	8.8	8.8	11.5	**9**
6	12.4	12.0	12.0	12.0	12.0	13.9	**12**
5	12.9	12.7	12.7	12.7	12.7	14.0	**13**
4	11.2	10.8	10.8	10.8	10.8	11.5	**11**
3	9.7	9.4	9.3	9.3	9.4	9.7	**9**
2	7.6	7.3	7.3	7.3	7.3	7.4	**7**
1	4.3	3.9	3.9	3.9	3.9	4.0	**4**
Base Columns Springs	0.20	0.24		0.24		0.20	**0.22**

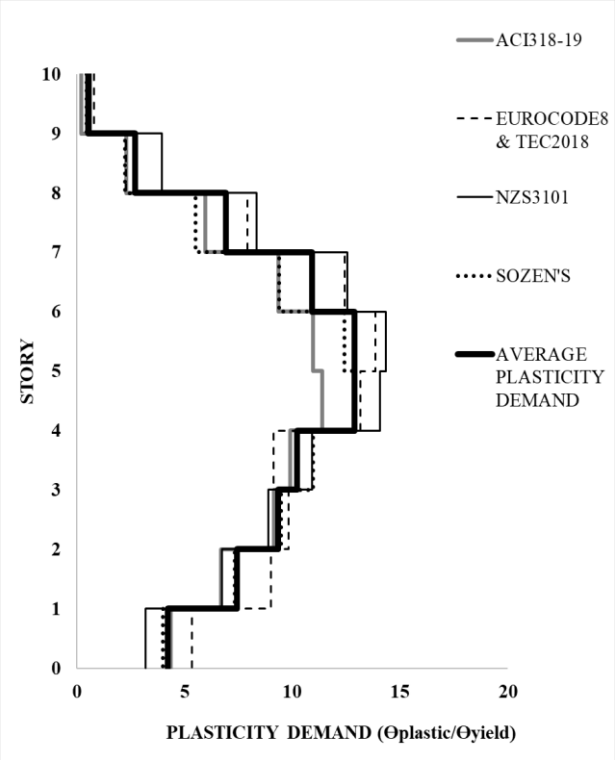

Figure 23. Plasticity demand of the system per effective stiffness procedure

3.3.2.3. H1-Run 3

Maximum roof displacements (mm), maximum roof drift ratios, periods and the deviations from the measured values in Cecen's report are presented Tables 31 and 32. Interstory drift ratio diagram at maximum roof displacement instant is also illustrated in Figure 24.

Table 31. Maximum roof displacements for H1-R3, nonlinear

CECEN H1-RUN3				
Linear System				
	Maximum Roof Displacement (mm)	**Maximum Roof Drift Ratio**	**Period (Sec)**	**Deviation from Measured (%)**
Gross Stiffness	43	0.019	0.24	58
ACI 318-19 & TEC2018	80	0.035	0.37	21
Eurocode 8 & SOZEN'S	79	0.034	0.34	22
NZS 3101-2006	87	0.038	0.41	14
CSA A23.3-14	77	0.034	0.36	24
Nonlinear System				
	Maximum Roof Displacement (mm)	**Maximum Roof Drift Ratio**	**Period (Sec)**	**Deviation from Measured (%)**
Gross Stiffness	59	0.026	0.30	42
ACI 318-19	86	0.038	0.48	15
Eurocode 8 & TEC2018	101	0.044	0.62	0
NZS 3101-2006	75	0.033	0.45	26
SOZEN'S	72	0.031	0.39	29
CECEN H1-RUN3	**101**	0.044	**0.34**	**0**

Table 32. Interstory drift ratio at maximum roof displacements for H1-R3, nonlinear

H1-R3 Interstory Drift Ratio at Max. Roof Displacement, Nonlinear					
STORY #	**ACI318-19**	**EUROCODE8 & TEC2018**	**NZS3101**	**SOZEN'S**	**CECEN H1-R2**
10	0.015	0.019	0.022	0.017	0.058
9	0.025	0.031	0.034	0.024	0.029
8	0.036	0.045	0.045	0.032	0.062
7	0.046	0.057	0.050	0.039	0.065
6	0.051	0.064	0.049	0.043	0.060
5	0.052	0.065	0.044	0.043	0.045
4	0.050	0.060	0.035	0.041	0.052
3	0.047	0.051	0.027	0.037	0.032
2	0.037	0.036	0.017	0.028	0.026
1	0.016	0.014	0.006	0.012	0.014
Base	0.000	0.000	0.000	0.000	0.000

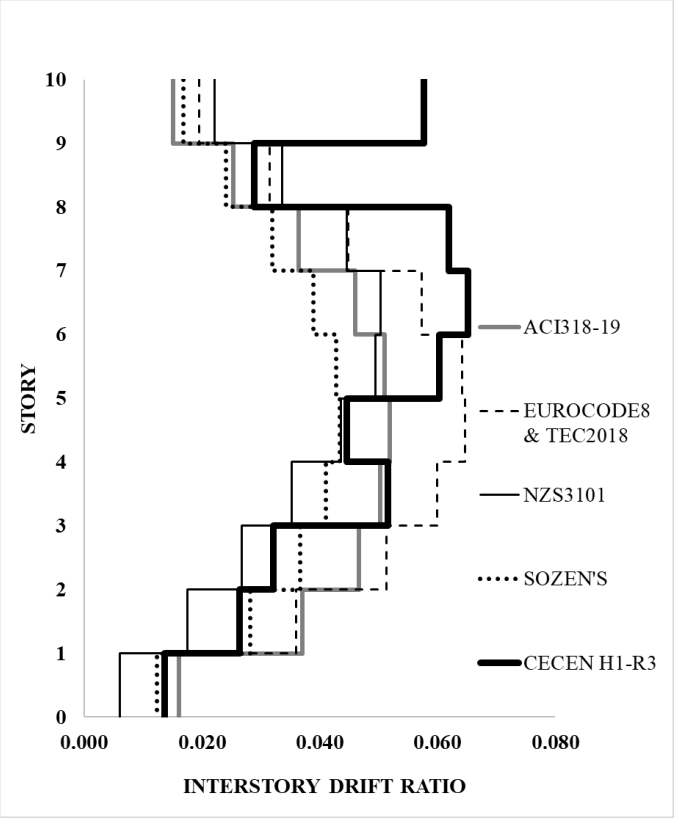

Figure 24. H1-R3 interstory drift ratio diagram, nonlinear

3.3.3. Dynamic Time-History Analysis for Frame H2

The second test frame is H2. A similar approach to H1 is followed for its simulations. Linear and nonlinear analyses are performed for each base excitation. Runs are representative of the Sozen's and the seismic code approaches and a simulation with the gross stiffness.

The results of the analyses are evaluated in terms of maximum roof displacement and the interstory-drift ratio at the instant of maximum roof displacement.

3.3.3.1. H2-Run 1

Maximum roof displacements (mm), maximum roof drift ratios, periods and the deviations from the measured values in Cecen's report are presented in Tables 33 and 34. Interstory drift ratio diagram at maximum roof displacement instant is also illustrated in Figure 25.

Table 33. Maximum roof displacements for H2-R1, nonlinear

CECEN H2-RUN1				
Linear System				
	Maximum Roof Displacement (mm)	**Maximum Roof Drift Ratio**	**Period (Sec)**	**Deviation from Measured (%)**
Gross Stiffness	6	0.003	0.24	33
ACI 318-19 & TEC2018	11	0.005	0.37	22
Eurocode 8 & SOZEN'S	9	0.004	0.34	0
NZS 3101-2006	11	0.005	0.41	22
CSA A23.3-14	10	0.004	0.36	11
Nonlinear System				
	Maximum Roof Displacement (mm)	**Maximum Roof Drift Ratio**	**Period (Sec)**	**Deviation from Measured (%)**
Gross Stiffness	6	0.003	0.30	33
ACI 318-19	11	0.005	0.48	22
Eurocode 8 & TEC2018	14	0.006	0.62	56
NZS 3101-2006	11	0.005	0.45	22
SOZEN'S	12	0.005	0.39	33
CECEN H2-RUN1	**9**	0.004	**0.34**	**0**

Table 34. Interstory drift ratio at max. roof disp. for H2-R1, nonlinear

H2-R1 Interstory Drift Ratio at Max. Roof Displacement, Nonlinear					
STORY #	**ACI318-19**	**EUROCODE 8 & TEC2018**	**NZS3101**	**SOZEN'S**	**CECEN H2-R1**
10	0.002	0.004	0.003	0.001	0.000
9	0.004	0.006	0.005	0.002	0.002
8	0.006	0.006	0.006	0.003	0.004
7	0.007	0.007	0.006	0.005	0.003
6	0.007	0.007	0.006	0.008	0.006
5	0.006	0.007	0.006	0.009	0.005
4	0.006	0.007	0.005	0.009	0.007
3	0.005	0.007	0.005	0.008	0.005
2	0.004	0.006	0.005	0.006	0.005
1	0.002	0.003	0.002	0.003	0.004
Base	0.000	0.000	0.000	0.000	0.000

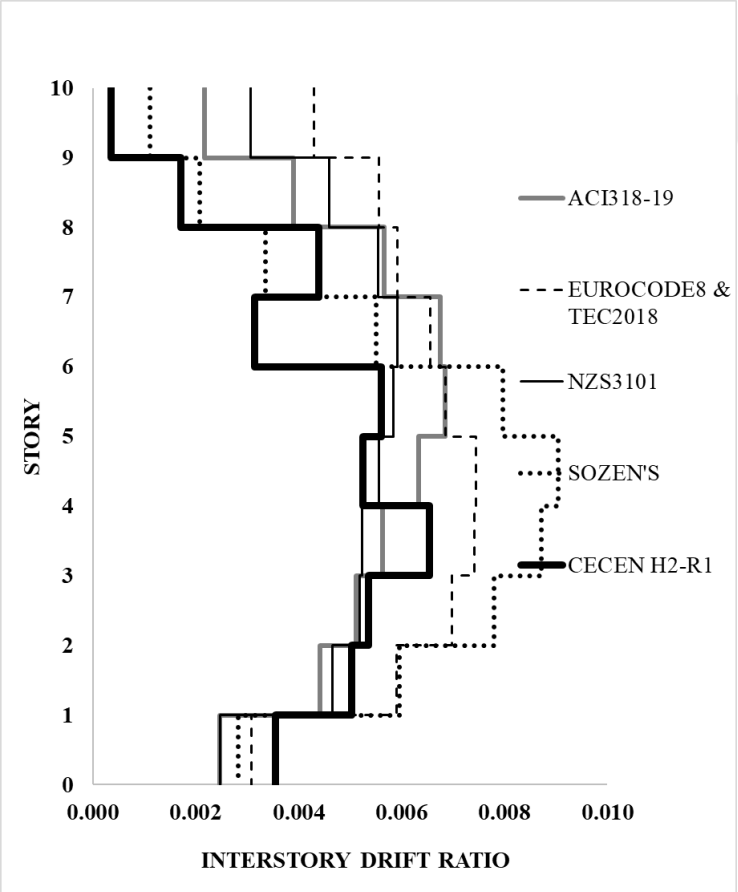

Figure 25. H2-R1 interstory drift ratio diagram, nonlinear

3.3.3.2. H2-Run 2

Maximum roof displacements (mm), maximum roof drift ratios, periods and the deviations from the measured values in Cecen's report are presented in Tables 35 and 36. Interstory drift ratio diagram at maximum roof displacement instant is also illustrated in Figure 26.

Table 35. Maximum roof displacements for H2-R2, nonlinear

CECEN H2-RUN2				
Linear System				
	Maximum Roof Displacement (mm)	**Maximum Roof Drift Ratio**	**Period (Sec)**	**Deviation from Measured (%)**
Gross Stiffness	12	0.005	0.24	33
ACI 318-19 & TEC2018	20	0.009	0.37	11
Eurocode 8 & SOZEN'S	19	0.008	0.34	6
NZS 3101-2006	21	0.009	0.41	17
CSA A23.3-14	19	0.008	0.36	6
Nonlinear System				
	Maximum Roof Displacement (mm)	**Maximum Roof Drift Ratio**	**Period (Sec)**	**Deviation from Measured (%)**
Gross Stiffness	12	0.005	0.30	33
ACI 318-19	22	0.010	0.48	22
Eurocode 8 & TEC2018	22	0.010	0.62	22
NZS 3101-2006	17	0.007	0.45	6
SOZEN'S	15	0.007	0.39	17
CECEN H2-RUN2	**18**	0.008	**0.34**	**0**

Table 36. Interstory drift ratio at max. roof disp. for H2-R2, nonlinear

H2-R2 Interstory Drift Ratio at Max. Roof Displacement, Nonlinear					
STORY #	**ACI318-19**	**EUROCODE8 & TEC2018**	**NZS3101**	**SOZEN'S METHOD**	**CECEN H2-R2**
10	0.003	0.004	0.003	0.002	0.001
9	0.005	0.007	0.005	0.003	0.006
8	0.010	0.009	0.009	0.005	0.006
7	0.015	0.010	0.012	0.007	0.008
6	0.016	0.012	0.013	0.009	0.012
5	0.014	0.014	0.011	0.010	0.011
4	0.011	0.014	0.009	0.010	0.011
3	0.010	0.013	0.007	0.009	0.011
2	0.008	0.010	0.005	0.007	0.010
1	0.004	0.005	0.002	0.003	0.006
Base	0.000	0.000	0.000	0.000	0.000

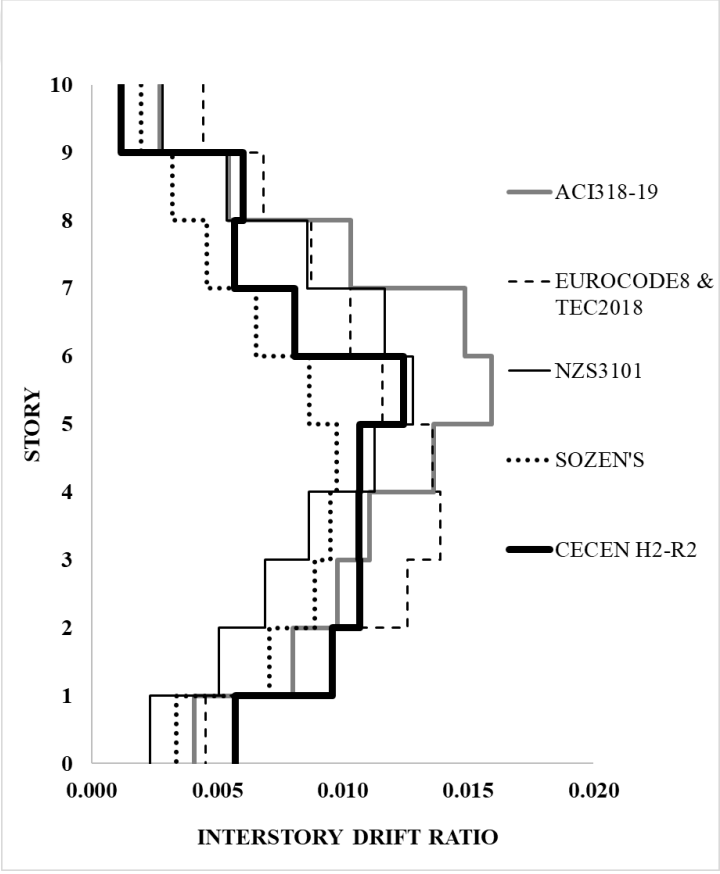

Figure 26. H2-R2 interstory drift ratio diagram, nonlinear

3.3.3.3. H2-Run 3

Maximum roof displacements (mm), maximum roof drift ratios, periods and the deviations from the measured values in Cecen's report are presented in Tables 37 and 38. Interstory drift ratio diagram at maximum roof displacement instant is also illustrated in Figure 27.

Table 37. Maximum roof displacements for H2-R3, nonlinear

CECEN H2-RUN3				
Linear System				
	Maximum Roof Displacement (mm)	**Maximum Roof Drift Ratio**	**Period (Sec)**	**Deviation from Measured (%)**
Gross Stiffness	19	0.008	0.24	21
ACI 318-19 & TEC2018	32	0.014	0.37	33
Eurocode 8 & SOZEN'S	30	0.013	0.34	25
NZS 3101-2006	34	0.015	0.41	42
CSA A23.3-14	30	0.013	0.36	25
Nonlinear System				
	Maximum Roof Displacement (mm)	**Maximum Roof Drift Ratio**	**Period (Sec)**	**Deviation from Measured (%)**
Gross Stiffness	19	0.008	0.3	21
ACI 318-19	27	0.012	0.48	13
Eurocode 8 & TEC2018	29	0.013	0.62	21
NZS 3101-2006	23	0.010	0.45	4
SOZEN'S	19	0.008	0.39	21
CECEN H2-RUN3	**24**	0.010	**0.34**	**0**

Table 38. Interstory drift ratio at max. roof disp. for H2-R3, nonlinear

H2-R3 Interstory Drift Ratio at Max. Roof Displacement, Nonlinear					
STORY #	**ACI318-19**	**EUROCODE8 & TEC2018**	**NZS3101**	**SOZEN'S**	**CECEN H2-R3**
10	0.003	0.008	0.003	0.002	0.004
9	0.005	0.012	0.006	0.004	0.009
8	0.010	0.016	0.010	0.006	0.010
7	0.014	0.021	0.013	0.009	0.014
6	0.018	0.022	0.015	0.012	0.017
5	0.019	0.018	0.015	0.013	0.013
4	0.017	0.013	0.013	0.012	0.011
3	0.016	0.009	0.012	0.011	0.011
2	0.013	0.005	0.009	0.009	0.010
1	0.005	0.001	0.004	0.004	0.006
Base	0.000	0.000	0.000	0.000	0.000

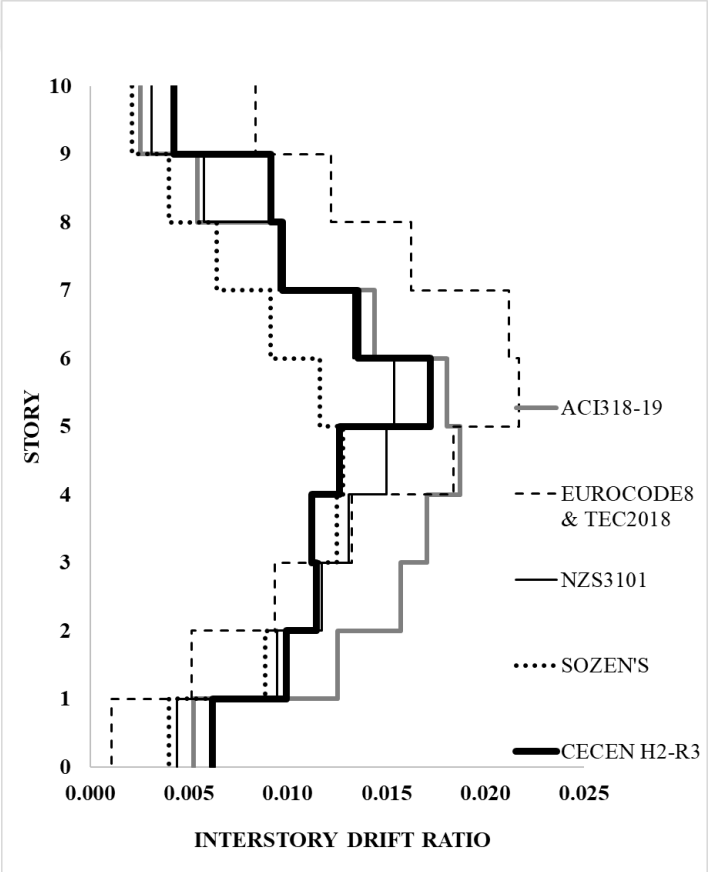

Figure 27. H2-R3 interstory drift ratio diagram, nonlinear

3.3.3.4. H2-Run 4

Maximum roof displacements (mm), maximum roof drift ratios, periods and the deviations from the measured values in Cecen's report are presented in Tables 39 and 40. Interstory drift ratio diagram at maximum roof displacement instant is also illustrated in Figure 28.

Table 39. Maximum roof displacements for H2-R4

CECEN H2-RUN4				
Linear System				
	Maximum Roof Displacement (mm)	**Maximum Roof Drift Ratio**	**Period (Sec)**	**Deviation from Measured (%)**
Gross Stiffness	19	0.008	0.24	27
ACI 318-19 & TEC2018	33	0.014	0.37	27
Eurocode 8 & SOZEN'S	30	0.013	0.34	15
NZS 3101-2006	34	0.015	0.41	31
CSA A23.3-14	30	0.013	0.36	15
Nonlinear System				
	Maximum Roof Displacement (mm)	**Maximum Roof Drift Ratio**	**Period (Sec)**	**Deviation from Measured (%)**
Gross Stiffness	19	0.008	0.3	27
ACI 318-19	27	0.012	0.48	4
Eurocode 8 & TEC2018	29	0.013	0.62	12
NZS 3101-2006	23	0.010	0.45	12
SOZEN'S	19	0.008	0.39	27
CECEN H2-RUN4	**26**	0.011	**0.34**	**0**

Table 40. Interstory drift ratio at max. roof disp. for H2-R4, nonlinear

H2-R4 Interstory Drift Ratio at Max. Roof Displacement, Nonlinear					
STORY #	**ACI318-19**	**EUROCODE8 & TEC2018**	**NZS3101**	**SOZEN'S**	**CECEN H2-R4**
10	0.002	0.008	0.003	0.002	0.008
9	0.005	0.012	0.006	0.004	0.028
8	0.010	0.016	0.010	0.006	0.006
7	0.015	0.021	0.013	0.009	0.023
6	0.018	0.022	0.015	0.012	0.010
5	0.019	0.019	0.015	0.013	0.013
4	0.017	0.014	0.013	0.013	0.013
3	0.016	0.010	0.012	0.011	0.011
2	0.012	0.005	0.009	0.009	0.009
1	0.005	0.001	0.004	0.004	0.005
Base	0.000	0.000	0.000	0.000	0.000

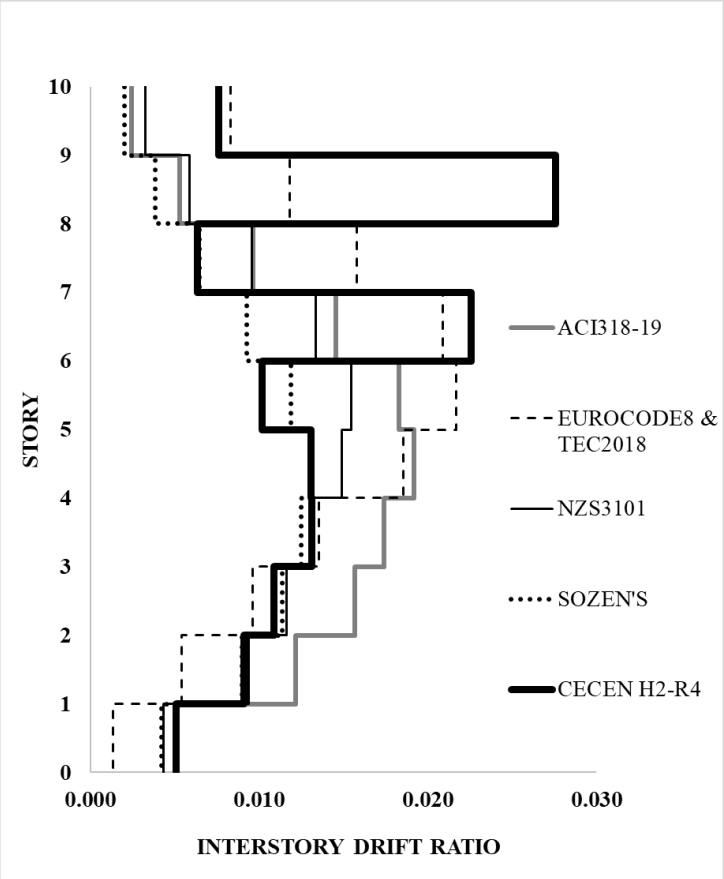

Figure 28. H2-R4 interstory drift ratio diagram, nonlinear

3.3.3.5. H2-Run 5

Maximum roof displacements (mm), maximum roof drift ratios, periods and the deviations from the measured values in Cecen's report are presented in Tables 41 and 42. Interstory drift ratio diagram at maximum roof displacement instant is also illustrated in Figure 29.

Table 41. Maximum roof displacements for H2-R5

CECEN H2-RUN5				
Linear System				
	Maximum Roof Displacement (mm)	**Maximum Roof Drift Ratio**	**Period (Sec)**	**Deviation from Measured (%)**
Gross Stiffness	28	0.012	0.24	28
ACI 318-19 & TEC2018	48	0.021	0.37	23
Eurocode 8 & SOZEN'S	45	0.020	0.34	15
NZS 3101-2006	51	0.022	0.41	31
CSA A23.3-14	44	0.019	0.36	13
Nonlinear System				
	Maximum Roof Displacement (mm)	**Maximum Roof Drift Ratio**	**Period (Sec)**	**Deviation from Measured (%)**
Gross Stiffness	27	0.012	0.30	31
ACI 318-19	39	0.017	0.48	0
Eurocode 8 & TEC2018	43	0.019	0.62	10
NZS 3101-2006	42	0.018	0.45	8
SOZEN'S	31	0.014	0.39	21
CECEN H2-RUN5	**39**	0.017	**0.34**	**0**

Table 42. Interstory drift ratio at max. roof disp. for H2-R5, nonlinear

H2-R5 Interstory Drift Ratio at Max. Roof Displacement, Nonlinear					
STORY #	**ACI318-19**	**EUROCODE8 & TEC2018**	**NZS3101**	**SOZEN'S**	**CECEN H2-R5**
10	0.006	0.009	0.007	0.003	0.012
9	0.011	0.019	0.014	0.006	0.045
8	0.017	0.031	0.021	0.012	0.005
7	0.021	0.035	0.026	0.018	0.036
6	0.024	0.030	0.029	0.022	0.015
5	0.024	0.023	0.027	0.022	0.020
4	0.023	0.016	0.023	0.020	0.017
3	0.021	0.013	0.018	0.017	0.014
2	0.016	0.009	0.013	0.012	0.012
1	0.007	0.003	0.005	0.003	0.007
Base	0.000	0.000	0.000	0.000	0.000

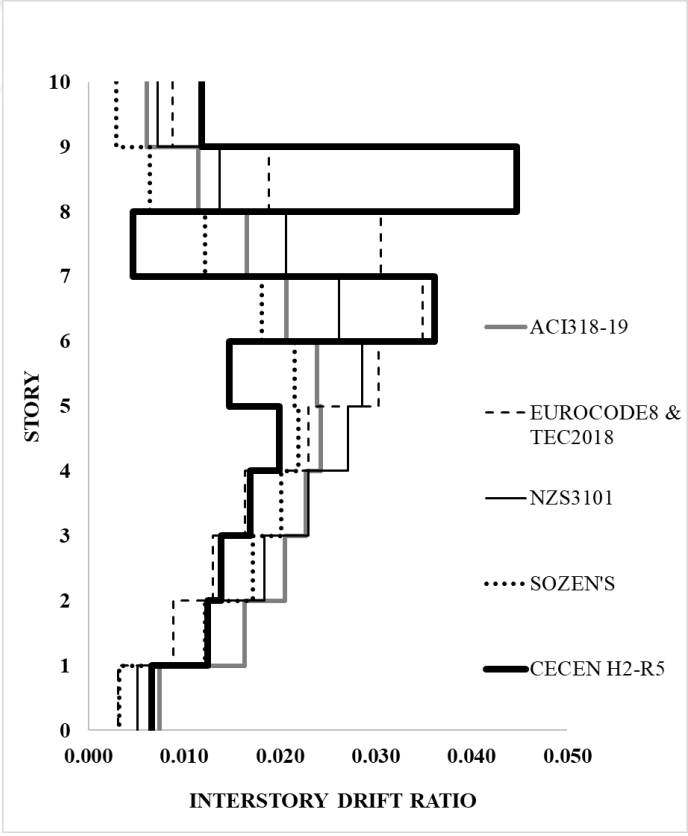

Figure 29. H2-R5 interstory drift ratio diagram, nonlinear

3.3.3.6. H2-Run 6

Maximum roof displacements (mm), maximum roof drift ratios, periods and the deviations from the measured values in Cecen's report are presented in Tables 43 and 44. Interstory drift ratio diagram at maximum roof displacement instant is also illustrated in Figure 30.

Table 43. Maximum roof displacements for H2-R6

CECEN H2-RUN6				
Linear System				
	Maximum Roof Displacement (mm)	**Maximum Roof Drift Ratio**	**Period (Sec)**	**Deviation from Measured (%)**
Gross Stiffness	36	0.016	0.24	40
ACI 318-19 & TEC2018	64	0.028	0.37	7
Eurocode 8 & SOZEN'S	60	0.026	0.34	0
NZS 3101-2006	67	0.029	0.41	12
CSA A23.3-14	59	0.026	0.36	2
Nonlinear System				
	Maximum Roof Displacement (mm)	**Maximum Roof Drift Ratio**	**Period (Sec)**	**Deviation from Measured (%)**
Gross Stiffness	40	0.017	0.30	33
ACI 318-19	57	0.025	0.48	5
Eurocode 8 & TEC2018	74	0.032	0.62	23
NZS 3101-2006	54	0.024	0.45	10
SOZEN'S	47	0.021	0.39	22
CECEN H2-RUN6	**60**	0.026	**0.34**	**0**

Table 44. Interstory drift ratio at max. roof disp. for H2-R6, nonlinear

H2-R6 Interstory Drift Ratio at Max. Roof Displacement, Nonlinear					
STORY #	**ACI318-19**	**EUROCODE8 & TEC2018**	**NZS3101**	**SOZEN'S**	**CECEN H2-R6**
10	0.009	0.015	0.009	0.005	0.023
9	0.014	0.027	0.018	0.012	0.041
8	0.021	0.039	0.029	0.020	0.011
7	0.031	0.045	0.036	0.027	0.053
6	0.039	0.045	0.038	0.031	0.019
5	0.041	0.044	0.035	0.031	0.032
4	0.037	0.041	0.028	0.029	0.027
3	0.030	0.035	0.022	0.024	0.022
2	0.020	0.023	0.014	0.017	0.022
1	0.007	0.008	0.006	0.007	0.010
Base	0.000	0.000	0.000	0.000	0.000

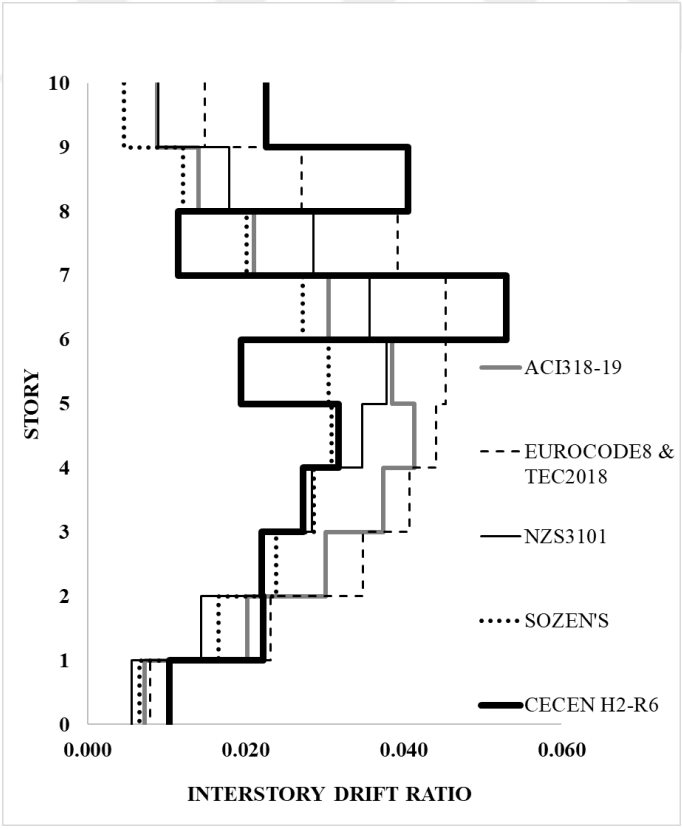

Figure 30. H2-R6 interstory drift ratio diagram, nonlinear

3.3.3.7. H2-Run 7

Maximum roof displacements (mm), maximum roof drift ratios, periods and the deviations from the measured values in Cecen's report are presented in Tables 45 and 46. Interstory drift ratio diagram at maximum roof displacement instant is also illustrated in Figure 31.

Table 45. Maximum roof displacements for H2-R7

CECEN H2-RUN7				
Linear System				
	Maximum Roof Displacement (mm)	**Maximum Roof Drift Ratio**	**Period (Sec)**	**Deviation from Measured (%)**
Gross Stiffness	41	0.018	0.24	59
ACI 318-19 & TEC2018	77	0.034	0.37	23
Eurocode 8 & SOZEN'S	77	0.034	0.34	23
NZS 3101-2006	81	0.035	0.41	19
CSA A23.3-14	74	0.032	0.36	26
Nonlinear System				
	Maximum Roof Displacement (mm)	**Maximum Roof Drift Ratio**	**Period (Sec)**	**Deviation from Measured (%)**
Gross Stiffness	56	0.024	0.3	44
ACI 318-19	83	0.036	0.48	17
Eurocode 8 & TEC2018	101	0.044	0.62	1
NZS 3101-2006	72	0.031	0.45	28
SOZEN'S	71	0.031	0.39	29
CECEN H2-RUN7	100	0.044	**0.34**	**0**

Table 46. Interstory drift ratio at max. roof disp. for H2-R7, nonlinear

H2-R7 Interstory Drift Ratio at Max. Roof Displacement, Nonlinear					
STORY #	**ACI318-19**	**EUROCODE8 & TEC2018**	**NZS3101**	**SOZEN'S**	**CECEN H2-R7**
10	0.014	0.018	0.015	0.015	0.046
9	0.022	0.032	0.025	0.023	0.096
8	0.030	0.049	0.035	0.031	0.015
7	0.041	0.059	0.042	0.039	0.122
6	0.053	0.061	0.045	0.042	0.006
5	0.057	0.063	0.043	0.043	0.049
4	0.053	0.061	0.038	0.039	0.037
3	0.043	0.053	0.033	0.035	0.028
2	0.031	0.036	0.026	0.028	0.024
1	0.012	0.013	0.012	0.013	0.012
Base	0.000	0.000	0.000	0.000	0.000

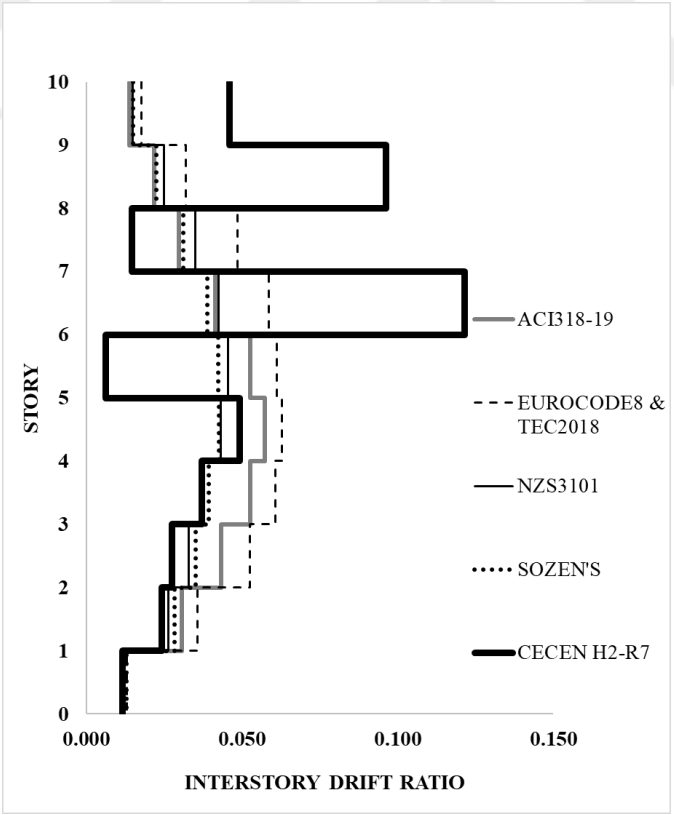

Figure 31. H2-R7 interstory drift ratio diagram, nonlinear

3.3.4. Properties of the Selected Ground Motion Set

A ground motion set was selected to test the performance of the numerical models under representative seismic action. This ground motion set consists of eleven different earthquake records. The properties of the acceleration records of the selected set, which was originally gathered by (Sönmez 2020), are provided in Table 47.

As mentioned earlier, the ground motions (El Centro, 1940) used in Cecen's experiments were compressed by a coefficient of 2.5 to have a demand beyond the constant acceleration region for the test frames scaled by a coefficient of 1/12. Similarly, all earthquake records in the selected ground motion set are compressed with the same coefficient.

The selected ground motion records were not suitable to define the targeted demand in their original form. Therefore, before the compression process, these records are scaled. The scaling process is carried out according to the Turkish Earthquake Code (TEC 2018). The reference demand was specified for Kadıköy, İstanbul, Turkey, as (Sönmez 2020). It was a DD2 type earthquake (10% probability in 50 years) and soil type ZD. The scaling process is explained in detail in Section 3.3.4.1.

Table 47. Properties of the original ground motion set

Properties of the Original Ground Motion Set	
Name	**PGA (g)**
RSN169 IMPERIAL	0.24
RSN178 IMPERIAL	0.27
RSN265 VICTORY	0.65
RSN316 WESTMORLAND	0.23
RSN549 CHALFANT	0.25
RSN721 SUPERSTITION HILLS	0.36
RSN848 LANDERS	0.28
RSN1115 KOBE	0.15
RSN1782 HECTOR	0.18
RSN5990 SIERRA	0.26
RSN6060 BIG BEAR	0.14

3.3.4.1. Scaling the Selected Ground Motion Set According to the TEC 2018 Procedure

Firstly, a reference region and the soil type shall be chosen for the scaling procedure. According to the TEC 2018, the soil types are ZA, ZB, ZC and ZD depending on the design acceleration spectrum. If the soil profile belongs to the ZA soil group, the ground display solid, hard rock form; ZB local soil classes display less weathered, medium-solid rocks texture; ZC local floor grade very tight sand, gravel and hard clay layers; ZD local ground grade gravel or clay layers; ZE local soil grade loose sand, soft clay floors; the ZF soil layers require site-specific research and assessment. Kadıköy/Istanbul, Turkey was chosen for this process. The soil type of Kadıköy location is the ZD.

According to TEC 2018, the scaling procedure of the second ground motion set is explained step by step below.

1. All acceleration records of the second ground motion set were corrected with either baseline correction or filtering with the help of SeismoSignal software(Source: Https://Seismosoft.Com/Products/Seismosignal/).

2. The response spectrums of the corrected acceleration records were obtained for the 2% viscous damping factor (ζ=2%).

3. Assuming that the natural dominant period of the frame (T_p) was 0.23 sec, the interval of the average period (T_{avg}) was calculated as below:

$$0.2\ T_p < T_{avg} < 1.5\ T_p$$

So, $0.046\ \text{sec} < T_{avg} < 0.345\ \text{sec}$

4. The mean accelerations between 0.046 and 0.345 sec were calculated for each response spectrum.

5. Elastic design spectrum of a coordinate in Kadiköy for the ZD soil was obtained from Turkey Disaster and Emergency Management Presidency (AFAD). Afterward, the mean accelerations of the design spectrum were calculated for the same period interval.

6. The mean accelerations of the response spectrums of the ground motion set were proportioned to that of the Kadıköy elastic design spectrum. These ratios were used as scaling coefficients.

The scaling coefficients and scaled peak ground motion accelerations are listed in Table 48.

Table 48. Properties of the scaled selected ground motion set for TEC 2018

Properties of the Scaled Second Ground Motion Set for TEC 2018		
Name	**PGA (g)**	**Scaling Coefficient**
RSN169 IMPERIAL	0.32	1.37
RSN178 IMPERIAL	0.29	1.1
RSN265 VICTORY	0.58	0.9
RSN316 WESTMORLAND	0.42	1.82
RSN549 CHALFANT	0.37	1.48
RSN721 SUPERSTITION HILLS	0.46	1.28
RSN848 LANDERS	0.31	1.1
RSN1115 KOBE	0.29	1.9
RSN1782 HECTOR	0.29	1.58
RSN5990 SIERRA	0.27	1.07
RSN6060 BIG BEAR	0.31	2.2

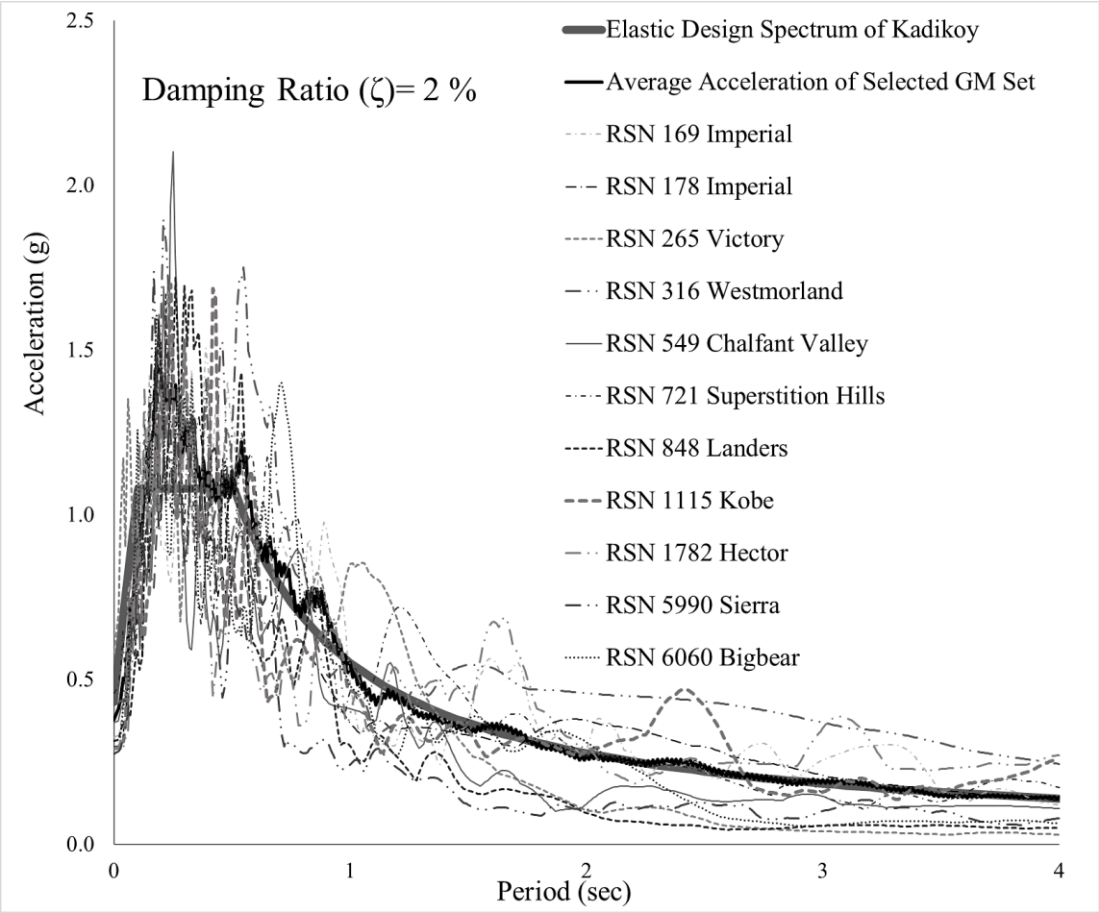

Figure 32. Individual and the average acceleration spectra of the selected GM set

3.3.4.2. Dynamic Time History Analysis Results of the Selected Ground Motion Set

The scaled and compressed acceleration records of the selected ground motion set are used as input records in OpenSees for dynamic time history analyses. The analyses are exerted for linear and nonlinear RC frames. The input acceleration records and maximum roof displacements are presented in the following.

3.3.4.2.1. RSN 169 Imperial

Maximum roof displacements (mm), maximum roof drift ratios, periods and the deviations from the average maximum roof displacements are presented in Tables 49 and 50. Interstory drift ratio diagram at the maximum roof displacement instant is also illustrated in Figure 33.

Table 49. Maximum roof displacements of RSN 169 Imperial

RSN169 IMPERIAL VALLEY			
Linear System			
	Maximum Roof Displacement (mm)	**Maximum Roof Drift Ratio**	**Deviation from Average (%)**
Gross Stiffness	12	0.005	45
ACI 318-19 & TEC 2018	24	0.010	9
Eurocode 8 & SOZEN'S	21	0.009	3
NZS 3101-2006	17	0.007	22
CSA A23.3-14	25	0.011	15
Average Max. Roof Disp.	22	0.009	**0**
Nonlinear System			
	Maximum Roof Displacement (mm)	**Maximum Roof Drift Ratio**	**Deviation from Average (%)**
Gross Stiffness	16	0.007	30
ACI 318-19	22	0.010	3
Eurocode 8 & TEC 2018	33	0.014	45
NZS 3101-2006	20	0.009	12
SOZEN'S	16	0.007	30
Average Max. Roof Disp.	23	0.010	**0**

Table 50. Interstory drift ratio at max. roof disp. for RSN169, nonlinear

RSN169 Interstory Drift Ratio at Max. Roof Displacement, Nonlinear					
STORY #	**ACI318-19**	**EUROCODE8 & TEC2018**	**NZS3101**	**SOZEN'S**	**AVERAGE DRIFT RATIO**
10	0.001	0.005	0.002	0.001	0.002
9	0.002	0.010	0.003	0.002	0.004
8	0.005	0.015	0.005	0.003	0.007
7	0.010	0.021	0.009	0.005	0.011
6	0.014	0.023	0.013	0.008	0.015
5	0.017	0.022	0.015	0.010	0.016
4	0.016	0.018	0.015	0.011	0.015
3	0.014	0.015	0.013	0.011	0.013
2	0.011	0.011	0.010	0.009	0.010
1	0.005	0.005	0.005	0.004	0.005
Base	0.000	0.000	0.000	0.000	0.000

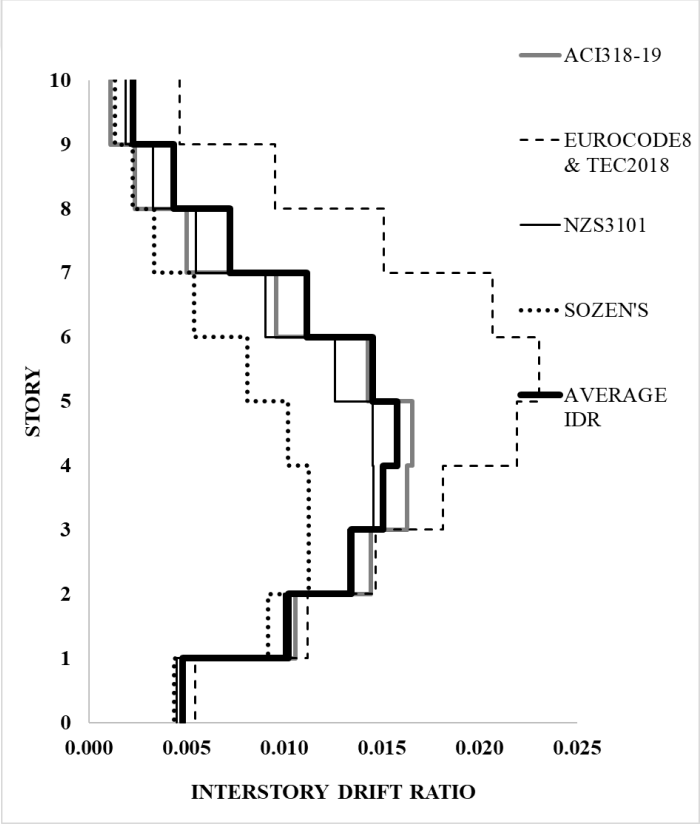

Figure 33. Interstory drift ratio diagram for RSN169, nonlinear

3.3.4.2.2. RSN 178 Imperial

Maximum roof displacements (mm), maximum roof drift ratios, periods and the deviations from the average maximum roof displacements are presented in Tables 51and 52. Interstory drift ratio diagram at the maximum roof displacement instant is also illustrated in Figure 34.

Table 51. Maximum roof displacements of RSN 178 Imperial

RSN178 IMPERIAL VALLEY			
Linear System			
	Maximum Roof Displacement (mm)	**Maximum Roof Drift Ratio**	**Deviation from Average (%)**
Gross Stiffness	11	0.005	35
ACI 318-19 & TEC 2018	17	0.007	0
Eurocode 8 & SOZEN'S	17	0.007	0
NZS 3101-2006	17	0.007	0
CSA A23.3-14	17	0.007	0
Average Max. Roof Disp.	17	0.007	**0**
Nonlinear System			
	Maximum Roof Displacement (mm)	**Maximum Roof Drift Ratio**	**Deviation from Average (%)**
Gross Stiffness	18	0.008	25
ACI 318-19	25	0.011	4
Eurocode 8 & TEC 2018	30	0.013	25
NZS 3101-2006	21	0.009	13
SOZEN'S	20	0.009	17
Average Max. Roof Disp.	24	0.010	**0**

Table 52. Interstory drift ratio at max. roof disp. for RSN178, nonlinear

RSN178 Interstory Drift Ratio at Max. Roof Displacement, Nonlinear					
STORY #	**ACI318-19**	**EUROCODE8 & TEC2018**	**NZS3101**	**SOZEN'S**	**AVERAGE DRIFT RATIO**
10	0.003	0.006	0.002	0.003	0.003
9	0.006	0.008	0.003	0.006	0.006
8	0.010	0.013	0.006	0.010	0.010
7	0.013	0.018	0.011	0.012	0.014
6	0.016	0.020	0.015	0.013	0.016
5	0.017	0.019	0.017	0.012	0.016
4	0.015	0.017	0.015	0.011	0.014
3	0.012	0.016	0.012	0.009	0.012
2	0.010	0.011	0.008	0.007	0.009
1	0.005	0.005	0.003	0.003	0.004
Base	0.000	0.000	0.000	0.000	0.000

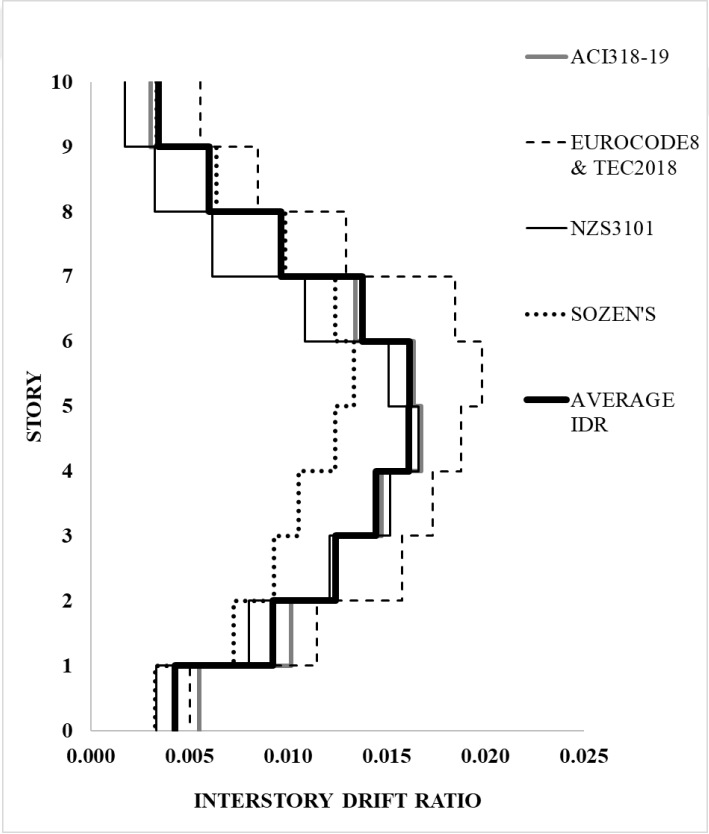

Figure 34. Interstory drift ratio diagram for RSN178, nonlinear

3.3.4.2.3. RSN 265 Victory

Maximum roof displacements (mm), maximum roof drift ratios, periods and the deviations from the average maximum roof displacements are presented in Tables 53 and 54. Interstory drift ratio diagram at the maximum roof displacement instant is also illustrated in Figure 35.

Table 53. Maximum roof displacements of RSN 265 Victory

RSN265 VICTORY			
Linear System			
	Maximum Roof Displacement (mm)	**Maximum Roof Drift Ratio**	**Deviation from Average (%)**
Gross Stiffness	14	0.006	41
ACI 318-19 & TEC 2018	24	0.010	1
Eurocode 8 & SOZEN'S	19	0.008	20
NZS 3101-2006	29	0.013	22
CSA A23.3-14	23	0.010	3
Average Max. Roof Disp.	24	0.010	**0**
Nonlinear System			
	Maximum Roof Displacement (mm)	**Maximum Roof Drift Ratio**	**Deviation from Average (%)**
Gross Stiffness	16	0.007	27
ACI 318-19	18	0.008	18
Eurocode 8 & TEC 2018	29	0.013	32
NZS 3101-2006	17	0.007	23
SOZEN'S	24	0.010	9
Average Max. Roof Disp.	22	0.010	**0**

Table 54. Interstory drift ratio at max. roof disp. for RSN265, nonlinear

RSN265 Interstory Drift Ratio at Max. Roof Displacement, Nonlinear					
STORY #	**ACI318-19**	**EUROCODE8 & TEC2018**	**NZS3101**	**SOZEN'S**	**AVERAGE DRIFT RATIO**
10	0.001	0.007	0.002	0.002	0.003
9	0.001	0.013	0.003	0.005	0.006
8	0.003	0.019	0.005	0.010	0.009
7	0.006	0.022	0.007	0.014	0.012
6	0.009	0.020	0.010	0.017	0.014
5	0.012	0.017	0.012	0.018	0.015
4	0.014	0.013	0.012	0.016	0.014
3	0.014	0.010	0.011	0.012	0.012
2	0.011	0.006	0.008	0.009	0.009
1	0.005	0.002	0.004	0.004	0.004
Base	0.000	0.000	0.000	0.000	0.000

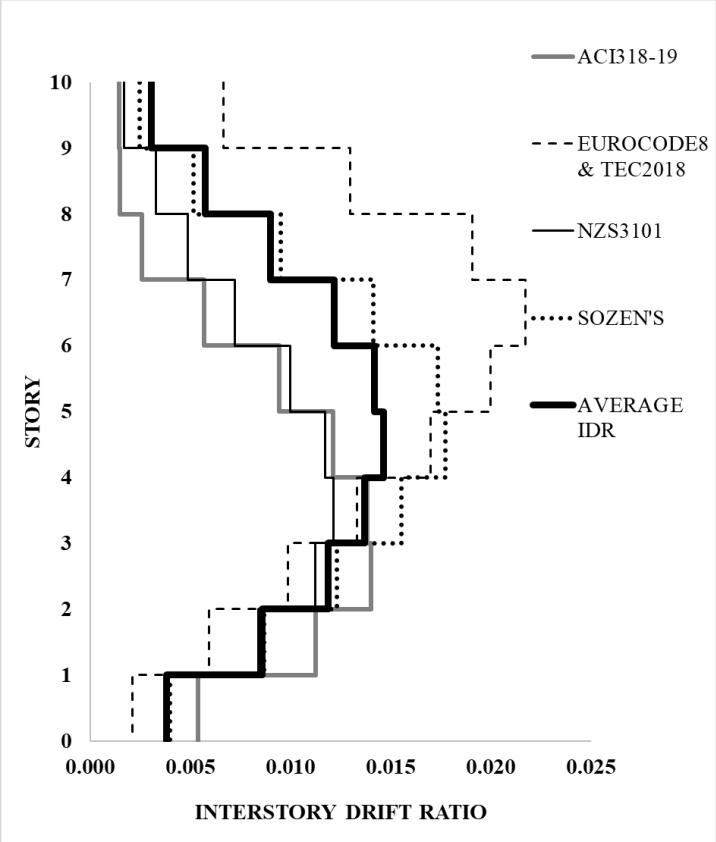

Figure 35. Interstory drift ratio diagram for RSN265, nonlinear

3.3.4.2.4. RSN 316 Westmorland

Maximum roof displacements (mm), maximum roof drift ratios, periods and the deviations from the average maximum roof displacements are presented in Tables 55 and 56. Interstory drift ratio diagram at the maximum roof displacement instant is also illustrated in Figure 36.

Table 55. Maximum roof displacements of RSN 316 Westmorland

RSN316 WESTMORLAND			
Linear System			
	Maximum Roof Displacement (mm)	**Maximum Roof Drift Ratio**	**Deviation from Average (%)**
Gross Stiffness	21	0.009	3
ACI 318-19 & TEC 2018	22	0.010	1
Eurocode 8 & SOZEN'S	21	0.009	3
NZS 3101-2006	23	0.010	6
CSA A23.3-14	21	0.009	3
Average Max. Roof Disp.	22	0.009	**0**
Nonlinear System			
	Maximum Roof Displacement (mm)	**Maximum Roof Drift Ratio**	**Deviation from Average (%)**
Gross Stiffness	30	0.013	25
ACI 318-19	30	0.013	25
Eurocode 8 & TEC 2018	80	0.035	100
NZS 3101-2006	20	0.009	50
SOZEN'S	30	0.013	25
Average Max. Roof Disp.	40	0.017	**0**

Table 56. Interstory drift ratio at max. roof disp. for RSN316, nonlinear

RSN316 Interstory Drift Ratio at Max. Roof Displacement, Nonlinear					
STORY #	**ACI318-19**	**EUROCODE8 & TEC2018**	**NZS3101**	**SOZEN'S**	**AVERAGE DRIFT RATIO**
10	0.001	0.009	0.002	0.004	0.004
9	0.003	0.020	0.003	0.008	0.008
8	0.007	0.033	0.005	0.012	0.014
7	0.013	0.044	0.008	0.016	0.020
6	0.018	0.050	0.011	0.019	0.025
5	0.021	0.052	0.014	0.020	0.027
4	0.022	0.049	0.015	0.018	0.026
3	0.022	0.044	0.014	0.016	0.024
2	0.017	0.033	0.012	0.012	0.019
1	0.007	0.015	0.005	0.005	0.008
Base	0.000	0.000	0.000	0.000	0.000

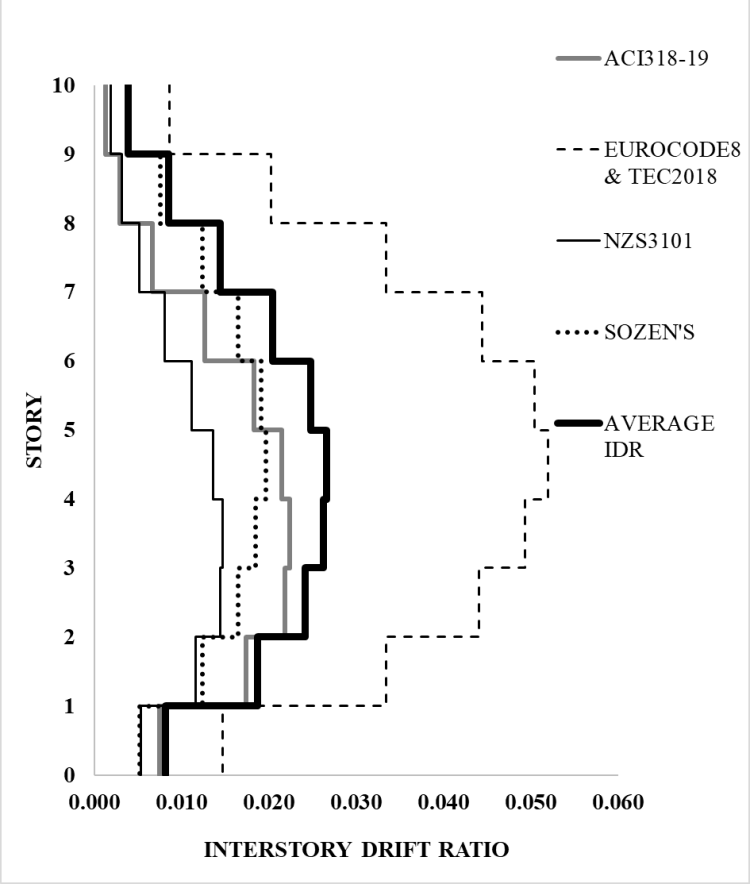

Figure 36. Interstory drift ratio diagram for RSN316, nonlinear

3.3.4.2.5. RSN 549 Chalfant

Maximum roof displacements (mm), maximum roof drift ratios, periods and the deviations from the average maximum roof displacements are presented in Tables 57 and 58. Interstory drift ratio diagram at the maximum roof displacement instant is also illustrated in Figure 37.

Table 57. Maximum roof displacements of RSN 549 Chalfant

RSN549 CHALFANT			
Linear System			
	Maximum Roof Displacement (mm)	**Maximum Roof Drift Ratio**	**Deviation from Average (%)**
Gross Stiffness	11	0.005	35
ACI 318-19 & TEC 2018	17	0.007	0
Eurocode 8 & SOZEN'S	16	0.007	6
NZS 3101-2006	19	0.008	12
CSA A23.3-14	16	0.007	6
Average Max. Roof Disp.	17	0.007	**0**
Nonlinear System			
	Maximum Roof Displacement (mm)	**Maximum Roof Drift Ratio**	**Deviation from Average (%)**
Gross Stiffness	10	0.004	49
ACI 318-19	21	0.009	8
Eurocode 8 & TEC 2018	22	0.010	13
NZS 3101-2006	20	0.009	3
SOZEN'S	15	0.007	23
Average Max. Roof Disp.	20	0.009	**0**

Table 58. Interstory drift ratio at max. roof disp. for RSN549, nonlinear

RSN549 Interstory Drift Ratio at Max. Roof Displacement, Nonlinear					
STORY #	**ACI318-19**	**EUROCODE8 & TEC2018**	**NZS3101**	**SOZEN'S**	**AVERAGE DRIFT RATIO**
10	0.002	0.003	0.003	0.002	0.003
9	0.004	0.006	0.006	0.003	0.005
8	0.007	0.009	0.009	0.005	0.008
7	0.010	0.011	0.011	0.008	0.010
6	0.011	0.012	0.012	0.010	0.011
5	0.013	0.012	0.012	0.011	0.012
4	0.014	0.012	0.011	0.010	0.012
3	0.014	0.013	0.011	0.008	0.011
2	0.012	0.011	0.008	0.005	0.009
1	0.006	0.006	0.004	0.002	0.005
Base	0.000	0.000	0.000	0.000	0.000

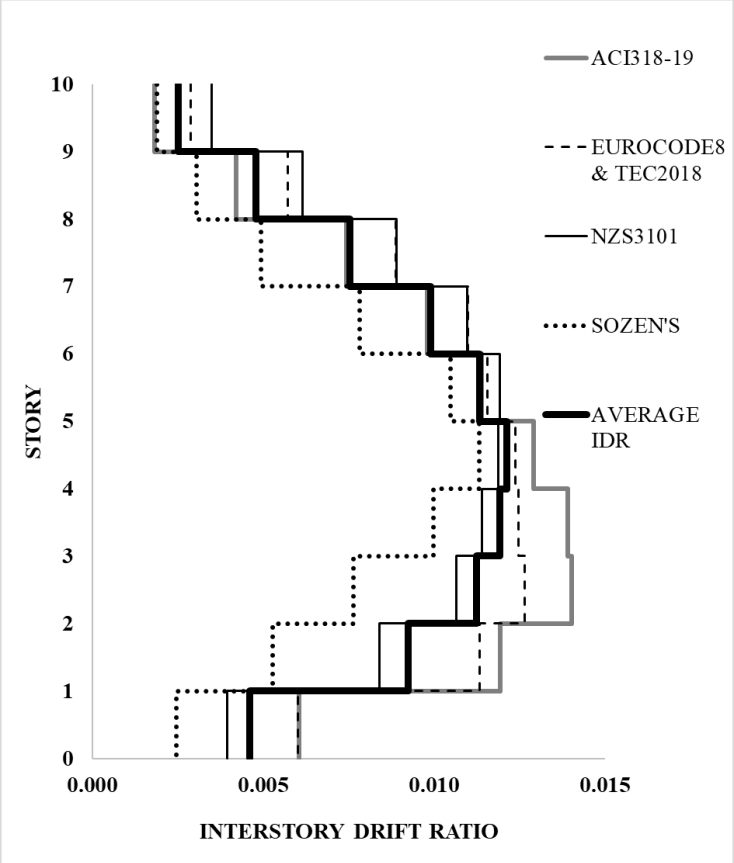

Figure 37. Interstory drift ratio diagram for RSN549, nonlinear

3.3.4.2.6. RSN 721 Superstition Hills

Maximum roof displacements (mm), maximum roof drift ratios, periods and the deviations from the average maximum roof displacements are presented in Tables 59 and 60. Interstory drift ratio diagram at the maximum roof displacement instant is also illustrated in Figure 38.

Table 59. Maximum roof displacements of RSN 721 Superstition

RSN721 SUPERSTITION			
Linear System			
	Maximum Roof Displacement (mm)	**Maximum Roof Drift Ratio**	**Deviation from Average (%)**
Gross Stiffness	16	0.007	30
ACI 318-19 & TEC 2018	23	0.010	0
Eurocode 8 & SOZEN'S	23	0.010	0
NZS 3101-2006	22	0.010	4
CSA A23.3-14	24	0.010	4
Average Max. Roof Disp.	23	0.010	**0**
Nonlinear System			
	Maximum Roof Displacement (mm)	**Maximum Roof Drift Ratio**	**Deviation from Average (%)**
Gross Stiffness	25	0.011	28
ACI 318-19	29	0.013	16
Eurocode 8 & TEC 2018	40	0.017	16
NZS 3101-2006	38	0.017	10
SOZEN'S	31	0.014	10
Average Max. Roof Disp.	35	0.015	**0**

Table 60. Interstory drift ratio at max. roof disp. for RSN721, nonlinear

RSN721 Interstory Drift Ratio at Max. Roof Displacement, Nonlinear					
STORY #	**ACI318-19**	**EUROCODE8 & TEC2018**	**NZS3101**	**SOZEN'S**	**AVERAGE DRIFT RATIO**
10	0.004	0.005	0.004	0.003	0.004
9	0.008	0.009	0.008	0.006	0.008
8	0.014	0.017	0.014	0.010	0.014
7	0.018	0.025	0.022	0.015	0.020
6	0.019	0.027	0.023	0.019	0.022
5	0.019	0.027	0.023	0.022	0.023
4	0.017	0.024	0.026	0.022	0.022
3	0.014	0.021	0.021	0.020	0.019
2	0.010	0.015	0.014	0.014	0.013
1	0.005	0.006	0.002	0.005	0.004
Base	0.000	0.000	0.000	0.000	0.000

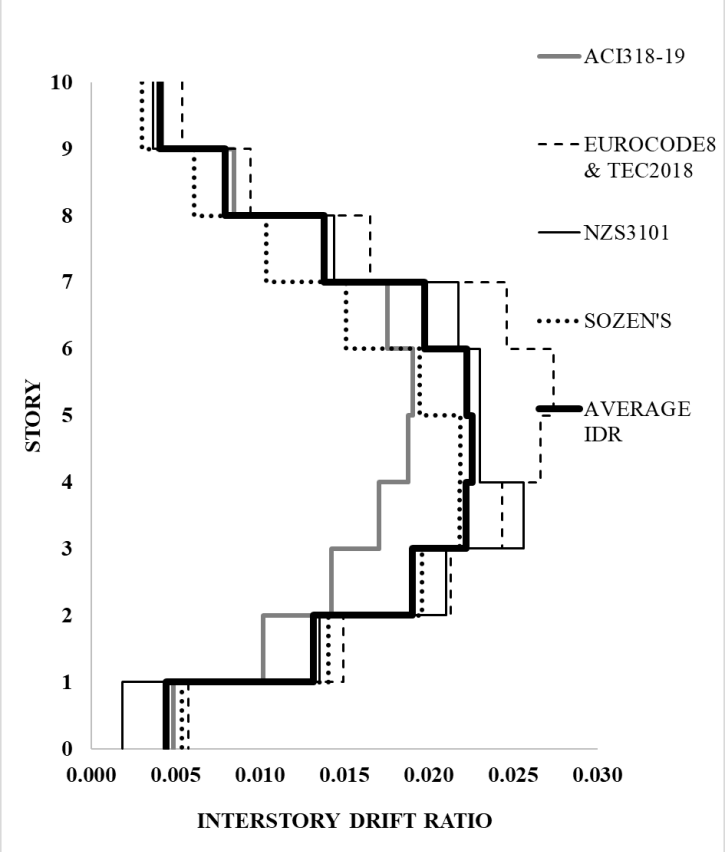

Figure 38. Interstory drift ratio diagram for RSN721, nonlinear

3.3.4.2.7. RSN 848 Landers

Maximum roof displacements (mm), maximum roof drift ratios, periods and the deviations from the average maximum roof displacements are presented Tables 61 and 62. Interstory drift ratio diagram at the maximum roof displacement instant is also illustrated in Figure 39.

Table 61. Maximum roof displacements of RSN 848 Landers

RSN848 LANDERS			
Linear System			
	Maximum Roof Displacement (mm)	**Maximum Roof Drift Ratio**	**Deviation from Average (%)**
Gross Stiffness	10	0.004	38
ACI 318-19 & TEC 2018	15	0.007	8
Eurocode 8 & SOZEN'S	19	0.008	17
NZS 3101-2006	14	0.006	14
CSA A23.3-14	17	0.007	5
Average Max. Roof Disp.	16	0.007	**0**
Nonlinear System			
	Maximum Roof Displacement (mm)	**Maximum Roof Drift Ratio**	**Deviation from Average (%)**
Gross Stiffness	12	0.005	31
ACI 318-19	19	0.008	9
Eurocode 8 & TEC 2018	19	0.008	9
NZS 3101-2006	19	0.008	9
SOZEN'S	13	0.006	26
Average Max. Roof Disp.	18	0.008	**0**

Table 62. Interstory drift ratio at max. roof disp. for RSN848, nonlinear

RSN848 Interstory Drift Ratio at Max. Roof Displacement, Nonlinear					
STORY #	**ACI318-19**	**EUROCODE8 & TEC2018**	**NZS3101**	**SOZEN'S**	**AVERAGE DRIFT RATIO**
10	0.003	0.003	0.003	0.003	0.003
9	0.006	0.006	0.006	0.006	0.006
8	0.008	0.008	0.009	0.008	0.008
7	0.009	0.010	0.011	0.010	0.010
6	0.010	0.010	0.012	0.010	0.010
5	0.010	0.010	0.012	0.008	0.010
4	0.010	0.010	0.010	0.006	0.009
3	0.011	0.010	0.008	0.003	0.008
2	0.009	0.009	0.006	0.000	0.006
1	0.005	0.005	0.003	0.000	0.003
Base	0.000	0.000	0.000	0.000	0.000

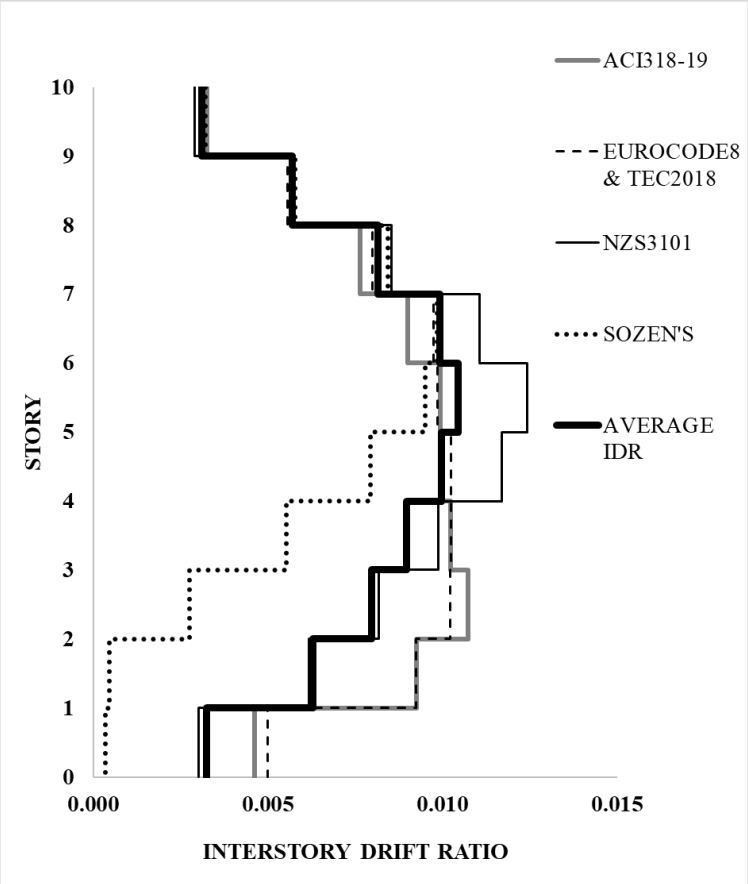

Figure 39. Interstory drift ratio diagram for RSN848, nonlinear

3.3.4.2.8. RSN 1115 Kobe

Maximum roof displacements (mm), maximum roof drift ratios, periods and the deviations from the average maximum roof displacements are presented in Tables 63 and 64. Interstory drift ratio diagram at the maximum roof displacement instant is also illustrated in Figure 40.

Table 63. Maximum roof displacements of RSN 1115 Kobe

RSN1115 KOBE			
Linear System			
	Maximum Roof Displacement (mm)	**Maximum Roof Drift Ratio**	**Deviation from Average (%)**
Gross Stiffness	12	0.005	35
ACI 318-19 & TEC 2018	20	0.009	8
Eurocode 8 & SOZEN'S	17	0.007	8
NZS 3101-2006	18	0.008	3
CSA A23.3-14	19	0.008	3
Average Max. Roof Disp.	19	0.008	**0**
Nonlinear System			
	Maximum Roof Displacement (mm)	**Maximum Roof Drift Ratio**	**Deviation from Average (%)**
Gross Stiffness	12	0.005	36
ACI 318-19	18	0.008	4
Eurocode 8 & TEC 2018	25	0.011	33
NZS 3101-2006	17	0.007	9
SOZEN'S	15	0.007	20
Average Max. Roof Disp.	19	0.008	**0**

Table 64. Interstory drift ratio at max. roof disp. for RSN1115, nonlinear

RSN1115 Interstory Drift Ratio at Max. Roof Displacement, Nonlinear					
STORY #	**ACI318-19**	**EUROCODE8 & TEC2018**	**NZS3101**	**SOZEN'S**	**AVERAGE DRIFT RATIO**
10	0.002	0.001	0.000	0.002	0.001
9	0.004	0.004	0.001	0.004	0.003
8	0.007	0.008	0.003	0.006	0.006
7	0.009	0.010	0.005	0.008	0.008
6	0.010	0.010	0.007	0.009	0.009
5	0.010	0.011	0.009	0.008	0.009
4	0.010	0.011	0.011	0.006	0.010
3	0.010	0.013	0.012	0.005	0.010
2	0.008	0.015	0.011	0.004	0.010
1	0.004	0.009	0.005	0.003	0.005
Base	0.000	0.000	0.000	0.000	0.000

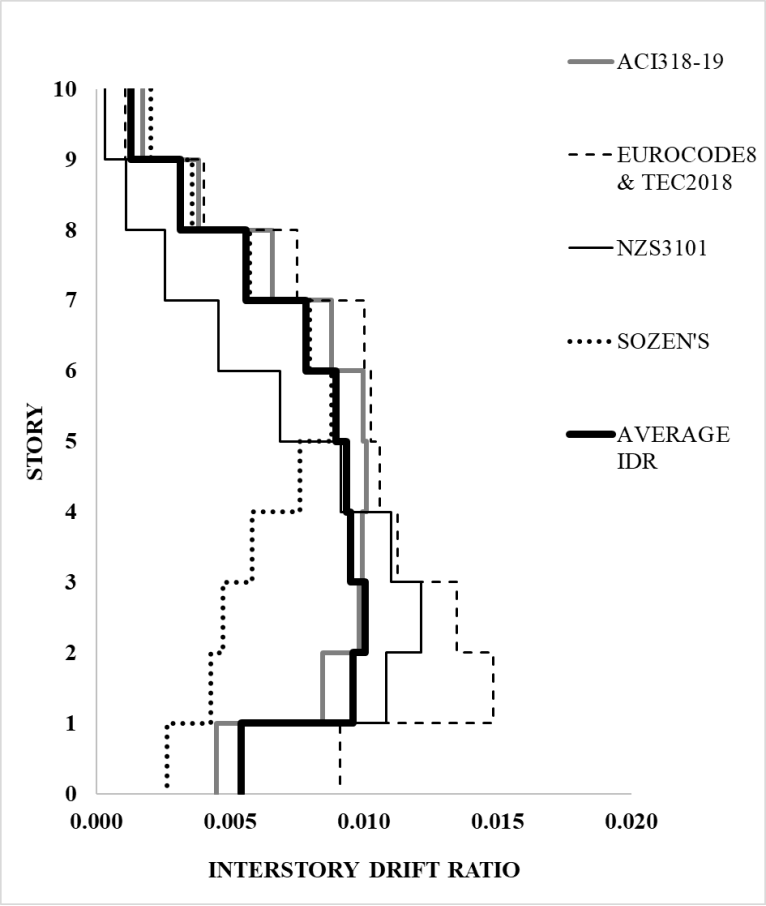

Figure 40. Interstory drift ratio diagram for RSN1115, nonlinear

3.3.4.2.9. RSN 1782 Hector

Maximum roof displacements (mm), maximum roof drift ratios, periods and the deviations from the average maximum roof displacements are presented in Tables 65 and 66. Interstory drift ratio diagram at the maximum roof displacement instant is also illustrated in Figure 40.

Table 65. Maximum roof displacements of RSN 1782 Hector

RSN1782 HECTOR			
Linear System			
	Maximum Roof Displacement (mm)	**Maximum Roof Drift Ratio**	**Deviation from Average (%)**
Gross Stiffness	8	0.003	57
ACI 318-19 & TEC 2018	20	0.009	8
Eurocode 8 & SOZEN'S	15	0.007	19
NZS 3101-2006	19	0.008	3
CSA A23.3-14	20	0.009	8
Average Max. Roof Disp.	**19**	0.008	**0**
Nonlinear System			
	Maximum Roof Displacement (mm)	**Maximum Roof Drift Ratio**	**Deviation from Average (%)**
Gross Stiffness	11	0.005	52
ACI 318-19	19	0.008	17
Eurocode 8 & TEC 2018	38	0.017	65
NZS 3101-2006	19	0.008	17
SOZEN'S	16	0.007	30
Average Max. Roof Disp.	**23**	0.010	**0**

Table 66. Interstory drift ratio at max. roof disp. for RSN1782, nonlinear

RSN1782 Interstory Drift Ratio at Max. Roof Displacement, Nonlinear					
STORY #	**ACI318-19**	**EUROCODE8 & TEC2018**	**NZS3101**	**SOZEN'S**	**AVERAGE DRIFT RATIO**
10	0.001	0.004	0.002	0.001	0.002
9	0.003	0.007	0.003	0.001	0.004
8	0.004	0.010	0.004	0.002	0.005
7	0.005	0.013	0.005	0.003	0.007
6	0.005	0.015	0.006	0.005	0.008
5	0.007	0.018	0.007	0.006	0.009
4	0.008	0.021	0.007	0.006	0.010
3	0.009	0.023	0.007	0.006	0.011
2	0.008	0.020	0.007	0.006	0.010
1	0.004	0.010	0.004	0.003	0.005
Base	0.000	0.000	0.000	0.000	0.000

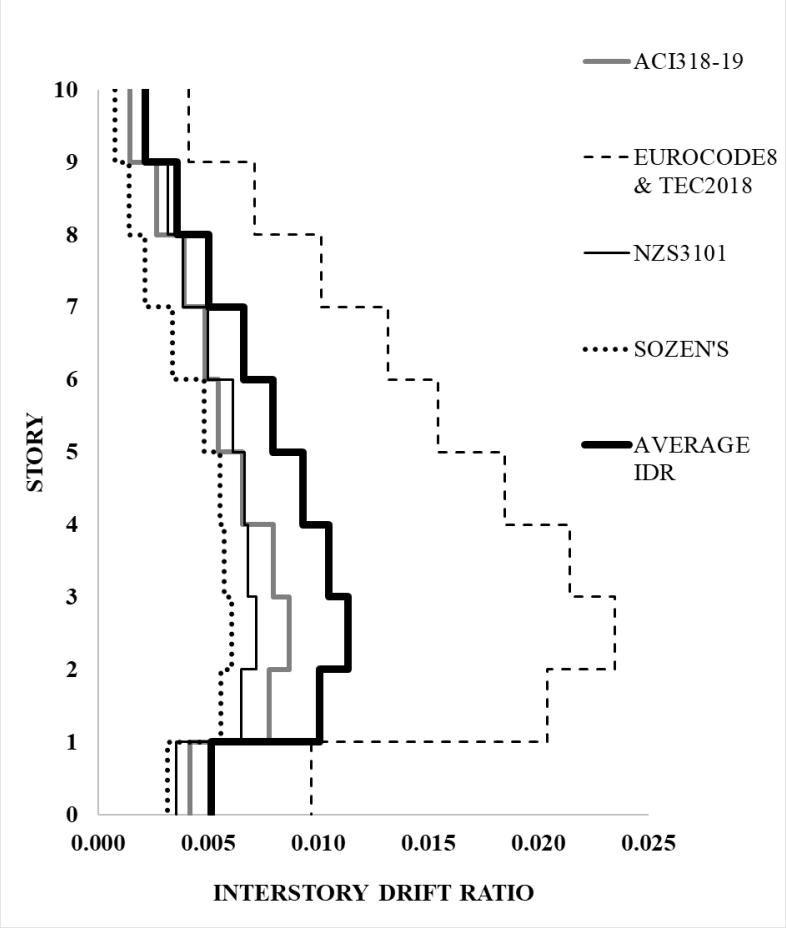

Figure 41. Interstory drift ratio diagram for RSN1782, nonlinear

3.3.4.2.10. RSN 5990 Sierra

Maximum roof displacements (mm), maximum roof drift ratios, periods and the deviations from the average maximum roof displacements are presented in Tables 67 and 68. Interstory drift ratio diagram at the maximum roof displacement instant is also illustrated in Figure 42.

Table 67. Maximum roof displacements of RSN 5990 Sierra

RSN5990 SIERRA			
Linear System			
	Maximum Roof Displacement (mm)	**Maximum Roof Drift Ratio**	**Deviation from Average (%)**
Gross Stiffness	9	0.004	12
ACI 318-19 & TEC 2018	11	0.005	7
Eurocode 8 & SOZEN'S	9	0.004	12
NZS 3101-2006	10	0.004	2
CSA A23.3-14	11	0.005	7
Average Max. Roof Disp.	**10**	0.004	**0**
Nonlinear System			
	Maximum Roof Displacement (mm)	**Maximum Roof Drift Ratio**	**Deviation from Average (%)**
Gross Stiffness	8	0.003	36
ACI 318-19	15	0.007	20
Eurocode 8 & TEC 2018	12	0.005	4
NZS 3101-2006	14	0.006	12
SOZEN'S	9	0.004	28
Average Max. Roof Disp.	**13**	0.005	**0**

Table 68. Interstory drift ratio at max. roof disp. for RSN5990, nonlinear

RSN5990 Interstory Drift Ratio at Max. Roof Displacement, Nonlinear					
STORY #	**ACI318-19**	**EUROCODE8 & TEC2018**	**NZS3101**	**SOZEN'S**	**AVERAGE DRIFT RATIO**
10	0.002	0.003	0.004	0.001	0.003
9	0.004	0.005	0.007	0.001	0.004
8	0.005	0.007	0.009	0.004	0.006
7	0.007	0.008	0.010	0.005	0.007
6	0.008	0.007	0.010	0.006	0.007
5	0.008	0.006	0.007	0.006	0.007
4	0.008	0.006	0.005	0.005	0.006
3	0.008	0.006	0.004	0.005	0.006
2	0.007	0.004	0.002	0.004	0.005
1	0.004	0.002	0.001	0.002	0.002
Base	0.000	0.000	0.000	0.000	0.000

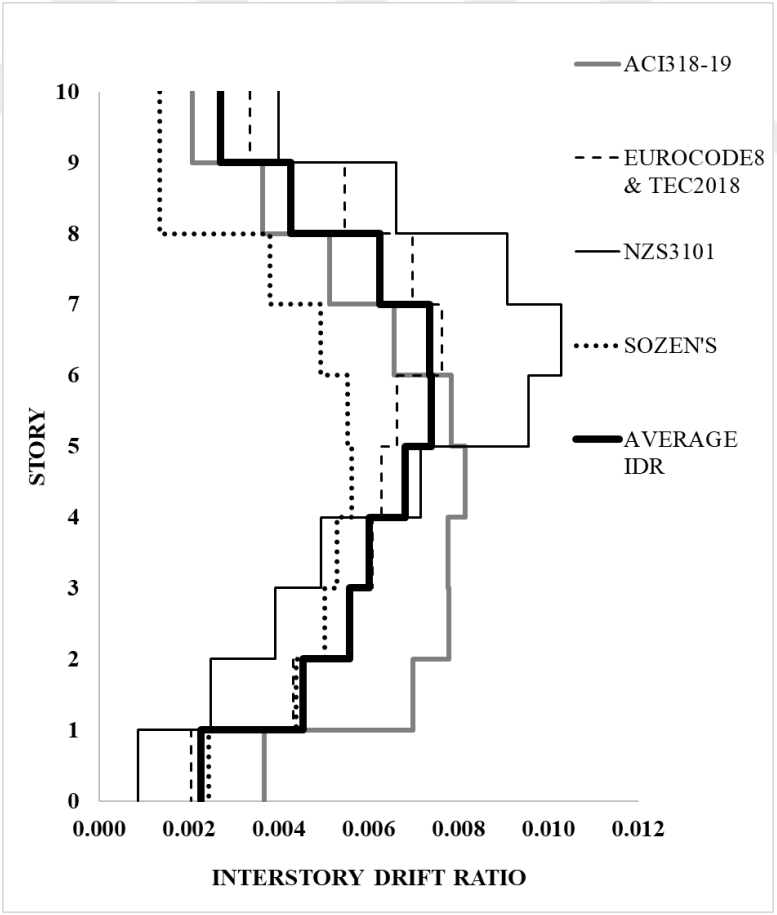

Figure 42. Interstory drift ratio diagram for RSN5990, nonlinear

3.3.4.2.11. RSN 6060 Big Bear

Maximum roof displacements (mm), maximum roof drift ratios, periods and the deviations from the average maximum roof displacements are presented in Tables 69 and 70. Interstory drift ratio diagram at the maximum roof displacement instant is also illustrated in Figure 43.

Table 69. Maximum roof displacements of RSN 6060 Big Bear

RSN6060 BIG BEAR			
Linear System			
	Maximum Roof Displacement (mm)	**Maximum Roof Drift Ratio**	**Deviation from Average (%)**
Gross Stiffness	11	0.005	41
ACI 318-19 & TEC 2018	19	0.008	3
Eurocode 8 & SOZEN'S	18	0.008	3
NZS 3101-2006	19	0.008	3
CSA A23.3-14	18	0.008	3
Average Max. Roof Disp.	**19**	0.008	**0**
Nonlinear System			
	Maximum Roof Displacement (mm)	**Maximum Roof Drift Ratio**	**Deviation from Average (%)**
Gross Stiffness	16	0.007	22
ACI 318-19	21	0.009	2
Eurocode 8 & TEC 2018	28	0.012	37
NZS 3101-2006	18	0.008	12
SOZEN'S	15	0.007	27
Average Max. Roof Disp.	**21**	0.009	**0**

Table 70. Interstory drift ratio at max. roof disp. for RSN6060, nonlinear

RSN6060 Interstory Drift Ratio at Max. Roof Displacement, Nonlinear					
STORY #	**ACI318-19**	**EUROCODE8 & TEC2018**	**NZS3101**	**SOZEN'S**	**AVERAGE DRIFT RATIO**
10	0.002	0.006	0.001	0.001	0.003
9	0.004	0.010	0.003	0.002	0.005
8	0.007	0.013	0.006	0.004	0.008
7	0.010	0.015	0.010	0.007	0.011
6	0.013	0.015	0.013	0.009	0.012
5	0.013	0.015	0.013	0.009	0.012
4	0.012	0.013	0.011	0.007	0.011
3	0.012	0.013	0.009	0.006	0.010
2	0.009	0.012	0.006	0.005	0.008
1	0.005	0.006	0.003	0.003	0.004
Base	0.000	0.000	0.000	0.000	0.000

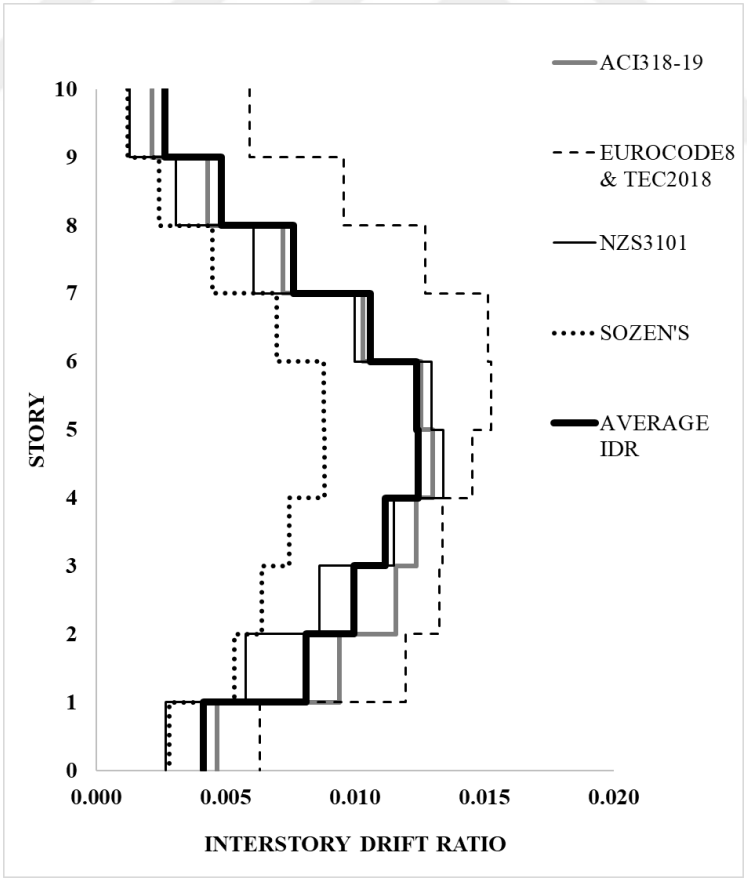

Figure 43. Interstory drift ratio diagram for RSN6060, nonlinear

Table 71 shows the average maximum roof drift ratios and the deviations from the general average for the selected ground motion sets.

Table 71. Average max. roof drift ratios and deviations from the general average for the selected ground motion set

Linear System		
	Average Max. Roof Drift Ratio	**% Deviation from General Average**
Gross Stiffness	0.005	35
ACI 318-19 & TEC 2018	0.008	0
Eurocode 8 & SOZEN'S	0.008	0
NZS 3101-2006	0.008	0
CSA A23.3-14	0.008	0
General Average Max. Roof Drift Ratio	0.008	0
Nonlinear System		
	Average Max. Roof Drift Ratio	**% Deviation from General Average**
Gross Stiffness	0.007	32
ACI 318-19	0.009	7
Eurocode 8 & TEC 2018	0.014	40
NZS 3101-2006	0.009	13
SOZEN'S	0.008	20
General Average Max. Roof Drift Ratio	0.010	0

CHAPTER 4

DISCUSSION OF RESULTS

4.1. Simulation of Cecen's Experiments

The calculated values of all runs for each set of Cecen's experiments are combined to observe the success of the effective stiffness procedures through average deviation from the measured values. The results for H1 runs are presented in Table 72. The gross averages show that all methods have similar results for linear analysis. All methods resulted in about a 10% deviation from the measured value. Nonlinear analyses results have a larger variation. Eurocode procedure seems to have a better fit for this run with the lowest covariance. The maximum deviation is for the Sozen's approach with 30% with a covariance of 12.4.

Table 72. Average and standard deviations of max. roof disp. for H1 runs

Average and Standard Deviations of each Procedure for H1 Runs		
Linear System		
	Average Deviation from Measured (%)	**σ (c.o.v)**
Gross Stiffness	47	21.8
ACI 318-19 & TEC 2018	10	4.6
Eurocode 8 & SOZEN'S	11	6.0
NZS 3101-2006	9	2.0
CSA A23.3-14	14	7.2
Nonlinear System		
	Average Deviation from Measured (%)	**σ (c.o.v)**
Gross Stiffness	38	17.1
ACI 318-19	14	6.3
Eurocode 8 & TEC 2018	3	0.4
NZS 3101-2006	22	9.32
SOZEN'S	30	12.38

H1-Run 2 is selected to investigate the plasticity demand of the system. The 2% peak roof drift is the reason of the selection. This value is about the seismic regulations' peak demand levels for design-level earthquakes. Plasticity demands are attempted to be reflected as the ratio of plastic rotations to yield rotations at the beam plastic hinges. The plasticity demands at the story levels could provide information about the distribution of the plasticity demand and the ductility level of the system. The results are summarized in Table 73. Maximum demands are observed on the fifth and sixth floors for all procedures. Considering the general uncertainty, it is not possible to tell that any method has superiority on the others. ACI-318 developed the highest demands, and the NZS3101 developed the lowest demand. Others are positioned in between these two extremes. The variation on floor 6 is larger than other floors and around 20%. The maximum demand is observed on this floor. The high uncertainty of the ground motion in a design scenario diminishes the importance of the observed difference. Also, observing the variation of peak roof drift ratio for the runs indicates that it is not possible to generalize the difference for the runs. Interestingly, even though Sozen's approach has the highest deviation for the measured peak roof drift ratio for the given run, the calculated plasticity demands have the highest deviation for the Eurocode8 approach, which has the lowest deviation from the measured value.

Table 73. Average plasticity demand of the beam rotational springs for H1-R2

AVERAGE PLASTICITY DEMAND OF BEAM ROTATIONAL SPRINGS FOR H1-R2 (Θplastic/Θyield)				
STORY #	**ACI318-19**	**EUROCODE8 & TEC2018**	**NZS3101**	**SOZEN'S**
10	0	1	4	0
9	2	2	5	2
8	6	8	7	6
7	9	12	10	9
6	11	14	10	12
5	11	13	10	13
4	10	9	8	11
3	9	10	7	9
2	7	9	6	7
1	4	5	4	4
Base	0	0	0	0

The results for H2 runs are presented in Table 74. The gross averages show that for linear analysis, deviations are larger than the deviations from H1. Still, the highest value is 25% off the measured value. Sozen's Approach seems to have a better success for this set. The gross averages for the nonlinear analyses have a similar range. The maximum deviation is around 25%, and the methods have about 10% differences among each other. The covariances of the results are low. Data do not permit to state explicitly that any method is superior to others. However, it could be said that the maximum difference of 25% is a tolerable value, considering the uncertainty in design ground motion itself. Overall, comparison with the results of the analysis with gross stiffness values, the effective stiffness approach consistently carries the results closer to measured values. Also, the covariance of the effective stiffness procedures is lower than the covariance of the gross stiffness approach.

Table 74. Average and standard deviations of max. roof disp. for H2 Runs

Average and Standard Deviations of each Procedure for H2 Runs		
Linear System		
	Average Deviation from Measured (%)	**σ (c.o.v)**
Gross Stiffness	34	21.8
ACI 318-19 & TEC 2018	21	4.6
Eurocode 8 & SOZEN'S	13	6.0
NZS 3101-2006	25	2.0
CSA A23.3-14	14	7.2
Nonlinear System		
	Average Deviation from Measured (%)	**σ (c.o.v)**
Gross Stiffness	33	5.7
ACI 318-19	12	0.6
Eurocode 8 & TEC 2018	21	2.1
NZS 3101-2006	13	2.0
SOZEN'S	24	3.6

The results for the selected ground motion suite are organized by average deviations of maximum roof displacements ratios from the general average in Table 75. ACI 318 was observed to exhibit the highest success for both linear and nonlinear analyses in absolute numbers. Nevertheless, the deviation ranges are 4 to 8% for the

linear analysis and 12-34% for nonlinear analysis. Covariance values are low for all approaches. Considering the overall uncertainty, it could be said that all the methods are successful.

Table 75. Average deviations of max. roof disp. for the selected ground motion set

Average Deviations of Max. Roof Displacements for Selected Ground Motion Set		
Linear System		
	% Deviation from General Average	**σ (c.o.v)**
Gross Stiffness	34	2.1
ACI 318-19 & TEC 2018	4	0.2
Eurocode 8 & SOZEN'S	8	0.3
NZS 3101-2006	8	0.0
CSA A23.3-14	5	0.1
Nonlinear System		
	% Deviation from General Average	**σ (c.o.v)**
Gross Stiffness	33	2.3
ACI 318-19	12	0.5
Eurocode 8 & TEC 2018	34	2.9
NZS 3101-2006	15	0.9
SOZEN'S	22	1.5

4.2. Combined Roof Drift Results of Cecen Runs

The output of all Cecen runs is combined to evaluate the average success of the methods in terms of maximum roof drift ratio in linear and nonlinear analyses.

Linear maximum roof drift ratios of the test runs are combined and presented for each stiffness procedure in Table 76. If the results of procedures are compared with measured results, it could be seen that the deviation of the calculated to measured results is a maximum of about 30%. Considering the possible uncertainty in ground motion, these differences are tolerable values and could be accepted successfully.

Table 76. Maximum roof drift ratios of Cecen runs for linear analyses

Linear Max. Roof Drift Ratio					
	ACI318 & TEC	**Eurocode & Sozen's**	**NZS3101**	**CSA A23.3-14**	**Measured (Cecen)**
H1-R1	0.012	0.011	0.013	0.011	0.013
H1-R2	0.024	0.023	0.026	0.022	0.023
H1-R3	0.035	0.034	0.038	0.034	0.044
H2-R1	0.005	0.004	0.005	0.004	0.004
H2-R2	0.009	0.008	0.009	0.008	0.008
H2-R3	0.014	0.013	0.015	0.013	0.010
H2-R4	0.014	0.013	0.015	0.013	0.011
H2-R5	0.021	0.020	0.022	0.019	0.017
H2-R6	0.028	0.026	0.029	0.026	0.026
H2-R7	0.034	0.034	0.035	0.032	0.044

Nonlinear maximum roof drift ratios of the test runs are also presented for each stiffness procedure in Table 77. Again, the calculated to measured deviation is a maximum of about 30%. These differences are tolerable values considering the possible uncertainty in ground motion. Eurocode8 and TEC2018 provide the same maximum roof drift ratio with the measured ones for the most intense runs H1-R3 and H2-R7 in nonlinear analysis.

Table 77. Maximum roof drift ratios of Cecen runs for nonlinear analyses

Nonlinear Max. Drift Ratio					
	ACI318	**Eurocode & TEC**	**NZS3101**	**Sozen's**	**Measured (Cecen)**
H1-R1	0.011	0.012	0.009	0.008	0.013
H1-R2	0.020	0.024	0.021	0.018	0.023
H1-R3	0.038	0.044	0.033	0.031	0.044
H2-R1	0.005	0.006	0.005	0.005	0.004
H2-R2	0.010	0.010	0.007	0.007	0.008
H2-R3	0.012	0.013	0.010	0.008	0.010
H2-R4	0.012	0.013	0.010	0.008	0.011
H2-R5	0.017	0.019	0.018	0.014	0.017
H2-R6	0.025	0.032	0.024	0.021	0.026
H2-R7	0.036	0.044	0.031	0.031	0.044

Figure 44 shows the distribution of the measured and calculated maximum roof drift ratios for both linear and nonlinear analyses. The results are organized to observe variation in roof drift ratio percentages. Boundaries for 0.5 and 1% roof drift ratio deviations are provided in the figure. It could be observed that for the practical range the deviation is within 0.5% boundary. None of the procedures have a superiority. The variations for the large drift demand are a little larger than 1%. Except for the Eurocode8-TEC2018 nonlinear results, all the approaches calculate lower values at this demand level.

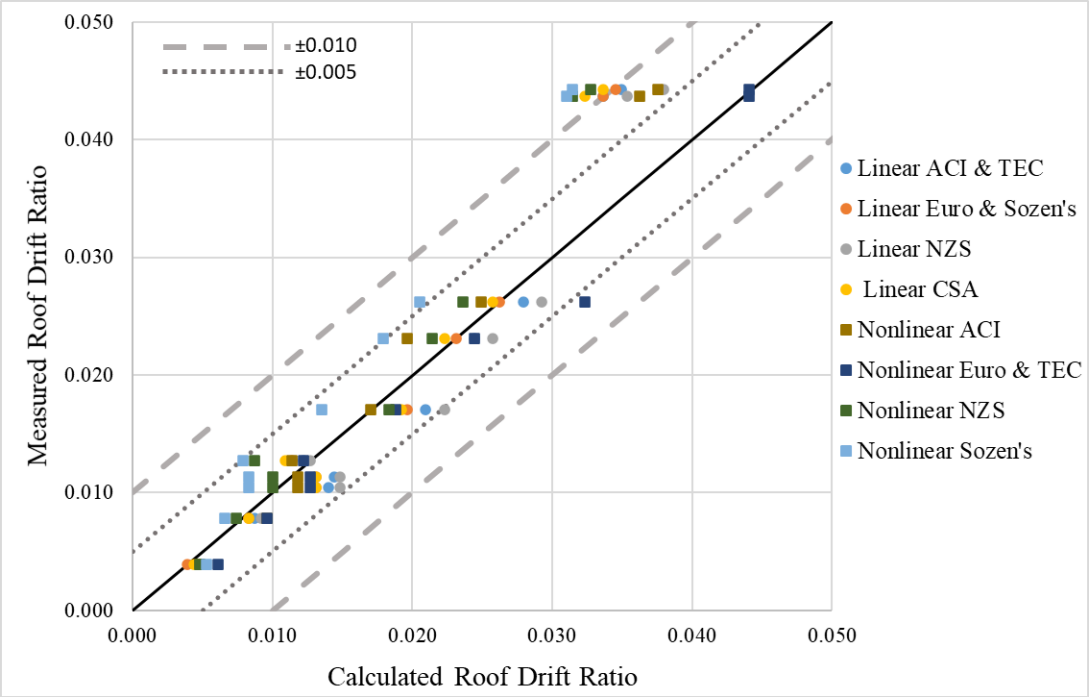

Figure 44. Calculated and measured maximum roof drift ratios

CHAPTER 5

SUMMARY AND CONCLUSIONS

5.1. Summary

This study aims to evaluate effective stiffness procedures of contemporary seismic design codes and some proposals for reinforced concrete structures. The effective stiffness approach is originally established for the application of the equal displacement rule. It states that the linear and nonlinear system displacement demands are about equal if the effective stiffness of the sustained drift levels is used in the linear system. Therefore, estimating the effective stiffness of reinforced concrete structures is considerably important for the seismic design. However, there is no mutual consent about determining the effective stiffness. Different approaches exist to define it. In the scope of this thesis, the effective stiffness approaches of the Turkish Earthquake Code (2018), Canadian Standards Association Design of Concrete Structures (CSA A.23.3-14), New Zealand Concrete Structures Standard (NZS3101-2006), Eurocode 8 (EN 1998-3), Building Code Requirement for Structural Concrete of American Concrete Institute (ACI318-19) and Sozen's approach are investigated in terms of effort in their execution. Comparison is made to see whether there is any clear advantage of the result obtained. A numerical study is performed to evaluate the effectiveness of the listed approaches. Two frames, which Cecen (1979) tested, are modeled by OpenSees software. Frames were designed as high ductility moment frames. Nonlinearity in frames is modeled by lumped plasticity approach through plastic hinges at the member ends. The rotational springs are defined as zero-length elements in the OpenSees material library. Steel-01 spring which could simulate bilinear moment-rotation relationship is used for defining the lumped nonlinearity of the frames.

Linear and nonlinear time history analyses are performed. Calculated values are compared with Cecen's (1979) test results. Also, a suite of ground motions with eleven earthquakes is selected. Linear and nonlinear dynamic analyses are performed with this suite for each effective stiffness procedure as well. The analyses results are compared in terms of maximum roof drifts, interstory drift ratios at maximum roof drift moment. Also,

the H1-R2 run of Cecen tests is evaluated in envelope drift levels, and plastic rotation values at maximum roof drift moment.

ACI318-19 and TEC 2018 have identical reduction factors in the linear system. ACI318-19 provided very close results in linear and nonlinear analyses in terms of maximum roof displacement for H1 and H2.

Eurocode8 suggests the identical reduction factors with Sozen's Approach and TEC 2018 in the linear system and nonlinear system, respectively. Furthermore, Eurocode8 gave tolerable results in linear analyses in terms of maximum roof displacement for H1. Also, it showed the best maximum roof displacement performance for H2.

NZS3101-2006 provided results with higher deviation than other procedures in terms of maximum roof displacement linear part. However, the results are still in tolerable limits. It was generally the second most successful procedure for maximum roof displacement in the nonlinear part. Also, this method exhibited acceptable distributions at interstory drift ratio diagrams.

CSA A23.3-14 was examined only in terms of the linear system. This procedure usually provided close results in maximum roof displacement for the runs with the lower spectrum intensity.

Sozen's Approach was a generally successful procedure for maximum roof displacement for linear analysis. The tolerable results also were obtained from this procedure in terms of maximum roof displacement in nonlinear.

5.2. Conclusions

The comparison of the calculated maximum roof drifts with the Cecen's (1979) test results show that all of the effective stiffness procedure provides results for linear and nonlinear analysis with a maximum of 25% and 30% deviation, respectively. None of the procedures has consistently a better estimation.

The investigation of the plastic demand for H1-Run2 shows that a better maximum roof drift estimation does not secure a better estimation of the plasticity demand. On the other hand, it could be said that the estimations of the procedures are not very different from each other.

The observed deviation levels are tolerable, considering the uncertainty in the expected ground motion. Hence, the procedures could be accepted as satisfactory. However, the level of accuracy does not warrant the complexity demanded by some of the approaches.

Results of the analysis with the suite of ground motions supported the results obtained from Cecen's tests. None of the procedures consistently have closer values to the calculated averages. But the deviation levels are in the same levels as the test result comparisons.

The Eurocode8-TEC2018 approach resulted better fit for the high demand Cecen Runs. The roof drift levels in these tests are about 4.5%. This approach defines much softer systems through the effective stiffness definitions. It is likely that other approaches are calibrated for the common design demand levels (2%), and their performance drops for higher demands. Still, their deviations are within the 1% interstory drift band.

If both the ease of application and the level of accuracy are considered, it could be stated that the simple approach proposed by Sozen is the most successful procedure.

REFERENCES

ACI 318-19. (2019). *Building Code Requirements for Structural Concrete*, Michigan. USA.

Cecen, Haluk. 1979. *Response of Ten Story, Reinforced Concrete Model Frames to Simulated Earthquakes*. University of Illinois at Urbana-Champaign.

CSA A23.3-14. (2014). *Design of Concrete Structure;* Canadian Standards Association, Canada.

"Datacenterhub - DEEDS." n.d. Accessed January 4, 2022. https://datacenterhub.org/deedsdv/publications/view/343.

Elwood, Kenneth J, and Jack P Moehle. 2006. "Idealized Backbone Model for Existing Reinforced Concrete Columns and Comparisons with FEMA 356 Criteria." *The Structural Design of Tall and Special Buildings* 15 (5): 553–69.

Eurocode 8. (1998). *Design of Structures for Earthquake Resistance;* European Standard EN1998-1.

Gulkan, Polat, and Mete Avni Sozen. 1971. "Response and Energy-Dissipation of Reinforced Concrete Frames Subjected to Strong Base Motions."

"Https://Opensees.Berkeley.Edu/Wiki/Index.Php/OpenSees_User." n.d.

"Https://Seismosoft.Com/Products/Seismosignal/." n.d.

"Https://Www.Ecf.Utoronto.ca/~bentz/R2k.Htm." n.d.

Moehle, Jack. 2015. *Seismic Design of Reinforced Concrete Buildings*. McGraw-Hill Education.

NZS 3101. (2006) *Concrete Structures Standard*; New Zealand Standards Association, Wellington, New Zealand.

Otani, Shunsuke. 1973. *Behavior of Multistory Reinforced Concrete Frames during Earthquakes*. University of Illinois at Urbana-Champaign.

Paulay, T, and M J N Priestly. 1992. "Structural Wall." *Seismic Design of Reinforced Concrete and Masonry Building*, 362–499.

Shibata, Akenori, and Mete A Sozen. 1976. "Substitute-Structure Method for Seismic Design in R/C." *Journal of the Structural Division* 102 (1): 1–18.

Sönmez, Egemen. 2020. "Manipulation of Structural Design Parameters to Mitigate the Concentrarion of Interstory Drift Ratios."

Sozen, Mete A. 2003. "The Velocity of Displacement." In *Seismic Assessment and Rehabilitation of Existing Buildings*, 11–28. Springer.

Sözen, Mete A. 2013. "WHY SHOULD DRIFT DRIVE DESIGN FOR EARTHQUAKE RESISTANCE?" In *Proceeding the 6th Civil Engineering Conference in Asia Region: Embracing the Future through Sustainability*.

Takeda, Toshikazu, Mete A Sozen, and N Norby Nielsen. 1970. "Reinforced Concrete Response to Simulated Earthquakes." *Journal of the Structural Division* 96 (12): 2557–73.

TEC. (2018). *Turkish Earthquake Code for Building Structures: Specifications for Design of Buildings under Earthquake Forces*; Presidency of Disaster and Emergency Management, 2018.

APPENDIX A

ACCELERATION TIME-HISTORIES OF THE SELECTED GROUND MOTION SET

A.1. Input Ground Motion Records Used in Chapter 3

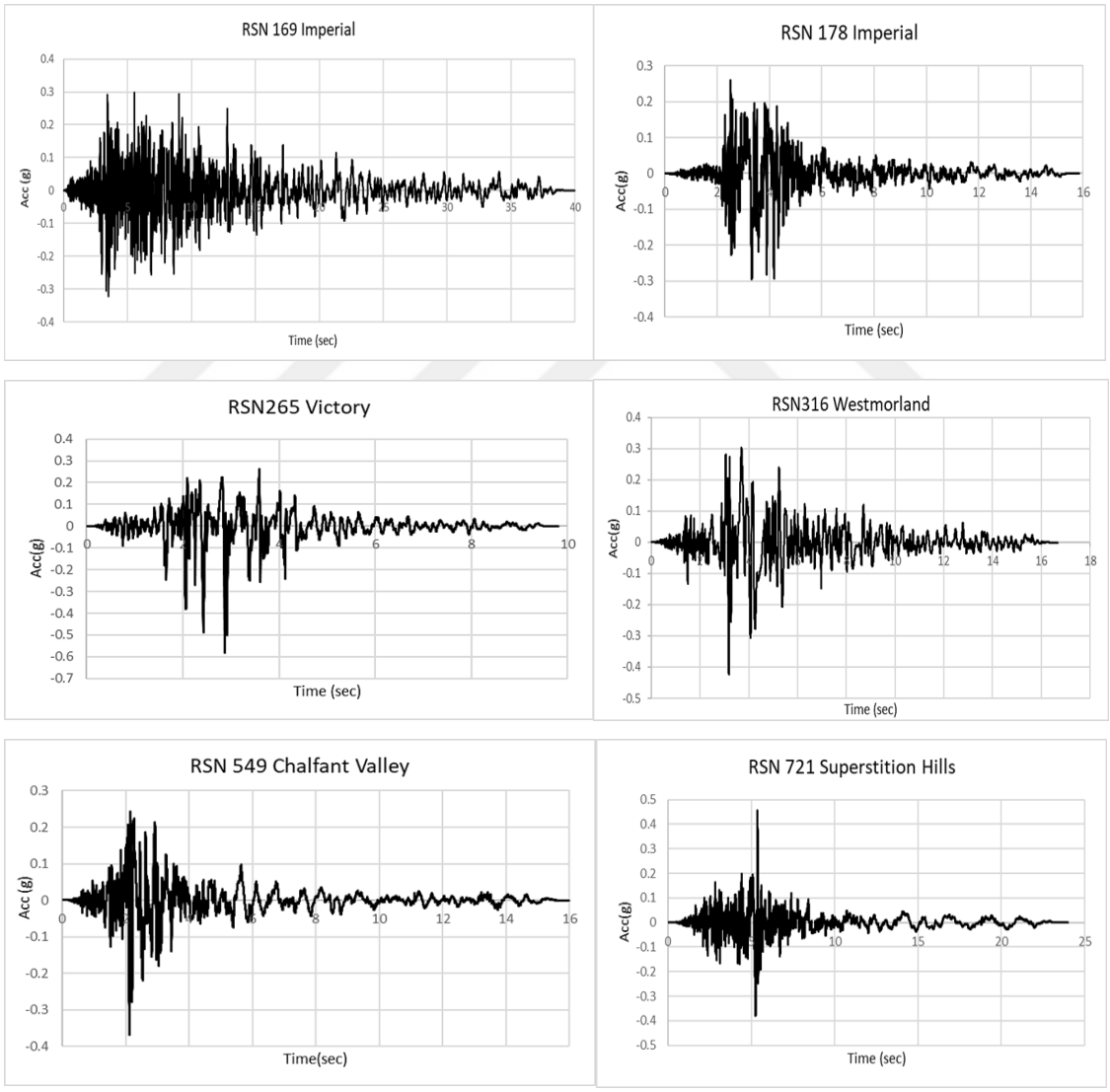

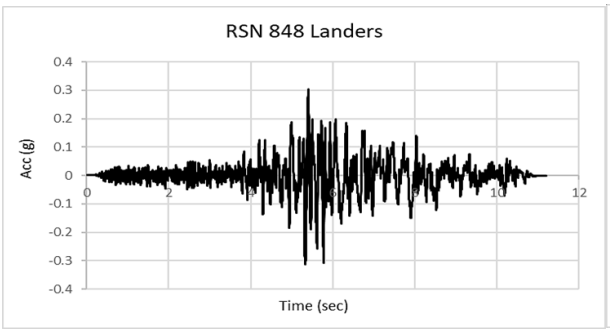
RSN 848 Landers
Acc (g)
Time (sec)

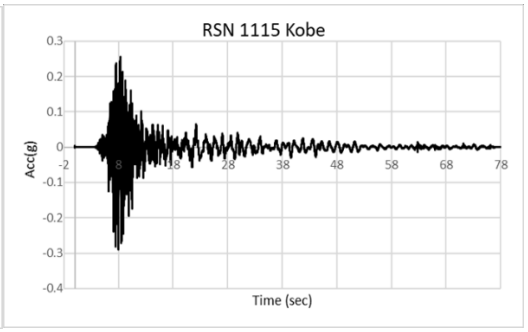
RSN 1115 Kobe
Acc(g)
Time (sec)

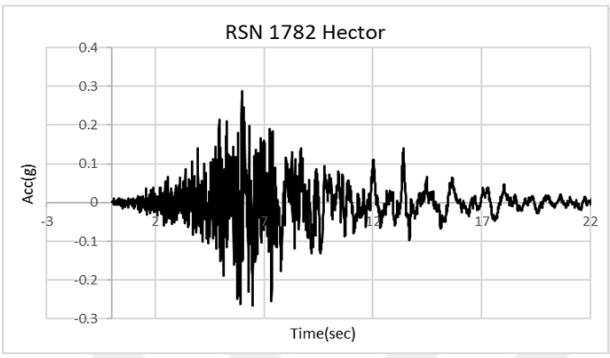
RSN 1782 Hector
Acc(g)
Time(sec)

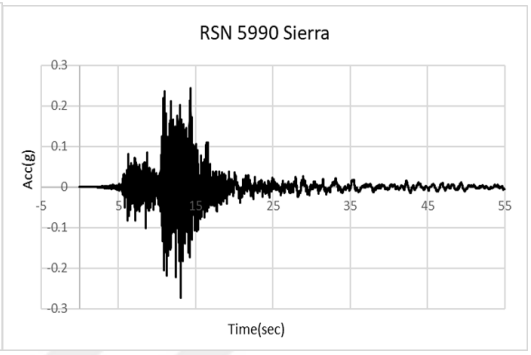
RSN 5990 Sierra
Acc(g)
Time(sec)

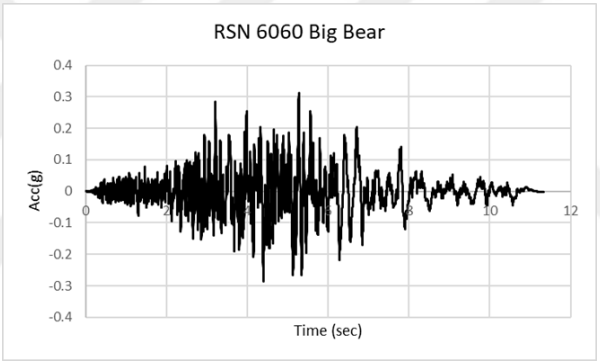
RSN 6060 Big Bear
Acc(g)
Time (sec)